Mode jumping and quasi-periodicity in nonlinear elastic structures

Everall, Paul Robert

Award date:
1999

Awarding institution:
University of Bath

MODE JUMPING AND QUASI-PERIODICITY IN NONLINEAR ELASTIC STRUCTURES

Submitted by

Paul Robert Everall

B.Eng

for the degree of
Doctor of Philosophy
of the University of Bath
1999

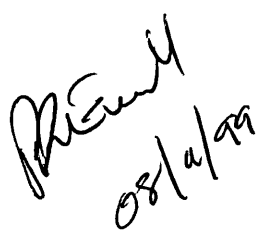

ProQuest LLC
789 East Eisenhower Parkway
P.O. Box 1346
Ann Arbor, MI 48106-1346

Abstract

It is well known that thin flat rectangular plates supported on their edges, under in-plane compressive loading, behave in a stable manner such that the induced wave pattern will continue to take extra load in the post-buckling regime. What is less obvious is the limit of this post-buckling stability, which is likely be marked by a dynamic mode jump to a new wave pattern with a reduced wavelength. Here the use of modern numerical methods, in conjunction with classical analytical techniques, allows a detailed investigation of mode jumping to be performed for a wide range of boundary conditions and all plate lengths.

For the axially-compressed strut supported by a stiffening nonlinear foundation — which forms a heuristic model for the more complicated plate problem — the full range of end conditions from simply-supported to clamped is examined. In the plate system, four separate combinations of simply-supported and clamped flexural conditions on the long (unloaded) and short (loaded) edges are considered, together with in-plane constraints ranging from free-to-pull-in to fully-restrained.

All possible mode interactions, for systems of all lengths, are presented in a concise form using the parameter space of Arnol'd tongues, borrowed from nonlinear dynamical systems theory. Each cusp describes the extent to which the system locks onto a particular wave, and also gives the ratio of the two competing wavelengths before and after mode jumping. This ratio is only rational at the extremes of simply-supported and clamped: for other boundary conditions it is irrational

and the associated buckle pattern quasi-periodic.

This work has been written up in four papers; three have been published (Hunt & Everall, 1999; Everall & Hunt, 1999a; Everall & Hunt, 1999b) and a further paper has been accepted (Everall & Hunt, 1999c).

Acknowledgements

It seems logical to begin with Dr Sally Clift who suggested I do a Ph.D., the EPSRC for the subsequent funding, and the University of Bath which has now been my home for seven years. However I am most indebted to my supervisor Professor Giles Hunt whose constant encouragement, patience and support gave me the motivation to finish. (I must also slip in a word of thanks to his wife Chrissie for the dinner parties.) A large acknowledgement must go to Dr Ahmer Wadee who, amongst many other things, introduced me to the various computer programs which made my Ph.D. possible. Professor Chris Budd, Dr Alan Champneys, Dr Ray Lawther and Dr Mark Peletier provided useful feedback on my research (the latter also donated a rather decent computer).

Then there are the other members of the office who kept me entertained (in alphabetical order): Richard Allen, Dr Oliver Boston, Colin Bowler, Ben Hicks, David Hole, Dr Richard McIntosh, Colin McPherson, Baomin Qi, Bill Taylor and Matt Warner. Also thanks to Dr Khurram Wadee whose only link with the office is the telephone during the numerous arguments with his brother Ahmer.

Finally an infinitely large word of thanks to my parents and sister for their continuing love and support, and a slightly smaller one to my other friends scattered around the world; Brendan Laing, Molly Molan & family, Nicola Hawkes & everyone else at the Stirling Graduate School, Alia Lodhi, Dr Yuan-Yao Li, Steven Kinnaird, Heidi Treharne and Martin Keylock.

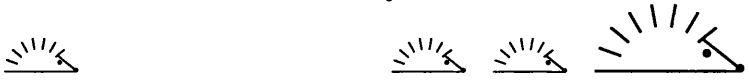

Contents

Abstract 1

Acknowledgements 3

List of Figures 9

Nomenclature 12

1 Introduction 14

1.1 Buckling phenomena 16

1.1.1 General behaviour 17

1.1.2 Analytical solutions 19

1.1.3 Modal analysis 24

1.1.4 Numerical methods 24

1.2 Mode interactions 25

1.2.1 Mode jumping 26

1.3 Dynamical systems 30

1.3.1 Discrete dynamical systems 32

1.3.2 Arnol'd tongues 33

1.4 Thesis outline 34

1.4.1 Simply-supported strut 35
1.4.2 Simply-supported plate 35
1.4.3 Effects of the boundary conditions 36
1.4.4 Conclusions and further work 36

2 Governing equations **37**

2.1 Total potential energy 39
2.1.1 Axially-compressed strut 39
2.1.2 Axially-compressed plate 43
2.2 Differential equations 51
2.2.1 Axially-compressed strut 51
2.2.2 Axially-compressed plate 53

3 Simply-supported strut **55**

3.1 Theory 57
3.1.1 Nondimensionalization 57
3.1.2 Linearization and root structure 58
3.1.3 Critical loads 60
3.2 Nonlinear energy formulation 62
3.2.1 Fundamental solution and initial bifurcations 64
3.3 Coupled behaviour 65
3.3.1 Stability 69
3.4 Numerical solutions 72
3.4.1 Reduction to first-order form 73

3.4.2 Comparison with analytical results 74
3.5 Passive contamination 77
3.6 Arnol'd tongues 81
3.6.1 Construction 82
3.6.2 Simply-supported strut 84
3.7 Concluding remarks 86

4 Simply-supported plate **88**

4.1 Differential equation 90
4.1.1 Nondimensionalization 90
4.2 Boundary conditions 91
4.2.1 Free-edged 92
4.2.2 Straight-edged 93
4.2.3 Clamped in-plane 94
4.3 Critical loads 95
4.4 Rayleigh–Ritz formulation 98
4.4.1 Energy integral 99
4.4.2 Passive contamination 100
4.5 Reduction to ODEs 102
4.5.1 Galerkin reduction 102
4.5.2 Boundary conditions 103
4.5.3 Reduction to first-order form 106
4.6 Full numerical solution 107
4.7 Validation 108

4.7.1 Uncoupled paths 108
4.7.2 Secondary bifurcations 109
4.8 Arnol'd tongues 111
4.9 Passive mode effects 113
4.9.1 Limit point instability 113
4.9.2 Stable secondary bifurcation 114
4.9.3 Unstable secondary bifurcation 115
4.9.4 Crossing of tongues 115
4.10 Concluding remarks 116

5 Effects of the boundary conditions **118**

5.1 Supercritical strut 119
5.1.1 Energy integral and differential equation 119
5.1.2 Critical loads 121
5.1.3 Solution method 124
5.1.4 Arnol'd tongues 125
5.2 Axially-compressed plate 128
5.2.1 Boundary conditions 128
5.2.2 Critical loads 129
5.2.3 Reduction to ODEs 131
5.2.4 Arnol'd tongues 132
5.3 Concluding remarks 134

6 Conclusions and further work **135**

6.1 Further work 137

A Calculus of variations **139**

B Energy coefficients **142**

References **144**

List of Figures

1.1 Plate buckling behaviour 15

1.2 Linear buckling behaviour 17

1.3 Typical loading configurations 18

1.4 Some typical prismatic structures 19

1.5 Stable post-buckling behaviour 20

1.6 Unstable post-buckling behaviour 21

1.7 A typical mode jump 22

1.8 Supercritical strut link model 24

1.9 Simply-supported and clamped buckle patterns 25

1.10 Various in-plane boundary conditions 27

1.11 Unforced and forced pendulums 31

1.12 Poincaré map 32

1.13 Arnol'd tongues 33

2.1 Strut on an elastic foundation 39

2.2 Strut in bending 40

2.3 Strut end-shortening 42

2.4 Flat plate under compression 44

2.5 Plate end-shortening 47

2.6 Force equilibrium on a small element 49

3.1 Strut on an elastic foundation 57

3.2 Eigenvalues in the complex plane 59

3.3 Critical loads 61

3.4 Hyperbolic equilibrium paths 67

3.5 Elliptic equilibrium paths 68

3.6 Equilibrium paths with passive contamination 76

3.7 Comparison of solution profiles 80

3.8 Secondary buckling loads 81

3.9 Tongue showing interaction between 2 and 3 half-waves 83

3.10 Tongue showing interaction between 3 and 4 half-waves 84

3.11 Arnol'd tongues for the supercritical strut 85

4.1 Free-edged plate 92

4.2 Straight-edged plate 93

4.3 Clamped in-plane plate 95

4.4 Critical loads 97

4.5 Errors in total potential energy 108

4.6 Errors in secondary bifurcation positions 110

4.7 Arnol'd tongues for the clamped in-plane plate 111

4.8 Arnol'd tongues for the straight-edged plate 112

4.9 Limit point instability 113

4.10 Stable secondary bifurcation 114

4.11 Unstable secondary bifurcation 115

4.12 Crossing of tongues 116

5.1 Strut on an elastic foundation 120

5.2 Critical loads for the supercritical strut 123

5.3 Linear buckle patterns 124

5.4 Nonlinear buckle patterns 125

5.5 Arnol'd tongues for the supercritical strut 126

5.6 Secondary buckling loads 127

5.7 Plate buckle patterns for different boundary conditions 128

5.8 Critical loads for the plate with simply-supported long edges . . . 129

5.9 Critical loads for the plate with clamped long edges 131

5.10 Arnol'd tongues for the clamped in-plane plate 132

5.11 Arnol'd tongues for the straight-edged plate 133

Nomenclature

Subscripts x and y refer to the Cartesian coordinate system. Variables in brackets below denote nondimensional quantities. Dots ($\dot{}$) and primes ($'$) above variables represent partial differentiation with respect to x and y (or $\bar{x}$ and $\bar{y}$).

Axes and dimensions

x, y, z ($\bar{x}$, $\bar{y}$, $\bar{z}$)	Cartesian coordinates
u, v, w ($\bar{u}$, $\bar{v}$, $\bar{w}$)	Displacements in the x, y and z directions
L (l)	Length of plate or strut
s, t	Width and depth of strut (commonly written as b and d)
t	Plate thickness
r, r_x, r_y	Radii of curvature
θ, θ_x, θ_y	Angles of rotation

Material properties

E, G	Young's modulus and shear modulus
ν	Poisson's ratio (assumed to be 0.3)
$I = \frac{st^3}{12}$	Second moment of area (commonly written as $\frac{bd^3}{12}$)
$D = \frac{Et^3}{12(1-\nu^2)}$	Plate flexural rigidity (or plate constant)
K, C	Foundation spring stiffness and nonlinearity
$\mathcal{K}$ (κ)	Rotational spring stiffness

Stresses, strains, moments and loads

σ_x, σ_y, τ_{xy}	Direct and shear stresses
φ ($\bar{\varphi}$)	Stress function
ε_x, ε_y, γ_{xy}	Direct and shear strains
M, M_x, M_y	Bending moments
P, P_x, P_y (p, p_x, p_y)	Applied loads

Energy components

V, W	Total potential energy
U_b	Bending energy
U_f	Foundation energy
U_l	Work done by the applied load
U_m	Membrane energy
Δ	End shortening

Rayleigh–Ritz

a, b, c, d	Number of half-waves in buckle pattern
Q_a	Amplitude of mode with a half-waves
V_{aaaa}, V'_{aa}, etc.	Energy coefficients
P^a (p^a)	Critical load for mode with a half-waves

Chapter 1

Introduction

> "... it is obvious that irrational numbers are uninteresting to an engineer, since he is only concerned with approximations, and all approximations are rational."
>
> Hardy (1940)

The responses of structural members in axial compression which undergo bifurcational instabilities can typically be split into two parts: pre-buckling and post-buckling. Often the initial pre-buckling response is *linear* and, apart from a small amount of elastic compression, the member retains its unloaded shape. The limit of this behaviour is marked by a *critical load* where the member buckles, undergoing noticeable elastic or plastic deformation as it moves into the post-buckling regime. It is the *nonlinear* post-buckling behaviour of thin, flat, rectangular plates that is of interest here. Thin plates appear in a number of different structures and are also used to construct a wide range of prismatic members such as stiffened plates and box-sections; typical applications include aircraft, bridges, offshore platforms and ships.

When supported on all four edges, the load carried by a thin flat plate continues to increase after buckling, and therefore it might be expected that stability would

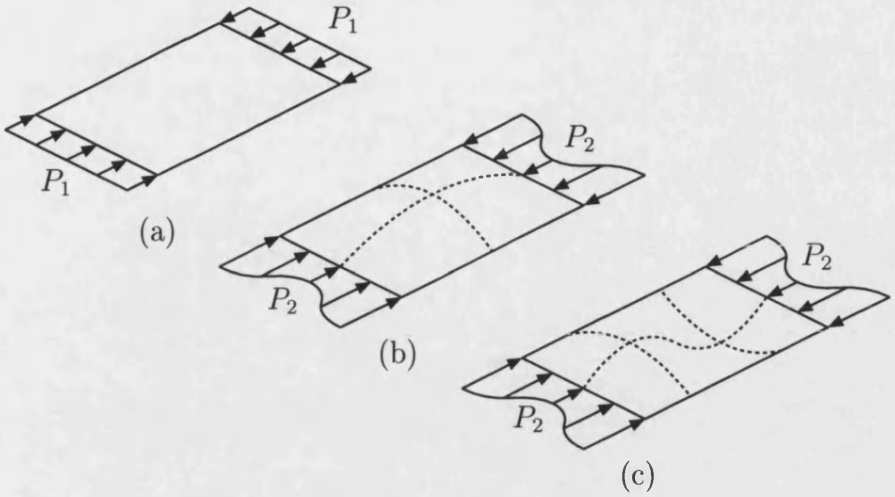

Figure 1.1: Plate buckling behaviour; (a) uniformly compressed state, (b) initial buckle pattern, (c) buckle pattern after mode jumping. $P_1 < P^C < P_2$.

be lost when yielding occurs. However a change in the buckle pattern has been observed experimentally *before* yielding takes place, implying a loss of stability earlier in the loading process. Take for example the rectangular plate shown in Fig. 1.1(a) which is in the uniformly compressed state (the applied load P_1 is less than the critical load P^C). When the critical load is reached the plate buckles — the shape being dependent on the boundary conditions and aspect ratio — with the amplitude of deflection increasing with further increases in load. At the load P_2 (say) there is a loss of stability marked by a sudden change in the buckle pattern; this behaviour is often termed "mode jumping". Figs. 1.1(b) and (c) show typical buckle patterns for a simply-supported plate, before and after mode jumping, where the number of half-waves has increased from one to two.

It is well known that for a simply-supported flat plate the post-buckling behaviour is periodic, with the buckle pattern containing a single wavelength and an integer number of half-waves along the length (Fig. 1.1). However with other boundary conditions the initial response is dependent on *two* wavelengths, the ratio of which is typically irrational, and hence the resulting behaviour is (in general) quasi-periodic.

This work aims to characterize the phenomenon of mode jumping in plates for a wide range of boundary conditions and lengths, comparing results from both analytical and numerical solution methods. An analogy with dynamical systems is used to present the results in a form reminiscent of Arnol'd tongues, which is found to highlight the effects of different boundary conditions in a succinct manner.

The remainder of this chapter introduces nonlinear buckling phenomena and the development of different solution techniques, with the emphasis on flat plates. It closes with a review of the previous research on mode jumping, background to dynamical systems and an outline of the work presented in this thesis.

1.1 Buckling phenomena

There are a number of textbooks covering the buckling of elastic structures in general (e.g. Timoshenko & Gere, 1961; Allen & Bulson, 1980; Ellinas *et al.*, 1984; Bazant & Cedolin, 1991) and on flat plates in particular (e.g. Timoshenko & Woinowsky-Krieger, 1959; Cox, 1963; Bulson, 1970; Szilard, 1974; Chia, 1980). General nonlinear theory of structural stability, used in the investigation of mode jumping, is covered in more specialized textbooks (see for example Croll & Walker (1972), Supple (1973) and Thompson & Hunt (1973; 1984)). The extensive use of both flat plates and prismatic structures means that their linear and nonlinear behaviour has received widespread attention — the theoretical and experimental research on plate behaviour is summarized by (for example) Walker (1984) and Chou & Rhodes (1997), although mode jumping is not covered in detail.

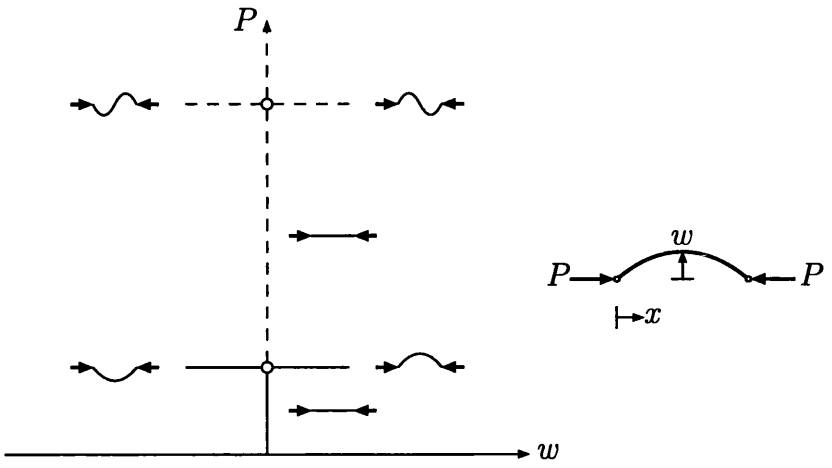

Figure 1.2: Equilibrium paths for the elastica. Stable paths are shown as solid lines and unstable paths as broken lines.

1.1.1 General behaviour

One common simple elastic structure is the axially-compressed strut or "elastica": Euler (1744) showed that non-zero solutions emerge from the flat state at discrete *critical loads*. Fig. 1.2 summarizes this behaviour in a load–deflection diagram, where all possible solutions of the governing equation under changing load form a number of equilibrium paths; the horizontal lines correspond to the first two "modes" for the simply-supported strut (one and two half sine-waves along the length). For the strut free of imperfections, there is equal probability of it buckling with either positive or negative deflection and hence the intersections between paths marking zero (pre-buckling) and non-zero (post-buckling) solutions are called branching or *bifurcation* points.

A similar load–deflection diagram can be constructed for the plate using the critical loads and buckling modes given by the linear equation, derived independently by Kirchhoff (1877) and Love (1892). This equation allows the small deflection response for different loading configurations, such as those shown in Fig. 1.3, to be calculated (Szilard (1974) defines "small" to be less than one-fifth of the plate thickness) — some typical applications are given in the classic textbook by Timoshenko & Gere (1961) and more recently by Allen & Bulson (1980). The

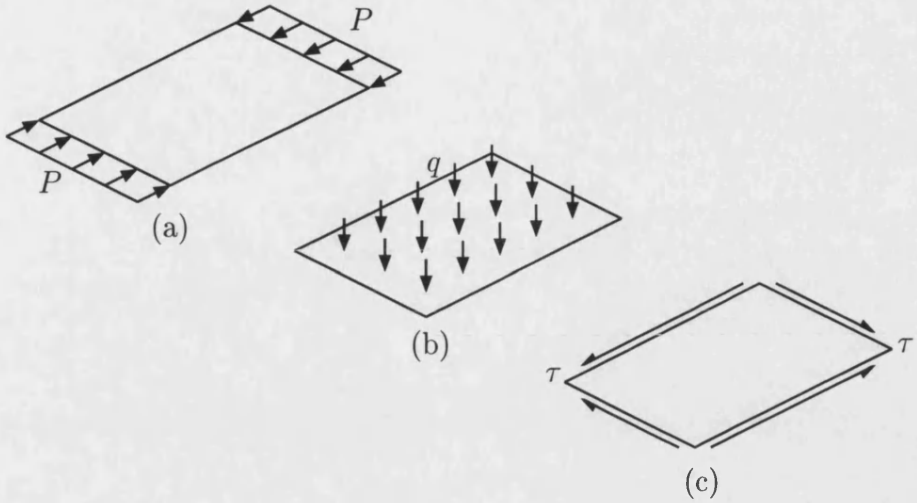

Figure 1.3: Some typical loading configurations; (a) in-plane (axial), (b) transverse and (c) shear.

in-plane boundary conditions are also important: in addition to altering the critical loads, careful selection allows more complex structures to be modelled as a series of flat plates. For example, Falconer & Chapman (1953) approximated each bay of a stiffened panel — used extensively in aircraft structures — as a plate with straight edges and, assuming periodic buckling, calculated the critical loads. A similar approach is used by the eigenvalue solver VICONOPT (Williams *et al.*, 1991) which computes the critical buckling and/or vibration modes of prismatic structures (see Fig. 1.4) and optimizes the geometry for a given set of constraints. Two books on the design of thin plates show further applications of this method for transverse (Aalami & Williams, 1975) and in-plane (Williams & Aalami, 1979) loading.

With interest in the construction of lighter and more efficient structures by aircraft engineers, the ability to utilize the large deflection post-buckling strength of plates became important — to explore this behaviour the more complex von Kármán equations (Foppl, 1907; von Kármán, 1910) have to be used. Exact solutions of these nonlinear equations are only possible with simply-supported boundaries and for a limited number of loading configurations (Levy, 1942). As a result a number of approximate solution methods were developed, many of which are described in detail by Szilard (1974). The lack of any general solution tech-

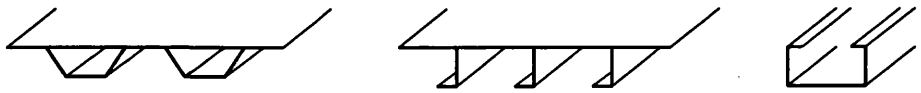

Figure 1.4: Some typical prismatic structures (taken from Anderson *et al.* (1983)).

niques meant that early approximations for the post-buckling of flat plates were based on experimental data. For example the "effective-width" concept (Winter, 1947) equates the nonuniform loading shown in Fig. 1.1 to a constant load acting over a reduced (effective) width. However this simple method assumes that failure occurs when the material yields (von Kármán *et al.*, 1932) rather than earlier in the post-buckling regime.

1.1.2 Analytical solutions

The first general approach for the modelling of nonlinear elastic structures was developed by Koiter (1945) who used the calculus of variations (Craggs, 1973) to minimize the potential energy of the structure, V, where (for the one-dimensional strut problem of Fig. 1.2)

$$V = \int \mathcal{L} \, \mathrm{d}x. \tag{1.1}$$

Here $\mathcal{L}$ is equivalent to the Lagrangian function in dynamical systems and x is the spatial coordinate. Note that this problem is also conservative, i.e. there is no loss of energy — in a dynamical systems context this is referred to as Hamiltonian. The first variations of V give the stationary points which, in turn, can be used to construct equilibrium paths describing the full nonlinear post-buckling behaviour. Koiter's work on struts, cylinders and plates showed that the response of an elastic structure in axial compression depends on the nature of the bifurcation point itself. Subcritical bifurcation leads to instability under conditions of controlled loading, whereas supercritical responses are stable, at least in the initial post-buckling range. The differences in buckle pattern are also significant, especially when the structure can be described as "long" ($x \to \infty$): subcritical responses

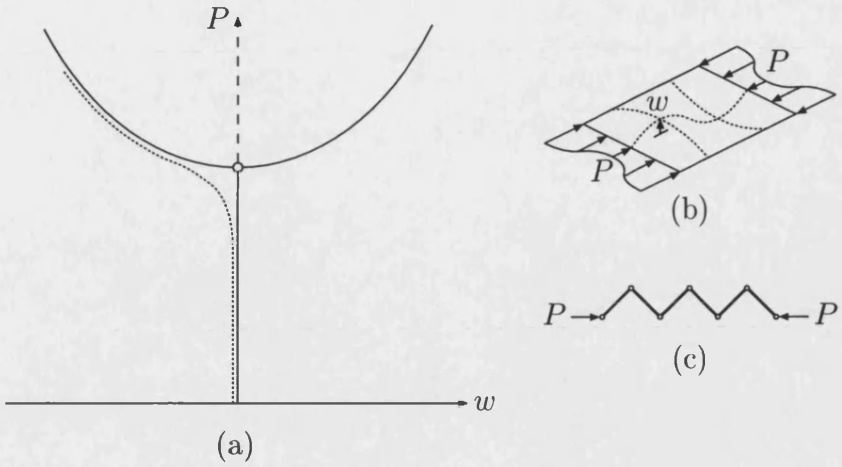

Figure 1.5: (a) Stable (supercritical) post-buckling behaviour. The dotted line shows the result of an added imperfection. (b) Periodic deflection of the axially-compressed plate. (c) Similar response for a link model (see p. 23).

show a tendency to localize while supercritical systems typically oscillate in some periodic or quasi-periodic manner. The thin flat plate considered here falls into the second category. The post-buckling shape is nondevelopable and therefore requires stretching of the mid-plane; this gives a positive post-buckling stiffness allowing increased loads to be supported. In contrast, the deformation of an axially-compressed cylinder (Fig. 1.6(b)) is unstable and there is a loss of stability after buckling. Typical load–deflection plots and buckle patterns for these two structures are sketched in Figs. 1.5 and 1.6 respectively.

Building on the work of Koiter — and in parallel to Sewell (1965; 1970) — Chilver and Thompson developed a general theory and perturbation method for post-buckling analysis, leading to the well known monograph by Thompson & Hunt (1973). The resulting *theory of elastic stability*, in a diagonalized formulation, assumes that the continuous system can be expressed by a series of "modes", with the modes themselves being picked out by linear eigenvalue analysis. For the simply-supported plate shown in Fig. 1.5(b) this gives

$$w = \left(Q_1 \sin \frac{\pi x}{L} + Q_2 \sin \frac{2\pi x}{L} + \cdots + Q_n \sin \frac{n\pi x}{L} \right) \sin \pi y, \qquad (1.2)$$

where w is the out-of-plane deflection. Substituting this modal approximation

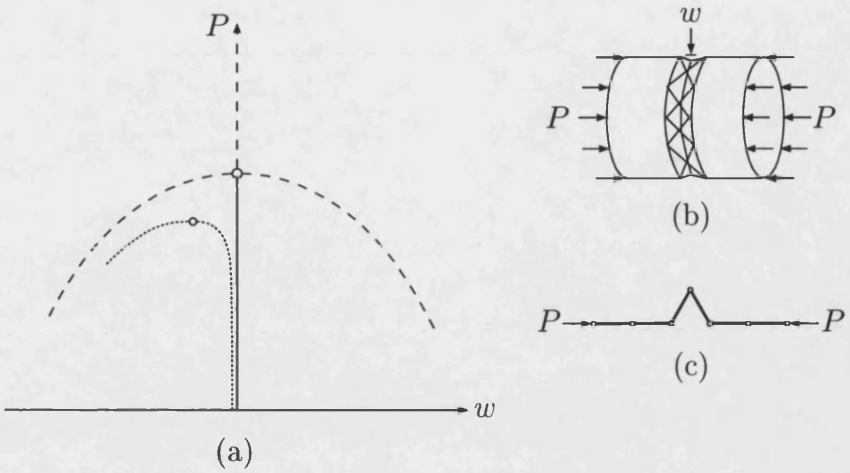

Figure 1.6: (a) Unstable (subcritical) post-buckling behaviour. The dotted line shows the result of an added imperfection. (b) Localized deflection of the axially-compressed cylinder. (c) Similar response for a link model (see p. 23).

into (1.1) and integrating gives an expression of the energy in terms of the amplitudes,

$$V = V(Q_1, Q_2, \ldots, Q_n), \tag{1.3}$$

which can then be used to describe the structural behaviour. Fundamental to this work are two axioms (Thompson & Hunt, 1973): a stationary value of the potential energy (1.3) with respect to *all* the generalized coordinates is necessary and sufficient for equilibrium; a relative minimum of the potential energy, again with respect to all the coordinates, is necessary and sufficient for stability of the equilibrium state.

Both these axioms are needed for the investigation of mode jumping. The first is used to generate the equilibrium paths — Fig. 1.5(a) illustrates the path for buckling into two half-waves, but paths corresponding to one, three and four half-waves etc. can also be plotted. These are called *uncoupled* paths as they consist primarily of a single mode. Solutions consisting of a mixture of buckle patterns can also be found: it is these *coupled* solutions which indicate the possibility of mode jumping. The second axiom can be used to show that the change in stability of a equilibrium path always coincides with either a limit point or

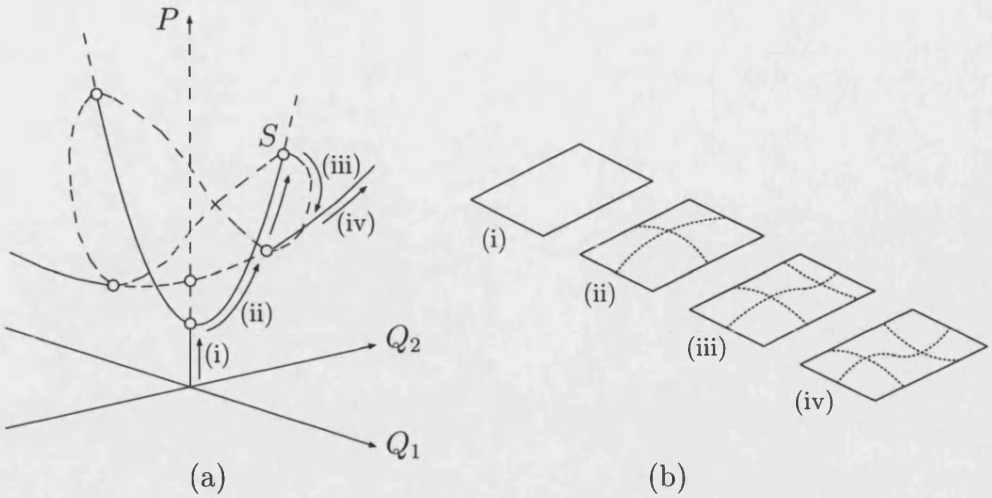

Figure 1.7: (a) Coupled solution paths (after Supple (1967)). Q_1 and Q_2 are the amplitudes of the one and two half-wave deflections respectively. (b) Buckle patterns; (i) pre-buckling, (ii) one half-wave, (iii) coupled and (iv) two half-waves.

the crossing of another path at a bifurcation point (Thompson & Hunt, 1973). Therefore the intersection of uncoupled and coupled paths is associated with the vanishing of a second derivative of V (Thompson & Hunt, 1984). Supple (1967) classified the coupled behaviour of any general two degree-of-freedom (d.o.f.) system ($Q_3 = \cdots = Q_n = 0$) according to the coefficients of the variables Q_1 and Q_2 in (1.3). In addition, by plotting the amplitudes of the two competing modes on separate axes, the coupled solution paths can be visualized in these dimensions for different structures; Fig. 1.7(a) shows a general form of the behaviour for a doubly-symmetric system such as the plate (Supple, 1970), with the corresponding buckle patterns sketched in Fig. 1.7(b). The lower uncoupled path (ii) loses stability at the *secondary bifurcation point* — where the uncoupled and coupled paths intersect (labelled S in Fig. 1.7(a)) — and hence mode jumping occurs. Solutions lying on the stable uncoupled path, with simply-supported boundary conditions, could also be called *mode locked*; i.e. the number of half-waves along the length of the plate remains constant. The limit of this mode locking is marked by the secondary bifurcation point.

Interest at this time was focused on unstable systems (Chilver, 1967; Supple, 1968; Thompson & Supple, 1973) where mode interactions and imperfections have

a greater impact on behaviour. The dotted line of Fig. 1.5 shows that despite the presence of an imperfection, introduced here as an initial out-of-flatness, the plate retains its stability. On the other hand, for the cylinder (Fig. 1.6) a relatively small imperfection can lead to a considerable loss of load carrying capability (Thompson & Hunt, 1973). The examination and portrayal of imperfections is also a central facet of *catastrophe theory* (Poston & Stewart, 1978); for example, the effects of certain additional transverse loads at a *compound bifurcation point* (where the critical loads for two different modes coincide) are described by the unfolding of a double cusp catastrophe (Magnus & Poston, 1977).

The two d.o.f. approximation studied by Supple highlights the coupled behaviour of nonlinear structures. However it is inevitable that interaction with other modes will occur for large deflections, further complicating the post-buckling response. Techniques such as the Lyapunov–Schmidt reduction (Golubitsky & Schaeffer, 1984), and the equivalent *elimination of passive coordinates* (Thompson & Hunt, 1984), allow high d.o.f. systems to be rewritten in terms of the major modes of interest, and hence enable a more rigorous analysis of the coupled behaviour.

Link models can also be analyzed using this theory. Constructed from just two basic elements — rotating rigid bodies and springs — their inherently simple behaviour allows the underlying response of nonlinear structures to be illustrated in an uncomplicated manner. For example, link models as shown in Figs. 1.5(c) and 1.6(c) have been used to highlight the differences between the periodic and localized responses of supercritical and subcritical systems respectively (Hunt *et al.*, 1989). In addition, Stein (1959a) used the three-link strut shown in Fig. 1.8(a) as a simplified model of the plate, with the stiffening nonlinear springs giving the system a supercritical post-buckling response. Stationary points of the system's potential energy — derived in terms of the amplitudes Q_1 and Q_2 — predict a mode jump from a symmetric ($Q_1 = Q_2$) to an antisymmetric ($Q_1 = -Q_2$) buckle pattern, shown in Figs. 1.8(a) and (b) respectively.

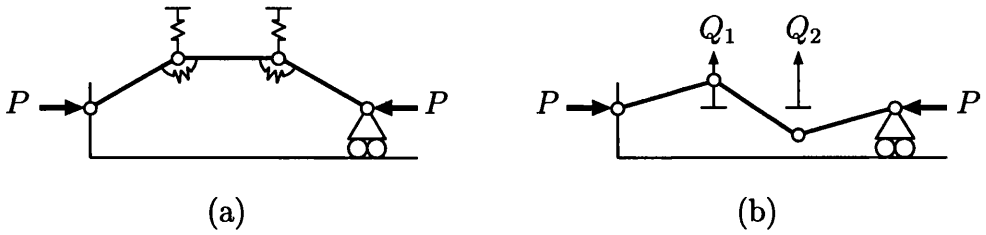

(a) (b)

Figure 1.8: Link model showing deflection patterns (a) before and (b) after mode jumping (after Stein (1959a)). Springs have been omitted from (b) for clarity.

1.1.3 Modal analysis

Unfortunately the modal techniques discussed above are only suitable for investigating the coupled behaviour of simply-supported plates. These boundary conditions are special in that the solutions are periodic (Fig. 1.9(a)) and can be approximated by a small number of modes — Supple (1970) suggests that a single mode portrayal is accurate up to about two-and-a-half times the critical load. For clamped boundaries there is a modulation of the buckle pattern (Fig. 1.9(b)), with amplitude decreasing towards the ends of the plate. In the post-buckling regime this response can only be approximated accurately by using a large number of modes. Uncoupled solutions can be found by using computers to calculate the amplitudes Q_1, Q_2 etc. (Yamaki, 1959; Yamaki, 1960) — an extreme example is provided by Watson (1998) who extrapolates to an infinite number of modes when finding the critical loads for clamped plates. Alternatively, multi-scale analysis attempts to overcome this limitation by assuming that the deflection is influenced by differing length scales, with the behaviour of Fig. 1.9(b) being approximated by a single periodic wave modulated by an overall amplitude variation (Potier-Ferry, 1983). However this approach is restricted to the initial post-buckling behaviour (Wadee *et al.*, 1997) and cannot locate secondary bifurcation points.

1.1.4 Numerical methods

The suitability of computers for repetitive and time consuming calculations has enabled techniques such as finite difference, finite element and stiffness-matrix

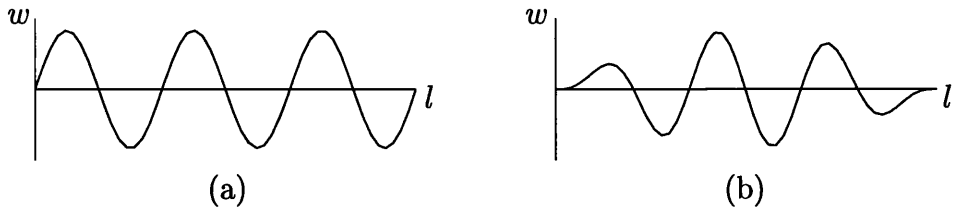

(a) (b)

Figure 1.9: Initial buckle pattern along the centreline of the plate; (a) simply-supported and (b) clamped boundary conditions.

methods to be implemented for high d.o.f. systems; early work was conducted at Cambridge, Imperial College and Swansea (see for example Dwight & Ratcliffe (1969), Williams & Walker (1975) and Zienkiewicz (1977) respectively). However, although the general approach of commercially available finite element programs — such as ANSYS (Swanson Analysis Systems, 1992) and ABAQUS (Hibbitt, Karlsson & Sorensen, 1997) — allows almost any structural geometry and the full range of boundary conditions to be modelled, these "black-box" codes may miss the solutions of practical significance as they can have difficulty coping with the inherent multiplicity of paths. More specialized programs, the boundary value solver AUTO (Doedel *et al.*, 1995) for example, are well suited to this type of problem: in addition to following solution paths under the parametric variation of (say) load, bifurcation points are located numerically (Seydel, 1994) allowing the full post-buckling behaviour to be explored. However AUTO solves ordinary differential equations and is therefore not obviously suitable for the two-dimensional (partial differential equation) plate and cylinder problems. Recent work (Riks *et al.*, 1996; Gervais *et al.*, 1997) has shown that the algorithms used in AUTO can also be applied to these 2D problems, although the resulting programs are relatively slow.

1.2 Mode interactions

The destabilizing effect of mode interactions in (for example) stiffened plates in the late 1960's and early 1970's (Murray, 1973) is now well known, having been highlighted for instance by the large failure rate of box girder bridges; this

prompted the testing of flat plates with various boundary conditions at Imperial College (Harding & Hobbs, 1979) and a revision of the bridge design code (Dowling *et al.*, 1988). Therefore the ability to deal with complex nonlinear interactions which lead to a loss of stability is very important.

The linear eigenvalue solver VICONOPT (Williams *et al.*, 1991) is currently being developed to include the nonlinear post-buckling behaviour of prismatic structures (Fig. 1.4) (Powell *et al.*, 1998); the phenomenon of mode jumping in flat plates, as explored here, may provide a good method for validating any predictions of coupled behaviour.

1.2.1 Mode jumping

The earliest work investigating the phenomena of mode jumping was by Stein (1959a; 1959b): in addition to the link model described above, a physical experiment showed multiple mode jumps — from 5 to 6 to 7 to 8 half-waves along the length — in an aluminium panel. Theoretical work which followed used analytical methods encompassed by the theory of elastic stability (Thompson & Hunt, 1973), while more recently numerical methods have predominated.

A wide range of boundary conditions have been covered in the last forty years, including various combinations of simply-supported and clamped long and short edges in conjunction with a number of in-plane constraints. The three most common constraints are shown in Figs. 1.10(a), (b) and (c): these are termed "free-edged", "straight-edged" and "clamped in-plane" respectively. In addition, a number of papers (Matkowsky & Putnick, 1974; Matkowsky *et al.*, 1980; Holder & Schaeffer, 1984) approach the problem from a mathematical viewpoint and use boundary conditions which are hard to interpret physically. With such a wide variety of possible boundary conditions, and the need to cover systems of all lengths, it is perhaps not surprising that (in general) only specific cases of mode jumping are given in the literature. With the added complication of the variety

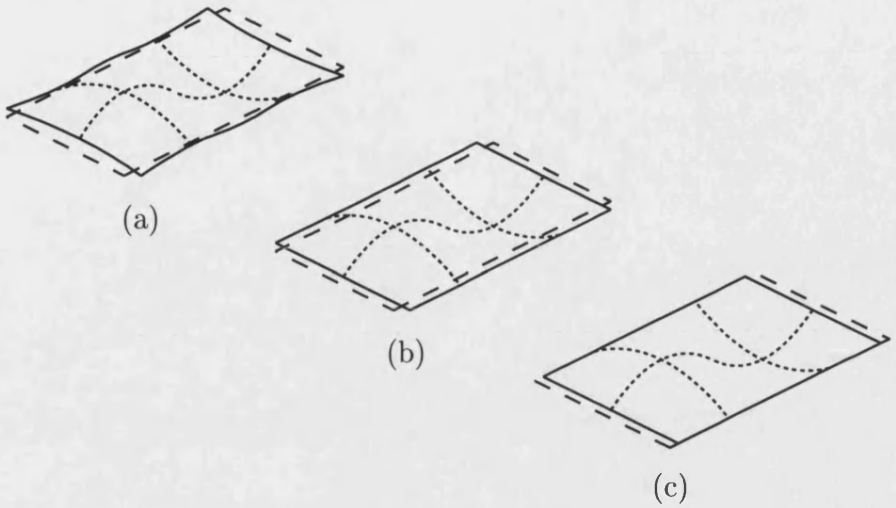

Figure 1.10: Simply supported plate with; (a) edges free to move, (b) all edges held straight and (c) long edges held rigidly apart. Broken lines show unloaded plate. Solid lines show (exaggerated) post-buckling shape.

of different solution methods — experimental, analytical and numerical — even giving qualitative conclusions on the effects of the boundary conditions is difficult, especially as there are often conflicting predictions of whether mode jumping will or will not occur.

However, for the same boundary conditions and in-plane constraints, apparently differing results can usually be attributed to the accuracy or otherwise of the solution method. For example, both two (Sharman & Humpherson, 1968; Supple, 1970; Wicks, 1988) and four (Uemura & Byon, 1977) d.o.f. modal approaches predict mode jumping in simply-supported plates for a number of discrete lengths. Maaskant & Roorda (1992) use a two d.o.f. approximation to cover a continuous range of lengths — however mode jumping is only predicted for a subset of the cases considered. In contrast, Nakamura & Uetani (1979) used previous work on the supercritical strut (Uetani, 1974) to develop a twenty term approximation of the deflected shape, such that it might be assumed that the effects of all significant contaminating modes were included. This comprehensive study of simply-supported plates clearly shows that mode jumping occurs in plates with either straight-edged or clamped in-plane constraints over the full range of aspect ratios considered (1.4–8). The secondary buckling loads are dependent on the

plate length and form a "saw-tooth" pattern (see Fig. 3.8, p. 81) — maximum values occur at lengths just to the right of the *compound bifurcation points* (where the critical loads for two different modes coincide) and decrease with increasing length until the next compound point is reached; here there is a step increase in load and the cycle repeats. Comparing the results for the clamped in-plane and straight-edged cases shows that mode jumping occurs at much higher amplitudes (and loads) for the latter and hence the destabilizing effects of passive modes are by this stage more significant.

Stoll (1994) uses a twelve d.o.f. model to predict mode jumping in a plate of aspect ratio 5.38:1 with either simply-supported or clamped short edges; in this instance the clamped case has the lesser post-buckling stability. Using analytical methods with clamped boundary conditions is unusual — the modulation of the buckle pattern (Fig. 1.9) means that these solutions are typically less accurate than for the simply-supported case. Numerical methods are more commonly used as they should give "near-exact" solutions for the deflected shape. However, finite element methods are relatively slow and mode jumping is only predicted for the individual cases considered (Uemura & Byon, 1978; Carnoy & Hughes, 1983). Riks *et al.* (1996) and Gervais *et al.* (1997) both present sophisticated finite element codes which track solution paths and log bifurcation points. Riks *et al.* (1996) compares results with experiments (see below), while Gervais *et al.* (1997) considers three sets of boundary conditions for a free-edged plate (Fig. 1.10(a)): all edges simply-supported; long edges simply-supported, short edges clamped; and all edges clamped. Mode jumping only occurs in the latter two cases — unfortunately direct comparison between these results is not possible as three different lengths are used. Secondary buckling loads for simply-supported plates have been calculated over a wide range of lengths (Nakamura & Uetani, 1979); there is no equivalent study with clamped boundary conditions and so the effect of length, especially near compound bifurcation points, cannot be determined. The work by Nakamura & Uetani (1979) and Gervais *et al.* (1997) also shows that the position of the compound bifurcation points, where the minimum secondary

buckling loads occur, are dependent on the boundary conditions. Therefore, qualitative comparisons between different boundary conditions will require a spread of results for each case.

A number of researchers have attempted quantitative validation of theoretical methods by comparing results with physical experiments. However comparisons (Schaeffer & Golubitsky, 1979; Stoll, 1994; Riks *et al.*, 1996) with the experiment by Stein (1959b) — effectively a straight-edged aluminium plate with simply-supported long edges and clamped short edges — and plates with either four simply-supported (Sharman & Humpherson, 1968; Johnson, 1990) or four clamped boundaries (Uemura & Byon, 1978; Carnoy & Hughes, 1983) are inconclusive. This is possibly explained by the difficulties in achieving the perfect simple or clamped support under experimental conditions, which are the easiest to implement theoretically. (This difficulty is highlighted by the photographs of experimental work on sandwich structures by Wadee (1999) for example.) Alternatively, Johnson (1990) suggests that initial imperfections may contribute to the poor agreement: it is well known from theoretical work (see for example Stoll, 1994) that the presence of small imperfections can lead to a significant drop in the secondary buckling load. Interestingly, the presence of a large imperfection may eliminate the phenomenon of mode jumping, the lack of bifurcation points leading to a complete smoothing of the loading path. Flexural boundary conditions falling between the extremes of simply-supported and clamped (Rhodes & Harvey, 1971) and constraints varying between straight-edged and clamped in-plane (Maaskant & Roorda, 1992) — which may be more representative of physical experiments — have not been studied in detail.

Other papers (Bauer & Reiss, 1965; Stroebel & Warner, 1973; Sridharan, 1983; Suchy *et al.*, 1985; Chien, 1989; Chien & Chen, 1997; Ikeda & Nakazawa, 1998) consider the problem of mode jumping in plates for individual cases, although they do not add anything new. Mode jumping has also been noted with other loading conditions: simultaneous axial and transverse loading (Levy *et al.*, 1944); a combination of bending and shear (Nakazawa *et al.*, 1993); axial loading with a

foundation (Cheng & Shang, 1997); and in laminated anisotropic plates (Jensen & Lagrac, 1988; Romeo & Frulla, 1994).

The supercritical response of the elastic strut supported by a nonlinear stiffening elastic foundation (Hui & Hansen, 1980; Potier-Ferry, 1983; Johnson, 1990) can be usefully allied to the axially-compressed flat plate. Surprisingly, despite being easier to solve, mode jumping in this one-dimensional model has only received isolated attention (Stein, 1959a; Uetani, 1974; Wu, 1993). The phenomenon of mode jumping has also been seen in axially-compressed cylinders (Yamaki, 1984; Riks *et al.*, 1996); unlike the plate where the number of half-waves increases in the direction of loading, here there is a *decrease* in the number of *circumferential* waves.

A number of general conclusions can be drawn from this work: when using a modal approach it is important to include the effects of contaminating modes; the secondary buckling load is very sensitive to the in-plane constraints, decreasing as movement is increasingly restrained; and plates with clamped short edges have less post-buckling stability than the simply-supported case, at least near a compound bifurcation point. The last two conclusions are, at best, only qualitative, the lack of a comprehensive study of all the various boundary conditions for a significant range of lengths meaning that their effects cannot be quantitatively evaluated.

1.3 Dynamical systems

Dynamical systems describe how systems evolve in time (a wide variety of examples are discussed by Thompson & Stewart, 1986) and hence their relevance to the static behaviour of elastic structures may not be immediately obvious. Take for example the unforced, undamped pendulum shown in Fig. 1.11(a). The amplitude of the large rotation θ at time t is described by the scaled nonlinear

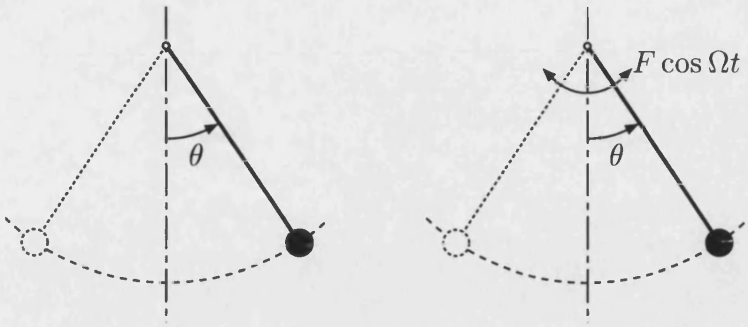

(a) (b)

Figure 1.11: (a) Unforced and (b) forced pendulum undergoing large deflections.

ordinary differential equation (ODE),

$$\frac{\mathrm{d}^2\theta}{\mathrm{d}t^2} + \sin\theta = 0. \tag{1.4}$$

The behaviour of the elastica (Fig. 1.2) is governed by the same nonlinear ODE, except that solutions vary in space (x) rather than time (t) (see for example Champneys *et al.*, 1997). Therefore much can be learned by treating spatial boundary value problems as though they were nonlinear initial value problems running in time. The understanding of subcritical behaviour has been further advanced by this analogy, with the localized response of the subcritical strut described by a homoclinic solution from the flat state to itself (Hunt & Wadee, 1991). Similarly, the phenomenon of mode jumping in supercritical structures can be linked to *mode locking* in nonlinear dynamical systems: if the pendulum is subjected to periodic forcing (Fig. 1.11(b)) then, depending on the amplitude of forcing and the ratio of the natural and forcing frequencies, it can exhibit either periodic (locking onto a integer multiple of the forcing frequency), quasi-periodic or chaotic behaviour. In numerical experiments, true quasi-periodic and chaotic responses cannot be seen because all real numbers are stored as a finite number of digits.

(a) (b) (c)

Figure 1.12: Poincaré map showing iterates 1000–1050 of (1.5) for $k = 1$ and (a) $\Omega = 0.35$, (b) $\Omega = 0.32$, (c) $\Omega = 0.29$.

1.3.1 Discrete dynamical systems

This behaviour is perhaps best illustrated with a discrete dynamical system (Sandefur, 1990). In contrast to dynamical systems like the pendulum which vary continuously, *discrete* systems are used to study quantities which only change at discrete points in time. The position (ω) of a nonlinear forced oscillator (Thompson & Stewart, 1986, p. 285) at the time-step $n + 1$ is given by

$$\omega_{n+1} = \omega_n + 2\pi\Omega + k \sin \omega_n, \tag{1.5}$$

where ω_n is the current position, Ω the ratio of the natural and forcing frequencies and k the amplitude of the nonlinearity. Plotting $\sin\omega$ against $\cos\omega$ gives a Poincaré map (in this case a circle map); Fig. 1.12 shows 50 iterations of (1.5) for three different values of Ω. (The first 1000 iterations are not plotted to eliminate any transient effects.) Figs. 1.12(a) and (c) show that the behaviour repeats every third and fourth iteration when $\Omega = 0.35$ and $\Omega = 0.29$ respectively, indicating that the response is periodic. However, when Ω is 0.32, the scattering of points of Fig. 1.12(b) indicates that the response is probably either quasi-periodic or chaotic, although in theory it could be periodic. Presenting the information in this manner is impractical as each only shows the behaviour for one value of Ω and k — in effect it is equivalent to Fig. 1.7(a) which shows the interaction between two specific modes at one particular length. An Arnol'd tongues plot (Arnol'd, 1965) summarizes mode locking in the forced oscillator for all values of

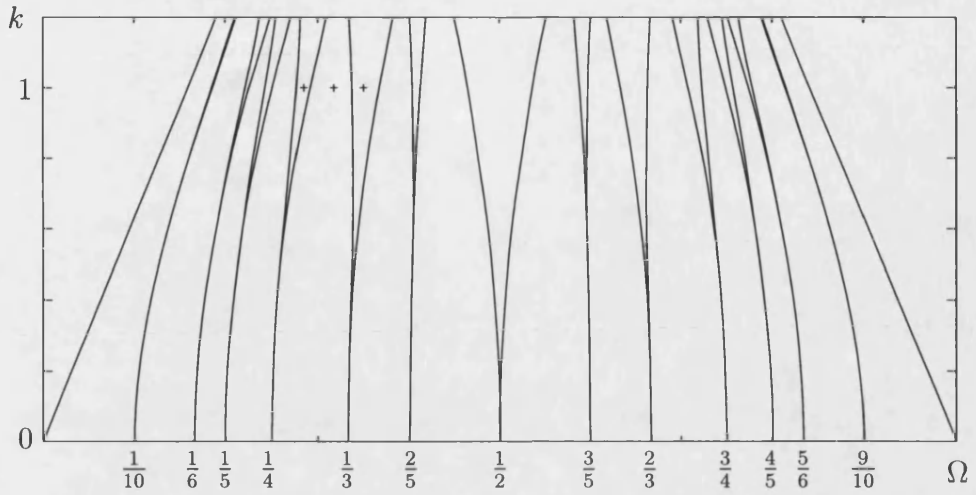

Figure 1.13: Arnol'd tongues for (1.5). The three crosses relate to the cases plotted in Fig. 1.12.

Ω and k: in the present thesis this same idea is used to show all mode interactions for all plate or strut lengths.

1.3.2 Arnol'd tongues

The mode locked behaviour of the forced oscillator can be determined from the steady-state frequency ratio $\bar{\Omega}$ (Hilborn, 1994), where

$$\bar{\Omega} = \lim_{n\to\infty} \frac{\omega_n + 2\pi\Omega + k\sin(\omega_n) - \omega_0}{2\pi n}. \tag{1.6}$$

If $\bar{\Omega}$ is rational then the solution will repeat after an integer number of time-steps, indicating that the behaviour is mode locked, while an irrational value implies a quasi-periodic or chaotic response. These values of $\bar{\Omega}$ can be used to construct an Arnol'd tongues plot — the cusp-shaped loci of Fig. 1.13 mark the positions of saddle node bifurcations in the parameter space of the ratio of the natural to forcing frequencies and the amplitude of the nonlinearity. Mode locked solutions lie within the tongues, and therefore the tips meet the real line at the positions of the rational numbers; quasi-periodic behaviour occurs in the regions outside the tongues. The three crosses plotted in Fig. 1.13 correspond to the examples shown

in Fig. 1.12; the two periodic solutions lie inside tongues and the quasi-periodic one lies outside. The ratio where the tongue meets the Ω axis gives the period — for the examples shown $\Omega = \frac{1}{3}$ and $\Omega = \frac{1}{4}$ indicate repetition after 3 and 4 time-steps respectively, confirmed by Figs. 1.12(a) and (c). Above $k = 1$ the tongues can cross leading to complex behaviour and a chaotic response (Thompson & Stewart, 1986).

Arnol'd tongues have been used in a diverse range of physical problems: frequency locking in lasers (Winful *et al.*, 1986); the mixing of chemicals in a tank reactor (Pugh *et al.*, 1986); predator-prey models in biology (Kot *et al.*, 1992); nonlinear digital filters (Galias, 1995); and Josephson junction arrays (Das *et al.*, 1996) for example. Although not always strictly Arnol'd tongues, all share two common features — a ratio of two frequencies plotted against a nondimensional amplitude and tongues which meet the frequency axis at rational positions. However, problems more closely related to mode jumping in the plate are the strut subjected to periodic forcing (Timoshenko & Gere, 1961) and the inverted pendulum (Acheson, 1993), both of which can be reduced to the Mathieu equation (Jordan & Smith, 1987). Mode locking for these systems occurs *outside* the tongues: this is opposite to the example above which is summarized in Fig. 1.13. For the strut and plate problems the cusps mark the locus of the secondary bifurcation points under changing length, and therefore regions outside the tongues relate to locking onto the uncoupled solution (see Fig. 1.7(a)). In addition to giving the limit of stability, the tongue representation also gives the ratio between the two natural frequencies (or wavelengths) of the interacting modes.

1.4 Thesis outline

Mode jumping has been predicted and observed for a variety of different loading conditions: here, to allow a wide range of boundary conditions to be considered, interest is restricted to the most common case of in-plane loading (Fig. 1.3(a)).

This also enables the strut on a stiffening elastic foundation to be used as a heuristic model for the plate; results presented in this thesis show clear similarities between the two systems. No new experimental data is presented in this thesis to validate the theoretical results: instead, existing models — whose derivation is given in the next chapter — are used to investigate the effects of boundary conditions in isolation from those due to imperfections.

1.4.1 Simply-supported strut

Mode jumping in the relatively straightforward strut model is presented in Chapter 3. Restriction to simply-supported boundaries allows the problem to be approached from two perspectives: the classical theory of elastic stability (Thompson & Hunt, 1973) and the modern numerical continuation code AUTO (Doedel *et al.*, 1995). The modal approach is used to find the secondary buckling loads, while comparisons with numerical results highlight the dominant contaminating modes. In addition, the analogy with mode locking in dynamical systems is introduced, showing how the secondary bifurcation points for all pairs of interacting modes at all lengths are described by an Arnol'd tongues plot (Hunt & Everall, 1999).

1.4.2 Simply-supported plate

The work on mode jumping reviewed above highlights the advantages and disadvantages of the two main solution methods: the analytical approach allows a wide range of results to be generated relatively quickly, but it is effectively restricted to simply-supported boundary conditions; numerical solutions are more accurate for the full range of boundary conditions but are more time consuming. Here a third approach is also used. The von Kármán equations are reduced to a series of ODEs using the Galerkin procedure and solved with AUTO. Solutions by this method — previously used for the axially-compressed cylinder (Lord *et al.*,

1997) — are compared with the full analytical and numerical solutions. The post-buckling behaviour for two sets of in-plane boundary conditions is again summarized using Arnol'd tongues. Finally, AUTO is used to explore the coupled behaviour in detail (Everall & Hunt, 1999a).

1.4.3 Effects of the boundary conditions

This new contribution is completed in Chapter 5, where a wide range of both flexural and in-plane boundary conditions are investigated. Presentation of the results in a consistent manner allows easy comparisons to be made, with changes in boundary conditions mirrored by changes in the shape of the Arnol'd tongues. The full range of flexural boundary conditions is considered for the strut, including those lying between the extremes of simply-supported and clamped (Everall & Hunt, 1999b; Everall, 1999); in the plate problem, four combinations of simply-supported and clamped boundaries are considered in conjunction with two sets of in-plane constraints (Everall & Hunt, 1999c; Everall & Hunt, 1999d).

1.4.4 Conclusions and further work

Chapter 6 draws the thesis to a close by summarizing the results and their possible implications for practical applications. A number of possible extensions to this work are also discussed.

Chapter 2

Governing equations

The thin elastic plate undergoing large lateral displacements is a classical problem with the roots dating back to von Kármán (1910) and beyond. The assumption of "thin" plates allows the theory of simple bending and plane stress to be used, removing any dependence on the z coordinate of a three-dimensional reference frame (see Fig. 2.4, p. 44) and thus simplifying the governing equations (generally known as the von Kármán large deflection equations). Obviously this formulation does not apply to all practical situations, and hence a number of alternative plate models have been developed for a variety of different geometries and materials. However in general these systems are more complex; the behaviour of "thick" plates for example is dependent on x, y and z (Reissner, 1947; Mindlin, 1951) and hence the equations are time-consuming to solve. Similarly, composite materials and laminated (layered) plates — commonly used where weight is important — introduce two further complications; anisotropic materials (whose properties are different in different directions) and compatibility between the different layers (see for example Szilard, 1974).

Mode jumping has been observed experimentally in composite and laminated plates (Jensen & Lagrac, 1988; Romeo & Frulla, 1994); however the complexity of the equations means that prediction of coupled behaviour either analytically or

numerically would be difficult. Therefore — as with the majority of the research discussed in the previous chapter — mode jumping in thin isotropic plates is considered here. The relative simplicity of the von Kármán equations means that the post-buckling stability can be compared for a wide range of boundary conditions (Fig. 1.10) and all plate lengths.

Although these equations only describe the *elastic* behaviour, the applied load to cause yielding (plastic behaviour) in thin plates is estimated (von Kármán *et al.*, 1932) to be several times the critical load (P^{C}). This is supported by experimental results (Stein, 1959b) where transition from elastic to plastic behaviour was observed at $2P^{C}$ for a plate with a width-to-thickness ratio of approximately 65 — more importantly this transition occurred *after* the first mode jump. It is therefore reasonable to assume that the post-buckling response remains in the elastic regime. In addition, the elastic behaviour of the strut conserves energy and so when the load is removed the system returns to the original flat state. If plastic deformation was included there would be dissipation of energy and the system would be nonconservative.

Two alternative but complementary formulations are used, the energy integral and the von Kármán equations; in this treatment the former is found more useful for analytical methods and the latter for numerical techniques. Both these representations are derived in detail in a number of textbooks (see for example Timoshenko & Gere (1961), Bulson (1970) and Szilard (1974)). Here the derivation of the total potential energy is outlined for the supercritical strut and plate in the next section: application of the calculus of variations is then used to convert these energy integrals into the equivalent differential equations.

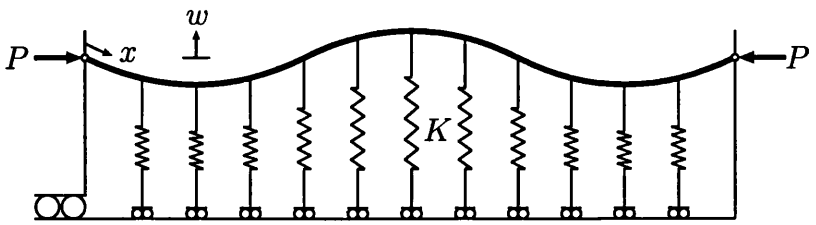

Figure 2.1: Strut on an elastic foundation.

2.1 Total potential energy

2.1.1 Axially-compressed strut

The total potential energy (V) for an incompressible elastic strut of length L ($0 < x < L$), compressed by an axial load P (which retains its magnitude and direction as the strut deflects) and supported by an elastic foundation — as shown in Fig. 2.1 — is the summation of three components: the energy required to bend the strut (U_b); the energy stored in the foundation (U_f); and the work done by the load (U_l). Substituting into Koiter's expression (1.1) gives

$$V = \int_0^L \mathcal{L}\, \mathrm{d}x = U_b + U_f - U_l. \tag{2.1}$$

The final term (U_l) is subtracted because it represents external work done rather than energy stored in the system.

The strut is incompressible and therefore the overall length will remain constant. However the action of bending will cause equal and opposite compressive and tensile stresses (see Fig. 2.2(a)) to occur at positions either side of the centreline (the neutral axis). The change in bending energy for a small element of length $\mathrm{d}x$, due to the applied moment M causing a rotation $\mathrm{d}\theta$, is given by

$$\mathrm{d}U_b = \frac{1}{2} M \mathrm{d}\theta. \tag{2.2}$$

By taking rotational equilibrium about A in Fig. 2.2 and rearranging, the moment

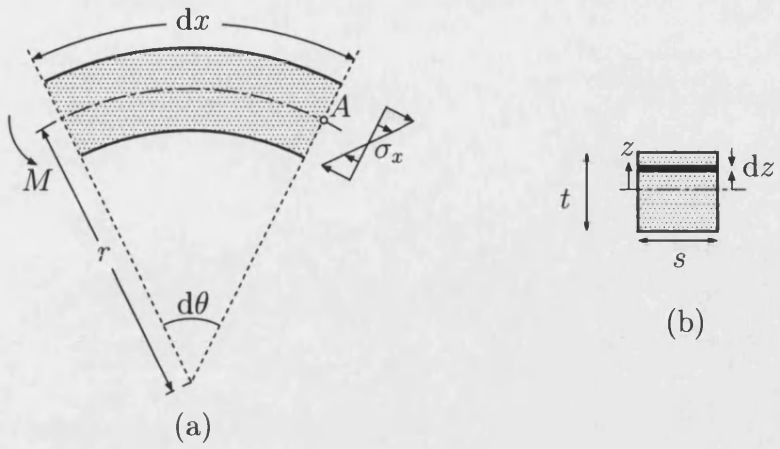

Figure 2.2: (a) Strut in bending. (b) Cross-section of the strut.

M can be expressed in terms of a stress distribution

$$M = \int_{-t/2}^{t/2} \sigma_x b z \, \mathrm{d}z. \tag{2.3}$$

(Note that bending out of the x-z plane is assumed to be absent.) Using the assumption that plane sections remain plane and perpendicular to the neutral axis, the strain ε_x at a distance z from the centreline is

$$\varepsilon_x = \frac{r\mathrm{d}\theta - (r-z)\mathrm{d}\theta}{r\mathrm{d}\theta} = \frac{z}{r}. \tag{2.4}$$

This assumption is only valid if both the depth d and the angle $\mathrm{d}\theta$ are "small", and is similarly relevant to the plate problem. The maximum allowable thickness (depth) is generally limited to one-tenth of the plate width (Szilard, 1974) — in practice the ratio is usually much smaller (Stein, 1959b; Watson, 1998) and thus it is not a significant limitation. Therefore although deflections may be several times the plate thickness, they are negligible in comparison to the length and hence the corresponding angles are also moderately small.

Considering for the moment a two-dimensional plate, the assumption of plane stress,

$$\sigma_z = 0, \quad \tau_{xz} = 0, \quad \tau_{yz} = 0, \tag{2.5}$$

and isotropic materials give the following Hooke's law stress-strain relationships (Timoshenko & Goodier, 1970),

$$\varepsilon_x = \frac{1}{E}(\sigma_x - \nu\sigma_y), \quad \varepsilon_y = \frac{1}{E}(\sigma_y - \nu\sigma_x), \quad \gamma_{xy} = \frac{1}{G}\tau_{xy} = \frac{2}{E}(1+\nu)\tau_{xy}, \quad (2.6)$$

where E is Young's modulus and ν is Poisson's ratio. Direct stress and strain are denoted by σ and ε and shear stress and shear strain by τ and γ: subscripts refer to the assumed Cartesian coordinate system. Rearranging gives

$$\sigma_x = \frac{E}{1-\nu^2}(\varepsilon_x + \nu\varepsilon_y), \quad \sigma_y = \frac{E}{1-\nu^2}(\varepsilon_y + \nu\varepsilon_x), \quad \tau_{xy} = \frac{E}{2(1+\nu)}\gamma_{xy}. \quad (2.7)$$

For the one-dimensional incompressible strut, σ_y and τ_{xy} in (2.6) are zero and hence the expression for σ_x reduces to

$$\sigma_x = E\varepsilon_x. \quad (2.8)$$

Using this expression to substitute strain (2.4) for stress in (2.3) gives

$$M = Eb\int_{-t/2}^{t/2}\left(\frac{z}{r}\right)z\,\mathrm{d}z = \frac{1}{r}E\frac{st^3}{12} = \frac{1}{r}EI, \quad (2.9)$$

where I is the second moment of area (more commonly written as $\frac{bd^3}{12}$). Combining the approximation for small angles (see Fig. 2.3)

$$\theta \approx \frac{\mathrm{d}w}{\mathrm{d}x} \Rightarrow \frac{\mathrm{d}\theta}{\mathrm{d}x} \approx \frac{\mathrm{d}^2w}{\mathrm{d}x^2} \quad (2.10)$$

with the expression for arc-length ($\mathrm{d}x = r\mathrm{d}\theta$) gives the radius r in terms of the vertical displacement w,

$$\frac{1}{r} = \frac{\mathrm{d}\theta}{\mathrm{d}x} \approx \frac{\mathrm{d}^2w}{\mathrm{d}x^2}. \quad (2.11)$$

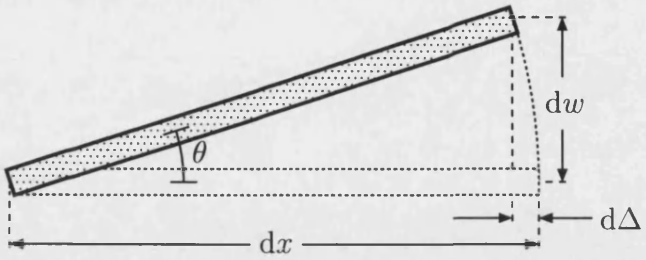

Figure 2.3: End-shortening.

Equations (2.2), (2.9) and (2.11) give

$$\mathrm{d}U_b = \frac{1}{2}M\mathrm{d}\theta = \frac{1}{2}\frac{1}{r}EI\mathrm{d}\theta = \frac{1}{2}EI\frac{\mathrm{d}^2w}{\mathrm{d}x^2}\mathrm{d}\theta = \frac{1}{2}EI\frac{\mathrm{d}^2w}{\mathrm{d}x^2}\frac{\mathrm{d}\theta}{\mathrm{d}x}\mathrm{d}x, \tag{2.12}$$

and a further substitution for θ (2.10) yields the bending energy for an element of length $\mathrm{d}x$;

$$\mathrm{d}U_b = \frac{1}{2}EI\left(\frac{\mathrm{d}^2w}{\mathrm{d}x^2}\right)^2\mathrm{d}x. \tag{2.13}$$

The deviation of the strut from the initial flat state causes the foundation to be either stretched or squashed. For convenience Fig. 2.1 shows a strut supported by a finite number of springs; in practice a continuous elastic foundation providing a force $Kw + Cw^3$ per-unit-length is used. The nonlinear component (Cw^3) is included to give a stable post-buckling response and provide a heuristic model for the plate. A cubic nonlinearity is chosen so that the resulting energy function carries a fundamental symmetry — containing only even powers of w — so positive and negative deflections, $w(x)$ and $-w(x)$, have the same energy. The energy stored in a foundation of length $\mathrm{d}x$ due to a deflection w is

$$\mathrm{d}U_f = \mathrm{d}x\int\left(Kw + Cw^3\right)\mathrm{d}w = \left(\frac{1}{2}Kw^2 + \frac{1}{4}Cw^4\right)\mathrm{d}x. \tag{2.14}$$

The work done by the load is given by $P\Delta$, where Δ is the total distance moved by the applied load P. Using Pythagoras' theorem and Fig. 2.3 the end-shortening

due to a rotation θ is

$$\mathrm{d}\Delta = \mathrm{d}x - \sqrt{\mathrm{d}x^2 - \mathrm{d}w^2} = \mathrm{d}x - \mathrm{d}x\sqrt{1 - \left(\frac{\mathrm{d}w}{\mathrm{d}x}\right)^2}. \tag{2.15}$$

This expression is simplified by again assuming small angles,

$$\mathrm{d}\Delta \approx \frac{1}{2}\left(\frac{\mathrm{d}w}{\mathrm{d}x}\right)^2 \mathrm{d}x, \tag{2.16}$$

and therefore work done for an elemental length is

$$\mathrm{d}U_l = P\mathrm{d}\Delta \approx \frac{1}{2}P\left(\frac{\mathrm{d}w}{\mathrm{d}x}\right)^2 \mathrm{d}x. \tag{2.17}$$

Substituting the expressions for bending energy (2.13), foundation energy (2.14) and work done (2.17) into (2.1) and integrating over the length gives the total potential energy for the strut of Fig. 2.1,

$$V = \int_0^L \left(\frac{1}{2}EI\ddot{w}^2 - \frac{1}{2}P\dot{w}^2 + \frac{1}{2}Kw^2 + \frac{1}{4}Cw^4\right) \mathrm{d}x, \tag{2.18}$$

where w represents deflection away from the foundation and dots denote differentiation with respect to x.

2.1.2 Axially-compressed plate

The total potential energy for a flat plate of unit width ($0 < y < 1$), length L ($0 < x < L$) and thickness t, under biaxial compression (shown in Fig. 2.4) is

$$V = \int_0^1 \int_0^L \mathcal{L}\, \mathrm{d}x\mathrm{d}y = U_b + U_m - U_l, \tag{2.19}$$

where U_b is bending energy, U_m is the membrane energy due to in-plane compressibility and U_l is the work done by the applied loads. Rewriting the equations

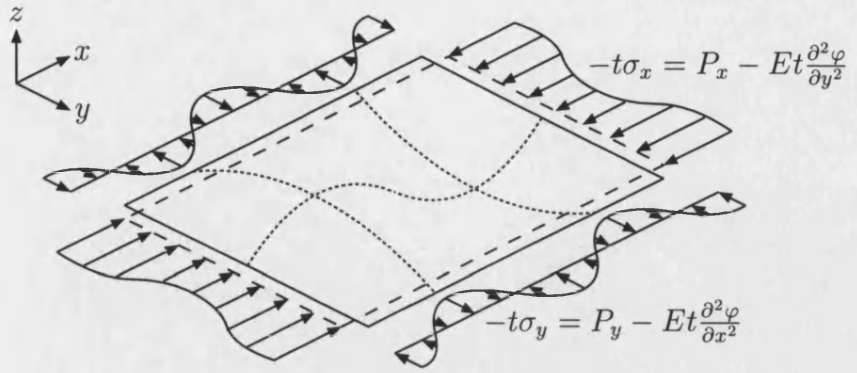

Figure 2.4: Flat plate under compression.

for ε_x (2.4), θ (2.10) and r (2.11) with subscripts to denote the relevant axes gives

$$\varepsilon_x = \frac{z}{r_x}, \quad \varepsilon_y = \frac{z}{r_y}, \tag{2.20}$$

$$\theta_x \approx \frac{\partial w}{\partial x}, \quad \theta_y \approx \frac{\partial w}{\partial y}, \tag{2.21}$$

and

$$\frac{1}{r_x} \approx \frac{\partial^2 w}{\partial x^2}, \quad \frac{1}{r_y} \approx \frac{\partial^2 w}{\partial y^2}. \tag{2.22}$$

In the plate problem U_b has components due to bending moments in the x and y directions and twisting moments providing shear stresses on the element faces. The energy due to curvature in the x direction for an element of size $\mathrm{d}x\mathrm{d}y$ is given by (2.3), with s replaced by $\mathrm{d}y$. Using the two-dimensional expression for

stress (2.7) and then substituting for the strains (2.20) and radii (2.22) gives

$$\begin{aligned} M_x &= \int_{-t/2}^{t/2} (\sigma_x z \mathrm{d}y)\ \mathrm{d}z \\ &= \frac{E}{1-\nu^2}\mathrm{d}y \int_{-t/2}^{t/2} (\varepsilon_x + \nu\varepsilon_y)\, z\ \mathrm{d}z \\ &= \frac{E}{1-\nu^2}\mathrm{d}y \int_{-t/2}^{t/2} \left(\frac{z}{r_x} + \nu\frac{z}{r_y}\right) z\ \mathrm{d}z \\ &= \frac{Et^3}{12(1-\nu^2)}\left(\frac{\partial^2 w}{\partial x^2} + \nu\frac{\partial^2 w}{\partial y^2}\right)\mathrm{d}y \\ &= D\left(\frac{\partial^2 w}{\partial x^2} + \nu\frac{\partial^2 w}{\partial y^2}\right)\mathrm{d}y, \end{aligned} \tag{2.23}$$

where D is the flexural rigidity of the plate, defined by

$$D = \frac{Et^3}{12(1-\nu^2)}, \tag{2.24}$$

and generally known as the plate constant. The bending energy due to M_x (2.2) is therefore

$$\begin{aligned} \mathrm{d}U_{b(M_x)} &= \frac{1}{2}M_x \mathrm{d}\theta_x = \frac{1}{2}D\left(\frac{\partial^2 w}{\partial x^2} + \nu\frac{\partial^2 w}{\partial y^2}\right)\mathrm{d}\theta_x \mathrm{d}y \\ &= \frac{1}{2}D\left(\frac{\partial^2 w}{\partial x^2} + \nu\frac{\partial^2 w}{\partial y^2}\right)\frac{\partial \theta_x}{\partial x}\ \mathrm{d}x\mathrm{d}y, \\ &= \frac{1}{2}D\left(\frac{\partial^2 w}{\partial x^2} + \nu\frac{\partial^2 w}{\partial y^2}\right)\frac{\partial^2 w}{\partial x^2}\ \mathrm{d}x\mathrm{d}y. \end{aligned} \tag{2.25}$$

The two other components can be derived in a similar manner (see for example Timoshenko & Gere (1961) or Bulson (1970)) and the total bending energy is

given by

$$\mathrm{d}U_b = \frac{1}{2}D\left[\left(\frac{\partial^2 w}{\partial x^2}+\nu\frac{\partial^2 w}{\partial y^2}\right)\frac{\partial^2 w}{\partial x^2}+\left(\frac{\partial^2 w}{\partial y^2}+\nu\frac{\partial^2 w}{\partial y^2}\right)\frac{\partial^2 w}{\partial y^2} + 2(1-\nu)\left(\frac{\partial^2 w}{\partial x \partial y}\right)^2\right]\mathrm{d}x\mathrm{d}y$$

$$= \frac{1}{2}D\left[\left(\frac{\partial^2 w}{\partial x^2}+\frac{\partial^2 w}{\partial y^2}\right)^2 - 2(1-\nu)\left(\frac{\partial^2 w}{\partial x^2}\frac{\partial^2 w}{\partial y^2}-\left(\frac{\partial^2 w}{\partial x \partial y}\right)^2\right)\right]\mathrm{d}x\mathrm{d}y. \quad (2.26)$$

The two second derivatives in the direction of the principal axes describe the curvature of a surface (Timoshenko & Woinowsky-Krieger, 1959): when both are zero the corresponding radii are infinite and the surface is flat; if one is non-zero then the deformation is cylindrical. Both these surfaces are *developable* and can be formed without stretching the mid-plane. In contrast, the buckling of a plate supported on all four edges has two non-zero derivatives, indicating curvature in both directions, called positive Gaussian curvature. This surface is *nondevelopable* and the mid-plane of the plate has to stretch. Consider the uniform stretching of the element $\mathrm{d}x\mathrm{d}y$ due to the stress σ_x. As with a spring the stored energy is $\frac{1}{2}\times$ Force $\times$ Distance, and therefore

$$\mathrm{d}U_{m(\sigma_x)} = \frac{1}{2}(\sigma_x t\mathrm{d}y)(\varepsilon_x \mathrm{d}x) = \frac{1}{2}t\,(\sigma_x\varepsilon_x)\,\mathrm{d}x\mathrm{d}y. \quad (2.27)$$

After adding similar components from σ_y and τ_{xy} (Timoshenko & Gere, 1961) the total energy due to in-plane stretching is

$$\mathrm{d}U_m = \frac{1}{2}t\,(\sigma_x\varepsilon_x+\sigma_y\varepsilon_y+\tau_{xy}\gamma_{xy})\,\mathrm{d}x\mathrm{d}y, \quad (2.28)$$

and substitution of (2.6) gives

$$\mathrm{d}U_m = \frac{1}{2}\frac{t}{E}\left(\sigma_x(\sigma_x-\nu\sigma_y)+\sigma_y(\sigma_y-\nu\sigma_x)+2(1+\nu)\tau_{xy}^2\right)\mathrm{d}x\mathrm{d}y. \quad (2.29)$$

It is this energy component which gives the stable post-buckling response, mod-

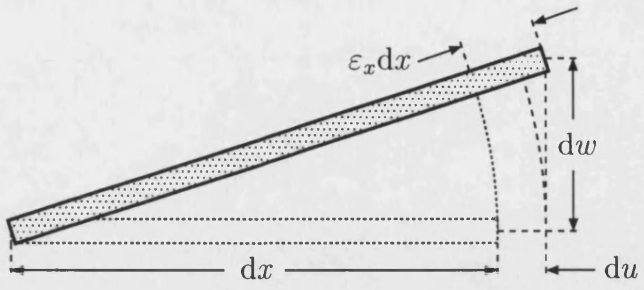

Figure 2.5: End-shortening.

elled in the one-dimensional strut system by the stiffening nonlinear component of the foundation.

With compressibility included to allow for stretching, the in-plane displacements (u and v in the x and y directions respectively) must also be included when calculating the end-shortening. Using the dimensions shown in Fig. 2.5 and the approximation for small angles, the mid-plane strain ε_x is

$$\varepsilon_x = \frac{\partial u}{\partial x} + \frac{1}{2}\left(\frac{\partial w}{\partial x}\right)^2. \tag{2.30}$$

The work done in the x direction per width $\mathrm{d}y$ (Force $\times$ Distance) is

$$\begin{aligned} \mathrm{d}U_{l(\sigma_x)} &= (t\sigma_x \mathrm{d}y)(\mathrm{d}u) = (t\sigma_x \mathrm{d}y)\left(\frac{\partial u}{\partial x}\mathrm{d}x\right) = t\sigma_x\left(\varepsilon_x - \frac{1}{2}\left(\frac{\partial w}{\partial x}\right)^2\right)\mathrm{d}x\mathrm{d}y \\ &= t\sigma_x\left(\frac{1}{E}(\sigma_x - \nu\sigma_y) - \frac{1}{2}\left(\frac{\partial w}{\partial x}\right)^2\right)\mathrm{d}x\mathrm{d}y. \end{aligned} \tag{2.31}$$

Similar expressions can be formulated for the work done by σ_y and τ_{xy} (Timoshenko & Gere, 1961):

$$\begin{aligned} \mathrm{d}U_{l(\sigma_y)} &= t\sigma_y\left(\frac{1}{E}(\sigma_y - \nu\sigma_x) - \frac{1}{2}\left(\frac{\partial w}{\partial y}\right)^2\right)\mathrm{d}x\mathrm{d}y, \\ \mathrm{d}U_{l(\tau_{xy})} &= t\tau_{xy}\left(\frac{1}{E}(1+\nu)\tau_{xy} - \frac{1}{2}\frac{\partial w}{\partial x}\frac{\partial w}{\partial y}\right)\mathrm{d}x\mathrm{d}y. \end{aligned} \tag{2.32}$$

Adding and integrating the separate contributions (2.26), (2.29), (2.31) and (2.32)

gives the total potential energy for the elastic plate:

$$
\begin{aligned}
V = \frac{1}{2}D\int_0^1\int_0^L \left(\frac{\partial^2 w}{\partial x^2}+\frac{\partial^2 w}{\partial y^2}\right)^2 - 2(1-\nu)\left(\frac{\partial^2 w}{\partial x^2}\frac{\partial^2 w}{\partial y^2}-\left(\frac{\partial^2 w}{\partial x \partial y}\right)^2\right)\mathrm{d}x\mathrm{d}y \\
+\frac{1}{2}\frac{t}{E}\int_0^1\int_0^L (\sigma_x+\sigma_y)^2 - 2(1+\nu)(\sigma_x\sigma_y-\tau_{xy}^2)\,\mathrm{d}x\mathrm{d}y \\
-\frac{1}{2}\frac{t}{E}\int_0^1\int_0^L \sigma_x\left(2(\sigma_x-\nu\sigma_y)-E\left(\frac{\partial w}{\partial x}\right)^2\right)\mathrm{d}x\mathrm{d}y \\
-\frac{t}{E}\int_0^1\int_0^L \tau_{xy}\left(2(1+\nu)\tau_{xy}-E\frac{\partial w}{\partial x}\frac{\partial w}{\partial y}\right)\mathrm{d}x\mathrm{d}y \\
-\frac{1}{2}\frac{t}{E}\int_0^1\int_0^L \sigma_y\left(2(\sigma_y-\nu\sigma_x)-E\left(\frac{\partial w}{\partial y}\right)^2\right)\mathrm{d}x\mathrm{d}y. \qquad (2.33)
\end{aligned}
$$

It is advantageous to split the stresses (σ_x, σ_y and τ_{xy}) into two components: one relating to uniform compression due to the average applied loads (P_x and P_y) and a stress function (φ) measuring the deviation from this uniformly compressed state, giving

$$
\sigma_x = E\frac{\partial^2\varphi}{\partial y^2}-\frac{P_x}{t},\quad \tau_{xy}=-E\frac{\partial^2\varphi}{\partial x\partial y},\quad \sigma_y = E\frac{\partial^2\varphi}{\partial x^2}-\frac{P_y}{t}. \qquad (2.34)
$$

For convenience P_x and P_y are defined to be positive in compression and act over a unit length in the x and y directions respectively. (It is assumed that there are no applied shear loads.) The expressions for φ are chosen because they automatically satisfy equilibrium on a small element (shown in Fig. 2.6 and normally used in the derivation of the governing differential equations) in the x and y directions,

$$
\begin{aligned}
\frac{\partial\sigma_x}{\partial x}+\frac{\partial\tau_{xy}}{\partial y} = E\left(\frac{\partial^3\varphi}{\partial x\partial^2 y}-\frac{\partial^3\varphi}{\partial x\partial^2 y}\right)=0, \\
\frac{\partial\sigma_y}{\partial y}+\frac{\partial\tau_{xy}}{\partial x} = E\left(\frac{\partial^3\varphi}{\partial^2 x\partial y}-\frac{\partial^3\varphi}{\partial^2 x\partial y}\right)=0. \qquad (2.35)
\end{aligned}
$$

Substituting (2.34) into (2.33), neglecting constant terms — which fall out in the

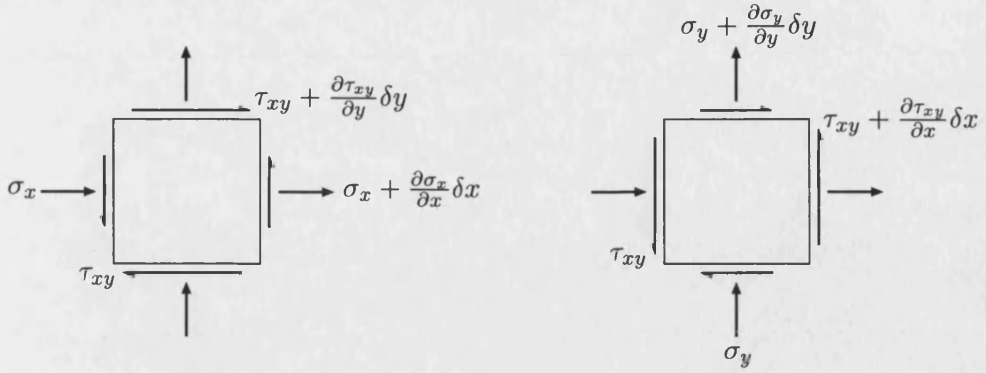

(a) (b)

Figure 2.6: Stresses acting on a small element in the (a) x and (b) y directions.

later differentiation — and simplifying, leaves

$$
\begin{aligned}
V = {} & \frac{1}{2}D\int_0^1\int_0^L \left(\frac{\partial^2 w}{\partial x^2}+\frac{\partial^2 w}{\partial y^2}\right)^2 - 2(1-\nu)\left(\frac{\partial^2 w}{\partial x^2}\frac{\partial^2 w}{\partial y^2}-\left(\frac{\partial^2 w}{\partial x \partial y}\right)^2\right)\mathrm{d}x\mathrm{d}y \\
& + \frac{1}{2}\frac{t}{E}\int_0^1\int_0^L \left(\frac{\partial^2 \varphi}{\partial x^2}+\frac{\partial^2 \varphi}{\partial y^2}\right)^2 - 2(1+\nu)\left(\frac{\partial^2 \varphi}{\partial x^2}\frac{\partial^2 \varphi}{\partial y^2}-\left(\frac{\partial^2 \varphi}{\partial x \partial y}\right)^2\right)\mathrm{d}x\mathrm{d}y \\
& - \frac{1}{2}\int_0^1\int_0^L \left(P_x - Et\frac{\partial^2 \varphi}{\partial y^2}\right)\left(\frac{\partial w}{\partial x}\right)^2 \mathrm{d}x\mathrm{d}y \\
& - Et\int_0^1\int_0^L \frac{\partial^2 \varphi}{\partial x \partial y}\frac{\partial w}{\partial x}\frac{\partial w}{\partial x}\,\mathrm{d}x\mathrm{d}y \\
& - \frac{1}{2}\int_0^1\int_0^L \left(P_y - Et\frac{\partial^2 \varphi}{\partial x^2}\right)\left(\frac{\partial w}{\partial y}\right)^2 \mathrm{d}x\mathrm{d}y. \qquad (2.36)
\end{aligned}
$$

This traditional notation is somewhat long-winded and so for the remainder of this thesis dots and primes are used to denote partial differentiation with respect

to x and y. Thus the previous equation can be rewritten as

$$\begin{aligned} V = {} & \frac{1}{2}D\int_0^1\int_0^L \left(\ddot{w}+\acute{w}\right)^2 - 2(1-\nu)\left(\ddot{w}\acute{w} - \dot{\acute{w}}^2\right)\,\mathrm{d}x\mathrm{d}y \\ & - \frac{1}{2}Et\int_0^1\int_0^L \left(\ddot{\varphi}+\acute{\varphi}\right)^2 - 2(1+\nu)\left(\ddot{\varphi}\acute{\varphi} - \dot{\acute{\varphi}}^2\right)\,\mathrm{d}x\mathrm{d}y \\ & - \frac{1}{2}\int_0^1\int_0^L \left(P_x - Et\acute{\varphi}\right)\dot{w}^2\,\mathrm{d}x\mathrm{d}y \\ & - Et\int_0^1\int_0^L \ddot{\varphi}\dot{w}\acute{w}\,\mathrm{d}x\mathrm{d}y \\ & - \frac{1}{2}\int_0^1\int_0^L \left(P_y - Et\ddot{\varphi}\right)\acute{w}^2\,\mathrm{d}x\mathrm{d}y. \end{aligned} \tag{2.37}$$

Integrating by parts gives an alternative (and possibly more familiar) form:

$$\begin{aligned} V = {} & \frac{1}{2}D\int_0^1\int_0^L \left(\ddot{w}+\acute{w}\right)^2 - 2(1-\nu)\left(\ddot{w}\acute{w} - \dot{\acute{w}}^2\right)\,\mathrm{d}x\mathrm{d}y \\ & + \frac{1}{2}Et\int_0^1\int_0^L \left(\ddot{\varphi}+\acute{\varphi}\right)^2 - 2(1+\nu)\left(\ddot{\varphi}\acute{\varphi} - \dot{\acute{\varphi}}^2\right)\,\mathrm{d}x\mathrm{d}y \\ & - \frac{1}{2}\int_0^1\int_0^L P_x\dot{w}^2\,\mathrm{d}x\mathrm{d}y \\ & - \frac{1}{2}\int_0^1\int_0^L P_y\acute{w}^2\,\mathrm{d}x\mathrm{d}y \\ & - Et\int_0^1\int_0^L \varphi\left(\nabla^4\varphi - \dot{\acute{w}}^2 + \ddot{w}\acute{w}\right)\,\mathrm{d}x\mathrm{d}y, \end{aligned} \tag{2.38}$$

where the last double integral is a Lagrange multiplier (Lord *et al.*, 1998) and $\nabla^4\varphi = \dddot{\varphi} + 2\,\ddot{\acute{\varphi}} + \acute{\acute{\acute{\varphi}}}$.

2.2 Differential equations

2.2.1 Axially-compressed strut

Equation (2.18) represents the total potential energy of the strut system. For equilibrium, V must be stationary: in the discrete general theory of elastic stability (Thompson & Hunt, 1973) a series of modes (1.2) are substituted, the integral evaluated and the stationary points found using the first derivatives; an alternative method is the calculus of variations which gives the stationary points in the form of a differential equation and a number of constraints. While solutions using a modal approach depend on the number and choice of modes, the differential equation can be solved numerically and the resulting solutions are *not* dependent on any prior assumptions of the deflected shape. The following analysis is a summary of the calculus of variations for this application.

The energy integral for the strut (2.18) is of the form

$$V = \int_0^L \mathcal{L}\,(w, \dot{w}, \ddot{w})\,\mathrm{d}x. \tag{2.39}$$

For equilibrium to be satisfied, the integral (V) of the Lagrangian ($\mathcal{L}$) must be stationary with respect to the spatial variable x, i.e. the first variation (Craggs, stationary with respect to the spatial variable x, i.e. the first variation (Craggs, 1973),

$$\delta V = \int_0^L \left(\frac{\partial \mathcal{L}}{\partial w}\delta w + \frac{\partial \mathcal{L}}{\partial \dot{w}}\delta \dot{w} + \frac{\partial \mathcal{L}}{\partial \ddot{w}}\delta \ddot{w} \right) \mathrm{d}x, \tag{2.40}$$

is zero. Integrating by parts gives

$$\begin{aligned} \delta V = &\int_0^L \frac{\partial \mathcal{L}}{\partial w}\delta w\,\mathrm{d}x + \left[\frac{\partial \mathcal{L}}{\partial \dot{w}}\delta w\right]_0^L - \int_0^L \frac{\mathrm{d}}{\mathrm{d}x}\left(\frac{\partial \mathcal{L}}{\partial \dot{w}}\right)\delta w\,\mathrm{d}x \\ &+ \left[\frac{\partial \mathcal{L}}{\partial \ddot{w}}\delta \dot{w} - \frac{\mathrm{d}}{\mathrm{d}x}\left(\frac{\partial \mathcal{L}}{\partial \ddot{w}}\right)\delta w\right]_0^L + \int_0^L \frac{\mathrm{d}^2}{\mathrm{d}x^2}\left(\frac{\partial \mathcal{L}}{\partial \ddot{w}}\right)\delta w\,\mathrm{d}x, \end{aligned} \tag{2.41}$$

and after substituting

$$\mathcal{L} = \frac{1}{2}EI\ddot{w}^2 - \frac{1}{2}P\dot{w}^2 + \frac{1}{2}Kw^2 + \frac{1}{4}Cw^4 \tag{2.42}$$

from (2.18) the following expression is obtained;

$$\delta V = \left[EI\ddot{w}\delta\dot{w} - \frac{\mathrm{d}}{\mathrm{d}x}(EI\ddot{w})\delta w + P\dot{w}\delta w\right]_0^L + \int_0^L \left(\frac{\mathrm{d}^2}{\mathrm{d}x^2}(EI\ddot{w}) + \frac{\mathrm{d}}{\mathrm{d}x}(P\dot{w}) + (Kw + Cw^3)\right)\delta w \, \mathrm{d}x. \tag{2.43}$$

For V to be stationary δV must disappear for all δw. Therefore the bracketed terms inside the integral must be zero, leading to the Euler equation

$$EI\,\ddddot{w} + P\ddot{w} + Kw + Cw^3 = 0. \tag{2.44}$$

Similarly the terms outside the integral must also vanish, giving the following constraint:

$$\left[EI\ddot{w}\delta\dot{w} - EI\dddot{w}\delta w + P\dot{w}\delta w\right]_0^L = 0. \tag{2.45}$$

As (2.44) is a fourth-order ODE, four boundary conditions are required. No vertical displacement at either end ($\delta w = 0$) eliminates the second and third terms, while the first term is satisfied by either simply-supported (free to rotate) or clamped (no rotation) ends. The boundary conditions for these two cases are defined respectively by

$$w(0) = w(L) = \ddot{w}(0) = \ddot{w}(L) = 0, \tag{2.46}$$

and

$$w(0) = w(L) = \dot{w}(0) = \dot{w}(L) = 0. \tag{2.47}$$

2.2.2 Axially-compressed plate

The plate problem is two-dimensional and hence the application of the calculus of variations is more complicated. The derivation of the first variation,

$$\begin{aligned}
\delta V = &\int_0^1 \Big[\big(D(\ddot{w} + \nu w'') - Et\varphi w''\big)\delta\dot{w} + 2\big(D(1-\nu) + Et\varphi\big)\dot{w}\delta w'\Big]_0^L \mathrm{d}y \\
&+ \int_0^L \Big[\big(D(w'' - \nu\ddot{w}) - Et\varphi\ddot{w}\big)\delta w'\Big]_0^1 \mathrm{d}x \\
&+ \int_0^1 \int_0^L \Big(D\nabla^4 w - \big(Et\varphi'' - P_x\big)\ddot{w} + 2Et\dot{\varphi}\dot{w} - \big(Et\ddot{\varphi} - P_y\big)w''\Big)\delta w \,\mathrm{d}x\mathrm{d}y \\
&- \int_0^1 Et\Big[\big(\ddot{\varphi} - \nu\varphi''\big)\delta\dot{\varphi} - \big(\ddot{\varphi} - \nu\varphi''\big)\delta\varphi + 2(1+\nu)\dot{\varphi}\delta\dot{\varphi}\Big]_0^L \mathrm{d}y \\
&- \int_0^L Et\Big[\big(\varphi'' - \nu\ddot{\varphi}\big)\delta\dot{\varphi} - \big(\varphi''' - \nu\dot{\varphi}''\big)\delta\varphi + 2(1+\nu)\,\dot{\varphi}'\delta\varphi\Big]_0^1 \mathrm{d}x \\
&+ \int_0^1 \int_0^L \Big(\nabla^4\varphi - \dot{w}^2 + \ddot{w}w''\Big)\delta\varphi \,\mathrm{d}x\mathrm{d}y, \qquad (2.48)
\end{aligned}$$

is given in Appendix A (Koiter, 1945). As this equation has to be zero with respect to each of the variables and their derivatives simultaneously, every term in the above expression is also zero. The third and sixth terms give two PDEs, commonly known as the von Kármán large deflection equations (von Kármán, 1910):

$$\begin{aligned}
D\nabla^4 w &= \big(Et\varphi'' - P_x\big)\ddot{w} - 2Et\dot{\varphi}\dot{w} + \big(Et\ddot{\varphi} - P_y\big)w'', \\
\nabla^4\varphi &= \dot{w}^2 - \ddot{w}w''. \qquad (2.49)
\end{aligned}$$

The first is an equilibrium and the second a compatibility equation.

Boundary conditions for w are given by the first two integrals. The assumption of no out-of-plane deflection on the edges of the plate implies that $w = \dot{w} = w'' = 0$ and $w = \dot{w} = \ddot{w} = 0$ on the short ($x = 0, L$) and long ($y = 0, 1$) boundaries

respectively. This leaves

$$\int_0^1 D\Big[\ddot{w}\delta\dot{w}\Big]_0^L \mathrm{d}y = 0, \qquad \int_0^L D\Big[\ddot{w}\delta\dot{w}\Big]_0^1 \mathrm{d}x = 0, \tag{2.50}$$

each of which is satisfied by either simply-supported or clamped boundary conditions. The boundary conditions on φ (the fourth and fifth terms of (2.48)) are more difficult. Using the earlier assumption that there are no applied shear stresses gives four boundary conditions,

$$\ddot{\varphi}(0,y) = \ddot{\varphi}(L,y) = \ddot{\varphi}(x,0) = \ddot{\varphi}(x,1) = 0, \tag{2.51}$$

which, noting that the rate-of-change of shear stress along the edges will also be zero, leaves:

$$\int_0^1 Et\Big[(\ddot{\varphi} - \nu\ddot{\varphi}'')\delta\dot{\varphi} - \ddot{\varphi}\delta\varphi\Big]_0^L \mathrm{d}y = 0, \tag{2.52}$$

$$\int_0^L Et\Big[(\ddot{\varphi}'' - \nu\ddot{\varphi})\delta\dot{\varphi}' - \ddot{\varphi}''\delta\varphi\Big]_0^1 \mathrm{d}x = 0. \tag{2.53}$$

Different sets of boundary conditions which satisfy these constraints are defined in Chapter 4 to model the three cases shown in Fig. 1.10: free-edged; straight-edged; and clamped in-plane.

Chapter 3

Simply-supported strut

While the supercritical strut considered here has been largely neglected, the strut supported by a nonlinear *softening* foundation has had a revival of interest, largely due to its heuristic role in the description of localized buckling (Hunt *et al.*, 1989; Champneys & Toland, 1993). Such responses are fundamentally subcritical (see Fig. 1.6), and interest has therefore centred on foundation nonlinearities that are either asymmetric (Hunt & Wadee, 1991) or symmetric but destabilizing (Wadee & Bassom, 1999). Much has been learned by treating the spatial boundary value problem as a nonlinear Hamiltonian initial value problem running in time; this dynamical systems approach describes the localized response as a homoclinic solution from the flat state to itself (see for example Champneys *et al.*, 1997). Thus the understanding of more complex problems such as the twisted rod (Champneys & Thompson, 1996) and the axially-compressed cylinder (Lord *et al.*, 1997), whose behaviour is also described by homoclinic solutions, has been further advanced by the analogy with the strut on a softening foundation.

Similarly, the periodic response of the axially-compressed strut on a stiffening foundation (Potier-Ferry, 1983) can be usefully allied to axially-compressed flat plates, where the nonlinear component of the foundation energy is analogous to the stabilizing effect of in-plane stretching. However, only a few researchers have

linked this heuristic model to the more difficult plate problem: Stein (1959a; 1959b) with the link model; the investigation of simply-supported struts by Uetani (1974) and plates by Nakamura & Uetani (1979); and the imperfection study of Johnson (1990).

As with the plate, instability under increasing load is expressed by a pair of imaginary eigenvalues — the two corresponding wavelengths give the possibility of doubly- or quasi-periodic behaviour — and hence the form of critical buckling is heavily reminiscent of the classical plate response (Timoshenko & Gere, 1961). However, in a finite-length system double or *compound* bifurcation points are found only sparsely; with simply-supported boundary conditions they occur when the ratio between the two eigenvalues is rational. Therefore a discrete bifurcation point will typically be encountered and the system will lock onto a single mode. As shown in Fig. 1.7, the limit of this mode locking is likely to be marked by a jump to a mode of a different wavelength; in both the plate and strut problems this change in mode number occurs along the length of the structure and, qualitatively, they should therefore have the same post-buckling response.

While the localized behaviour of subcritical structures relates to a homoclinic solution in nonlinear dynamical systems, mode jumping in the supercritical strut — and hence the axially-compressed plate — can be linked to the phenomenon of mode locking, summarized in the well known picture of Arnol'd tongues (Arnol'd, 1965). Here the two-dimensional space is marked by the ratio of the competing wavelengths and the amplitude at which mode jumping occurs, and shows interactions between any two modes and at all strut lengths. Certain regions of the tongues are determined to be of particular significance, marking the states where initially-stable supercritical paths of equilibria lose stability and induce the phenomenon of mode jumping.

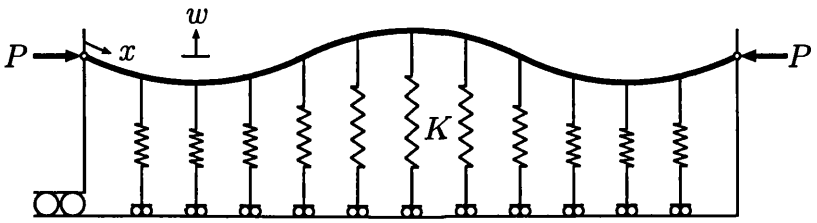

Figure 3.1: Strut on an elastic foundation.

3.1 Theory

Both the total potential energy and the differential equation for the axially-compressed elastic strut shown in Fig. 3.1 were derived in the previous chapter. Initially the differential equation (2.44),

$$EI\ddot{w}' + P\ddot{w} + Kw + Cw^3, \tag{3.1}$$

(where w represents deflection away from the foundation and dots denote differentiation with respect to x) is used to find the initial buckling modes and their corresponding critical loads. These modes are then substituted into the energy integral (2.18),

$$V = \int_0^L \left(\frac{1}{2}EI\ddot{w}^2 - \frac{1}{2}P\dot{w}^2 + \frac{1}{2}Kw^2 + \frac{1}{4}Cw^4\right)\mathrm{d}x, \tag{3.2}$$

giving a nonlinear energy formulation which, with the theory of elastic stability (Thompson & Hunt, 1973), allows the post-buckling stability to be investigated analytically.

3.1.1 Nondimensionalization

To simplify the equations without substituting specific values for the material properties (E, I), spring stiffness (K) and nonlinearity (C), it is useful to nondi-

mensionalize the Euler equation (3.1), giving

$$\ddddot{\bar{w}} + p\ddot{\bar{w}} + \bar{w} + \bar{w}^3 = 0, \tag{3.3}$$

where

$$\bar{w} = \sqrt{\frac{C}{K}}w, \quad p = \frac{P}{\sqrt{KEI}}, \tag{3.4}$$

and dots now denote differentiation with respect to $\bar{x}$ defined by,

$$\bar{x} = \sqrt[4]{\frac{K}{EI}}x. \tag{3.5}$$

The energy integral (3.2) can be nondimensionalized using the same relationships;

$$\bar{V} = \int_0^l \left(\frac{1}{2}\ddot{\bar{w}}^2 - \frac{1}{2}p\dot{\bar{w}}^2 + \frac{1}{2}\bar{w}^2 + \frac{1}{4}\bar{w}^4\right)\mathrm{d}\bar{x}. \tag{3.6}$$

3.1.2 Linearization and root structure

For small $\bar{w}$ the nonlinear term of equation (3.3) vanishes, leaving,

$$\ddddot{\bar{w}} + p\ddot{\bar{w}} + \bar{w} = 0. \tag{3.7}$$

If $\bar{w} = Ae^{\Lambda\bar{x}}$, the characteristic equation is

$$\Lambda^4 + p\Lambda^2 + 1 = 0, \tag{3.8}$$

and hence

$$\Lambda^2 = -\frac{p}{2} \pm \sqrt{\frac{p^2}{4} - 1}. \tag{3.9}$$

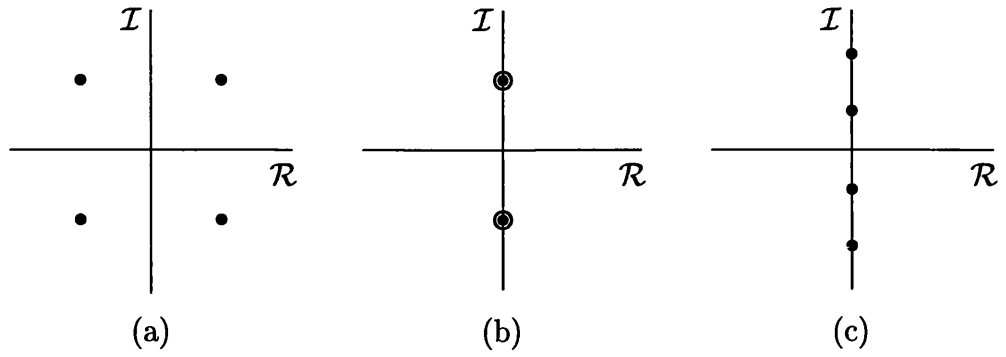

Figure 3.2: Eigenvalues of equation (3.7) in the complex plane; (a) $0 < p < 2$ — four complex eigenvalues, (b) $p = 2$ — two repeated imaginary eigenvalues, (c) $p > 2$ — four imaginary eigenvalues.

This leads to four eigenvalues,

$$\Lambda = \pm \mathrm{i} \sqrt{\frac{p}{2} \mp \sqrt{\frac{p^2}{4} - 1}}, \tag{3.10}$$

whose movement for $p > 0$ is summarized in Fig. 3.2. When $p \geq 2$ the values of Λ are pure imaginary — substituting them back into the initial expression ($\bar{w} = A\mathrm{e}^{\Lambda \bar{x}}$) gives the general solution

$$\bar{w} = A_1 \mathrm{e}^{\mathrm{i}\lambda_1 \bar{x}} + A_2 \mathrm{e}^{-\mathrm{i}\lambda_1 \bar{x}} + A_3 \mathrm{e}^{\mathrm{i}\lambda_2 \bar{x}} + A_4 \mathrm{e}^{-\mathrm{i}\lambda_2 \bar{x}} \tag{3.11}$$

where

$$\lambda_1 = \sqrt{\frac{p}{2} - \sqrt{\frac{p^2}{4} - 1}}, \quad \lambda_2 = \sqrt{\frac{p}{2} + \sqrt{\frac{p^2}{4} - 1}}. \tag{3.12}$$

Rewriting as a series of harmonic functions gives

$$\bar{w} = B_1 \sin \lambda_1 \bar{x} + B_2 \cos \lambda_1 \bar{x} + B_3 \sin \lambda_2 \bar{x} + B_4 \cos \lambda_2 \bar{x}, \tag{3.13}$$

where the negative eigenvalues have been absorbed by the real constants B_1, B_2, B_3 and B_4, obtainable from initial conditions in case of an initial value problem (IVP) and boundary conditions in the case of a boundary value problem (BVP). There are thus two possible periodic solutions to the linearized equation: if the

ratio of the wavelengths is rational a modulated periodicity can arise; if it is irrational, this will be replaced by quasi-periodicity.

3.1.3 Critical loads

If a strut of nondimensional length l has simply supported ends, $B_2 = B_4 = 0$ in (3.13) and only the sine terms apply. The solution may now involve combination of two waves of different wavelengths, but again only if their ratio is rational; if the two forms have a and b half-waves over the length l, wavelengths are $2l/a$ and $2l/b$ respectively, giving $\lambda_1 = a\pi/l$ (say) and $\lambda_2 = b\pi/l$, and hence $\lambda_1/\lambda_2 = a/b$. Quasi-periodicity, for which λ_1/λ_2 is irrational, is now necessarily absent, being only approachable in the limit as $l \to \infty$.

Typically a BVP solution will lock into a single wave. To demonstrate this the characteristic equation (3.8) is rewritten with p as the subject and Λ is substituted in terms of λ_1 to give the critical loads for buckling into a half-waves,

$$p^a = -\Lambda^2 - \frac{1}{\Lambda^2} = \lambda_1^2 + \frac{1}{\lambda_1^2} = \frac{a^2\pi^2}{l^2} + \frac{l^2}{a^2\pi^2}. \tag{3.14}$$

(Alternatively, working with (3.1) would have given the critical load

$$P^a = \frac{\pi^2 a^2 EI}{L^2} + \frac{L^2 K}{\pi^2 a^2}, \tag{3.15}$$

which repeats (3.14) in dimensional terms.)

Plotting p against l for each value of a gives the curves of Fig. 3.3, familiar also from the linear buckling of simply-supported plates (Timoshenko & Gere, 1961). The sequence is classical in nature. Each curve has a minimum at $p = 2$ (below which no buckling can occur) and is double-valued for $p > 2$: this corresponds to the two possible values of λ, where the shorter wavelengths ($\propto 1/\lambda_2$) lie to the left of the minimum and the longer wavelengths ($\propto 1/\lambda_1$) to the right. For any length l, the critical load for each mode a is found where the vertical line at l

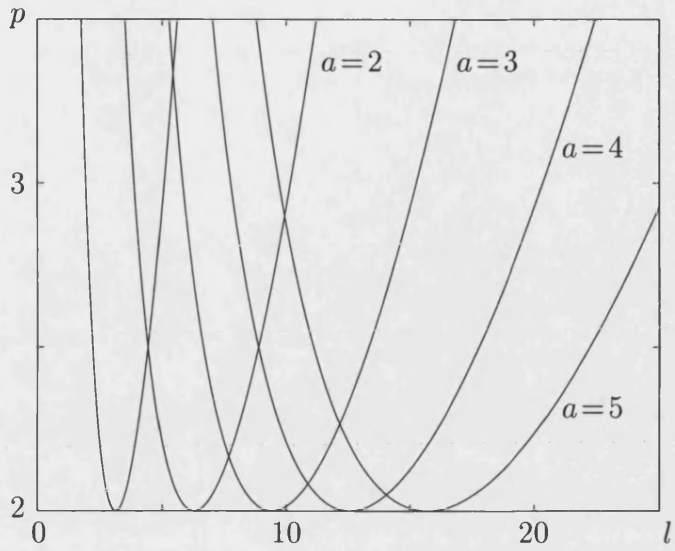

Figure 3.3: Critical load variations with length. (Note the curve $a = 1$ has not been labelled.)

intersects the corresponding curve. Typically this critical state will be discrete (Thompson & Hunt, 1973), although *compound* critical states also arise where two curves cross. The length at these points can be found by setting $p^a = p^b$ (3.14) and rearranging;

$$\begin{aligned} &\frac{a^2\pi^2}{l^2} + \frac{l^2}{a^2\pi^2} = \frac{b^2\pi^2}{l^2} + \frac{l^2}{b^2\pi^2} \\ &\Rightarrow \frac{\pi^2}{l^2}\left(a^2 - b^2\right) = \frac{l^2}{a^2b^2\pi^2}\left(a^2 - b^2\right) \\ &\Rightarrow l = \pi\sqrt{ab}. \end{aligned} \tag{3.16}$$

It is only at such intersection points that both λ_1 and λ_2 modes are allowable, giving the possibility of modulated periodicity. Although λ_1/λ_2 — given in terms of load by the following expression,

$$\frac{\lambda_1}{\lambda_2} = \frac{p}{2} - \sqrt{\frac{p^2}{4} - 1}, \tag{3.17}$$

— is irrational when $p^a \neq p^b$, the post-buckling form is periodic containing either a ($B_2 = B_3 = B_4 = 0$) or b ($B_1 = B_2 = B_4 = 0$) half-waves. If p^a is the minimum critical load, this uncoupled supercritical path would be expected to

be stable. However its stability may be curtailed by a secondary bifurcation marking a jump to a periodic solution of a different wavelength; the extent of locking onto the initial uncoupled mode is explored below using the full nonlinear energy formulation.

In the remainder of this chapter the nondimensional equations are used and the bar dropped.

3.2 Nonlinear energy formulation

For the BVP with simply-supported ends, the Fourier series representation,

$$w = \sum_{m=1}^{\infty} Q_m \sin \frac{m\pi x}{l}, \tag{3.18}$$

is available to express all possible equilibrium states in the nonlinear regime. Substituting a single mode of a half-waves into the nondimensionalized energy function (3.6) and integrating gives

$$V = \frac{1}{4}\frac{\pi^4 a^4}{l^3} Q_a^2 - \frac{1}{4}\frac{\pi^2 a^2}{l} p Q_a^2 + \frac{1}{4} l Q_a^2 + \frac{3}{32} l Q_a^4, \tag{3.19}$$

which, after rearranging and a substitution of p^a (3.14), simplifies to

$$V = \frac{3}{32} l Q_a^4 - \frac{1}{4}\frac{\pi^2 a^2}{l} \left(p - p^a\right) Q_a^2. \tag{3.20}$$

It is common practice (Thompson & Hunt, 1973) to rewrite this as

$$V = \frac{1}{24} V_{aaaa} Q_a^4 + \frac{1}{2} V'_{aa} \left(p - p^a\right) Q_a^2, \tag{3.21}$$

where

$$V_{aaaa} = \frac{\partial^4 V}{\partial Q_a^4} = \frac{9}{4} l, \quad V'_{aa} = \frac{\partial^3 V}{\partial Q_a^2 \partial p} = -\frac{1}{2}\frac{\pi^2 a^2}{l}. \tag{3.22}$$

Significantly (3.21) contains quadratic and quartic terms only; even after substitution of the full expression (3.18) all linear (e.g. Q_a) and cubic (e.g. Q_a^3) terms are absent and the quadratic form is diagonalized (i.e. there are no Q_aQ_b terms where $a \neq b$). No energy term can involve more than four different components, and any particular quartic term of interest can thus be determined from a summation of just four modes,

$$w = Q_a \sin\frac{a\pi x}{l} + Q_b \sin\frac{b\pi x}{l} + Q_c \sin\frac{c\pi x}{l} + Q_d \sin\frac{d\pi x}{l}, \tag{3.23}$$

where a, b, c and d are (as yet unspecified) positive integers. The total potential energy (3.6) for the full set of modes (3.18) can therefore be expressed in the following manner:

$$V = \frac{1}{24}\sum_{a=1}^{\infty}\sum_{b=1}^{\infty}\sum_{c=1}^{\infty}\sum_{d=1}^{\infty} V_{abcd}Q_aQ_bQ_cQ_d + \frac{1}{2}\sum_{a=1}^{\infty} V'_{aa}(p-p^a)Q_a^2. \tag{3.24}$$

It can readily be verified by a standard algebraic manipulation package such as MAPLE (Heck, 1996), that all the non-zero quartic coefficients are represented in the following list,

$$\begin{aligned}
V_{aaaa} &= \frac{9}{4}l,\\
V_{aabb} &= \frac{3}{2}l,\\
V_{aaab} &= -\frac{3}{4}l \text{ for } b = 3a,\\
V_{aabc} &= \frac{3}{4}l \text{ for } c = 2a - b,\\
&= -\frac{3}{4}l \text{ for } c = 2a + b,\\
V_{abcd} &= \frac{3}{4}l \text{ for } d = (a+b-c) \text{ or } (b+c-a) \text{ or } (c+a-b) \text{ or } (-a-b-c),\\
&= -\frac{3}{4}l \text{ for } d = (a-b-c) \text{ or } (b-c-a) \text{ or } (c-a-b) \text{ or } (a+b+c),
\end{aligned} \tag{3.25}$$

where a, b, c and d are all different from one another and again

$$V_{aaaa} = \frac{\partial^4 V}{\partial Q_a^4}, \quad V_{aabb} = \frac{\partial^4 V}{\partial Q_a^2 \partial Q_b^2}, \tag{3.26}$$

etc.

3.2.1 Fundamental solution and initial bifurcations

In general exact solutions require a large number of modes; however in practice only a relative small number can be used. This truncated Fourier series approximation is called a Rayleigh–Ritz analysis (Szilard, 1974). The first axiom of the theory of elastic stability (Thompson & Hunt, 1973) states that the equilibrium states for this potential energy function are given when all the first derivatives,

$$\frac{\partial V}{\partial Q_a}, \frac{\partial V}{\partial Q_b}, \cdots, \frac{\partial V}{\partial Q_n}, \tag{3.27}$$

are zero. The absence of constant terms in the resulting set of equilibrium equations means that a fundamental solution, $Q_a = Q_b = \cdots = Q_n = 0$, exists for all p.

Thompson & Hunt (1973) also state that the change in stability of a solution path always coincides with a limit point or the crossing of equilibrium paths; thus for a one degree-of-freedom (d.o.f.) system the intersection of the fundamental path with a supercritical uncoupled periodic solution is given where the second derivative of (3.21) is zero. Unsurprisingly, this linear eigenvalue result gives the same critical loads as (3.14).

This uncoupled solution emerges from the critical state as a pure sine wave but, because of the cubic nonlinearity (3.3), it is contaminated by odd-powered harmonics ($3a$, $5a$ etc.) as the deflection Q_a grows. A crude solution ignoring har-

monics ($Q_b = Q_c = \cdots = Q_n = 0$) is,

$$p = p^a - \frac{1}{6}\frac{V_{aaaa}}{V'_{aa}}Q_a^2. \tag{3.28}$$

Analytical solutions presented below are based on this simple one d.o.f. approximation with the harmonics ignored, and can be taken to be asymptotically correct as $Q_a \to 0$. The differences between asymptotic and full behaviours are explored later in Section 3.4 using the boundary value solver AUTO (Doedel *et al.*, 1995).

3.3 Coupled behaviour

Intersections of the curves of Fig. 3.3 identify two-fold compound critical states where two waves of different wavenumbers a and b have the same critical load. The defining potential function for this two d.o.f. system (excluding the special case $b = 3a$ when a V_{aaab} term must be included) is

$$\begin{aligned} V = {} & \frac{1}{24}V_{aaaa}Q_a^4 + \frac{1}{4}V_{aabb}Q_a^2Q_b^2 + \frac{1}{24}V_{bbbb}Q_b^4 \\ & + \frac{1}{2}V'_{aa}(p - p^a)Q_a^2 + \frac{1}{2}V'_{bb}(p - p^b)Q_b^2. \end{aligned} \tag{3.29}$$

The absence of cubic terms marks this as a *double-cusp catastrophe* (Thompson & Hunt, 1984) which, depending on relative sizes and signs of the coefficients, can take a number of different forms (Poston & Stewart, 1978). Differentiation of (3.29) with respect to Q_a and Q_b gives

$$\begin{aligned} \frac{\partial V}{\partial Q_a} &= \frac{1}{6}V_{aaaa}Q_a^3 + \frac{1}{2}V_{aabb}Q_aQ_b^2 + V'_{aa}(p - p^a)Q_a, \\ \frac{\partial V}{\partial Q_b} &= \frac{1}{2}V_{aabb}Q_a^2Q_b + \frac{1}{6}V_{bbbb}Q_b^3 + V'_{bb}(p - p^b)Q_b. \end{aligned} \tag{3.30}$$

All possible equilibrium states of this system are described by these two equations. For example, substitution of $Q_a = Q_b = 0$ gives the fundamental solution, while

$Q_a \neq Q_b = 0$ and $Q_a = 0 \neq Q_b$ leave equations for the uncoupled buckling into a and b half-waves respectively. Elimination of p leaves a single equation (Supple, 1967),

$$\left(3V'_{aa}V_{aabb} - V'_{bb}V_{aaaa}\right)Q_a^2 + \left(V'_{aa}V_{bbbb} - 3V'_{bb}V_{aabb}\right)Q_b^2 = 6V'_{aa}V'_{bb}\left(p^b - p^a\right), \quad (3.31)$$

which describes the coupled behaviour (for which Q_a and Q_b are both non-zero). Thus if coupled solutions do exist, they project onto the Q_a–Q_b base plane either as a hyperbola or an ellipse.

Both are found in the strut system. Substituting from the list of coefficients (3.25) gives,

$$\left(b^2 - 2a^2\right)Q_a^2 + \left(2b^2 - a^2\right)Q_b^2 = \frac{4}{3}\frac{\pi^2 a^2 b^2}{l^2}\left(p^b - p^a\right). \quad (3.32)$$

Without loss of generality it can be assumed that $a < b$, and hence the coefficient of the second term is always positive. If $a < b < \sqrt{2}a$, the first coefficient is negative and the hyperbolic form, with the equilibrium path behaviour shown schematically in Fig. 3.4, is obtained. Uncoupled paths appear at $p = p^a$ and $p = p^b$ on the fundamental path. A pair of secondary bifurcations, labelled accordingly either s_a or s_b, always appears on one of these paths. As the two critical states exchange positions on the fundamental path, the secondary bifurcations switch, such that they always appear on the upper uncoupled path. Therefore the lower uncoupled path is always stable and mode jumping cannot occur.

If on the other hand $b > \sqrt{2}a$, the first coefficient is positive and the elliptical form of Fig. 3.5 is obtained. For $p^a < p^b$ the right hand side of (3.32) is positive, and the ellipse intersects the uncoupled paths at the four secondary bifurcation positions shown as s_a and s_b. This is the situation for slightly shorter lengths than that of the compound state, just to the left of the relevant intersection point of Fig. 3.3. For longer lengths to the right of the intersection point, $p^a > p^b$, the right hand side of (3.32) is negative, and the coupled path vanishes. The equilibrium

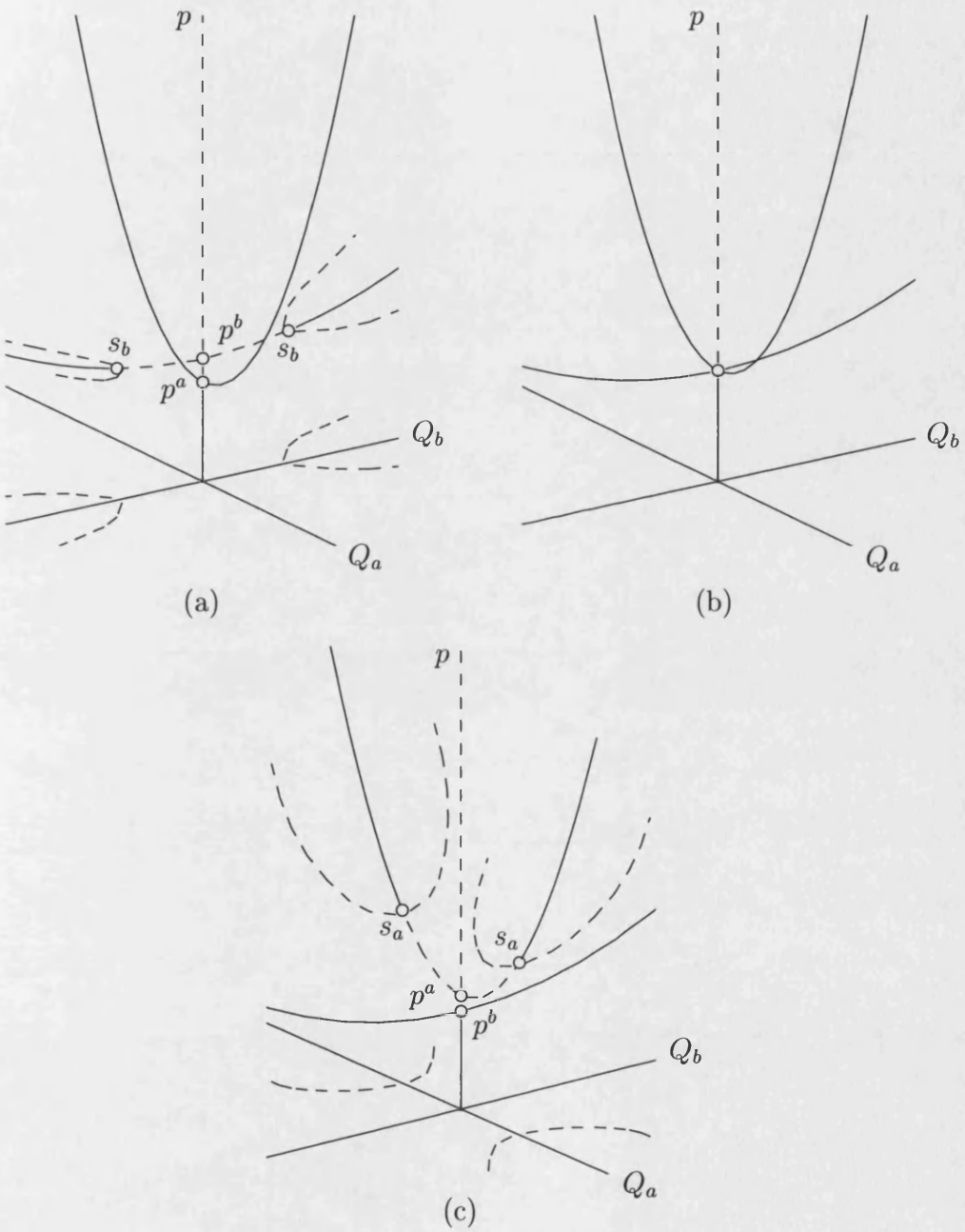

Figure 3.4: Equilibrium paths of energy function (3.29) when $b < \sqrt{2}a$; (a) $p^a < p^b$, (b) $p^a = p^b$, (c) $p^a > p^b$. Stable paths are shown as solid lines and unstable paths as broken lines.

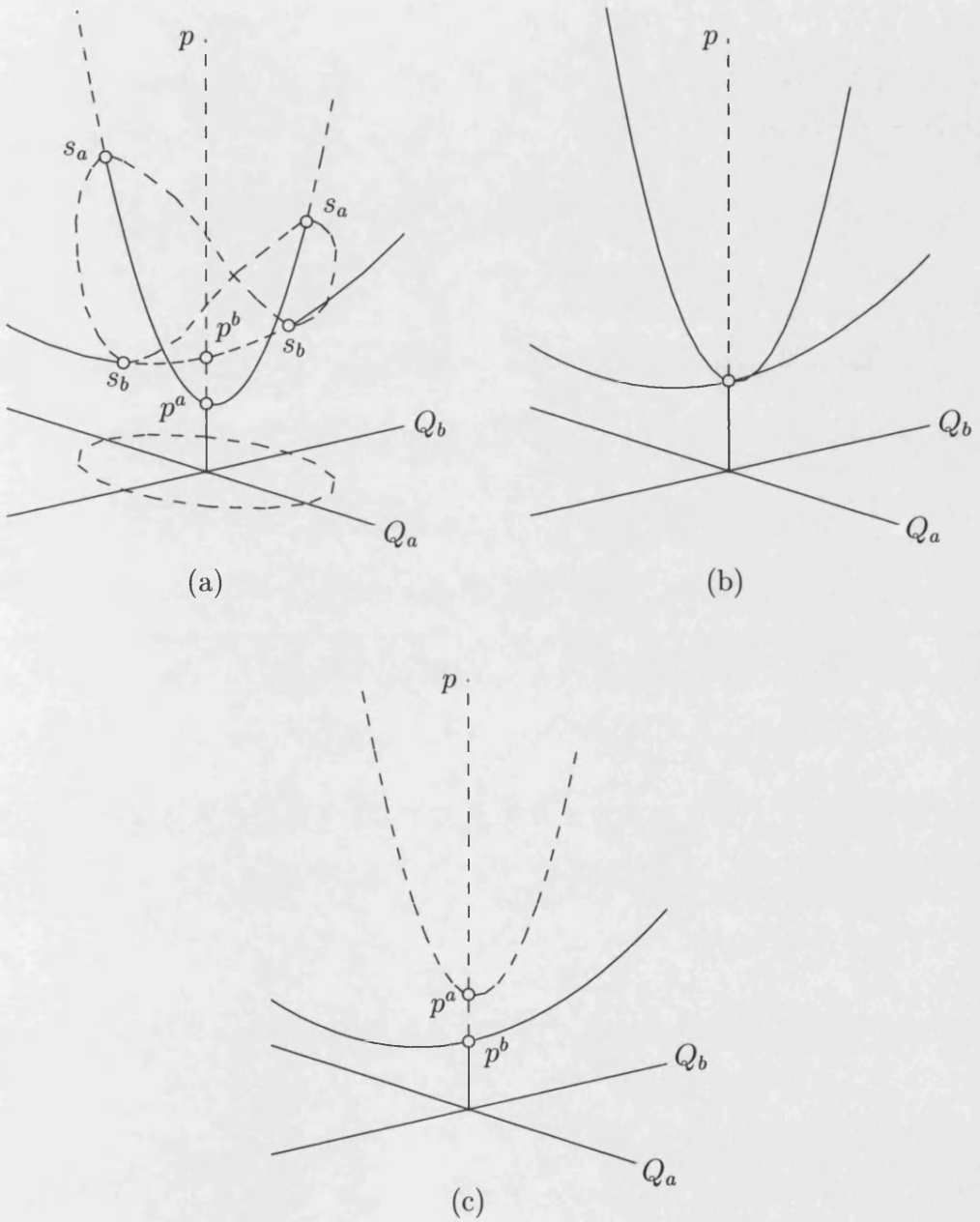

Figure 3.5: Equilibrium paths of energy function (3.29) when $b > \sqrt{2}a$; (a) $p^a < p^b$, (b) $p^a = p^b$, (c) $p^a > p^b$. Stable paths are shown as solid lines and unstable paths as broken lines.

configurations of Figs. 3.4 and 3.5 are explored in detail by Supple (1967).

3.3.1 Stability

Secondary bifurcation positions are readily determined from either (3.31) or (3.32) by setting $Q_a = 0$ or $Q_b = 0$ as appropriate. An alternative way of finding the intersection of the coupled and uncoupled paths is again to use the second axiom of the theory of elastic stability (Thompson & Hunt, 1973): here the linear eigenvalue analysis is performed on the uncoupled path ($Q_a \neq Q_b = 0$) and the secondary bifurcation points s_a are given when

$$\frac{\partial^2 V}{\partial Q_b^2} = \frac{1}{2} V_{aabb} Q_a^2 + V'_{bb}(p - p^b) = 0. \tag{3.33}$$

Elimination of p using (3.28) and rearranging gives

$$Q_{s_a} = \pm \sqrt{\frac{6 V'_{aa} V'_{bb}(p^b - p^a)}{3 V'_{aa} V_{aabb} - V'_{bb} V_{aaaa}}}, \tag{3.34}$$

which repeats the result given by (3.31). Alternatively, elimination of Q_a gives the secondary buckling load

$$p^{s_a} = \frac{V'_{aa} V_{aabb} p^a - V'_{bb} V_{aaaa} p^b}{3 V'_{aa} V_{aabb} - V'_{bb} V_{aaaa}}. \tag{3.35}$$

The stability of the secondary bifurcations is less straightforward however, and is best treated by expanding the potential function about the uncoupled equilibrium state via the incremental transformation,

$$Q_a = Q_{s_a} + q_a, \tag{3.36}$$

where Q_{s_a} is the secondary bifurcation point. Substitution into (3.29) then gives,

$$\begin{aligned} V = &\frac{1}{6}V_{aaaa}Q_{s_a}3q_a + \frac{1}{6}V_{aaaa}Q_{s_a}q_a^3 + \frac{1}{6}V_{aaaa}Q_{s_a}q_a^3 + \frac{1}{24}V_{aaaa}q_a^4 \\ &+ \frac{1}{4}V_{aabb}Q_{s_a}^2Q_b^2 + \frac{1}{2}V_{aabb}Q_{s_a}q_aQ_b^2 + \frac{1}{4}V_{aabb}q_a^2Q_b^2 \\ &+ \frac{1}{24}V_{bbbb}Q_b^4 + V'_{aa}(p-p^a)Q_{s_a}q_a + \frac{1}{2}V'_{aa}(p-p^a)q_a^2 + \frac{1}{2}V'_{bb}(p-p^b)Q_b^2. \end{aligned} \tag{3.37}$$

where terms dependent solely on Q_{s_a} have been ignored as they are constant in this analysis and hence have no effect on the equilibrium positions. Substituting the following expression, derived from (3.28),

$$V'_{aa}(p-p^a)Q_{s_a}q_a = -\frac{1}{6}V_{aaaa}Q_{s_a}^3q_a \tag{3.38}$$

cancels the linear terms in q_a, giving

$$\begin{aligned} V = &\frac{1}{4}V_{aaaa}Q_{s_a}^2q_a^2 + \frac{1}{6}V_{aaaa}Q_{s_a}q_a^3 + \frac{1}{24}V_{aaaa}q_a^4 \\ &+ \frac{1}{4}V_{aabb}Q_{s_a}^2Q_b^2 + \frac{1}{2}V_{aabb}Q_{s_a}q_aQ_b^2 + \frac{1}{4}V_{aabb}q_a^2Q_b^2 \\ &+ \frac{1}{24}V_{bbbb}Q_b^4 + \frac{1}{2}V'_{aa}(p-p^a)q_a^2 + \frac{1}{2}V'_{bb}(p-p^b)Q_b^2. \end{aligned} \tag{3.39}$$

It can be seen from (3.33) that at secondary bifurcation into Q_b the fourth and final terms cancel. Moreover for small q_a the second and third terms are small in comparison with the first, leaving

$$V \approx \frac{1}{4}V_{aaaa}Q_{s_a}^2q_a^2 + \frac{1}{2}V_{aabb}Q_{s_a}q_aQ_b^2 + \frac{1}{4}V_{aabb}q_a^2Q_b^2 + \frac{1}{24}V_{bbbb}Q_b^4 + \frac{1}{2}V'_{aa}(p-p^a)q_a^2. \tag{3.40}$$

After the substitution

$$\frac{1}{4}V_{aaaa}Q_{s_a}^2q_a^2 = -\frac{3}{2}V'_{aa}(p-p^a)q_a^2 \tag{3.41}$$

(again derived from (3.28)) this leaves,

$$V \approx \frac{1}{2}V_{aabb}Q_{s_a}q_aQ_b^2 + \frac{1}{4}V_{aabb}q_a^2Q_b^2 + \frac{1}{24}V_{bbbb}Q_b^4 - V'_{aa}(p-p^a)q_a^2. \tag{3.42}$$

The second term is small compared with the first and can be ignored. Differentiation with respect to q_a for equilibrium and rearranging gives the following first-order result for displacement away from the secondary bifurcation,

$$q_a = \frac{1}{4}\frac{V_{aabb}}{V'_{aa}(p-p^a)}\,Q_{s_a}Q_b^2. \tag{3.43}$$

Substituting this back into (3.42) gives (after a final substitution for $Q_{s_a}^2$) an effective fourth-order variation in Q_b which includes the passive variation in q_a:

$$V = \frac{1}{24}\left(V_{bbbb} - 9\frac{V_{aabb}^2}{V_{aaaa}}\right)Q_b^4. \tag{3.44}$$

On substitution from (3.25) this is found to be negative.

In the absence of instabilities with respect to other unspecified modes, the stability of the paths on and around the secondary bifurcations of Figs. 3.4 and 3.5 can now be summarized: where the uncoupled path passes from stable to unstable with increasing p, the coupled path is unstable and bends downwards with respect to the positive p axis; on the other hand, where the uncoupled path passes from unstable to stable with increasing p, the coupled path is still unstable but bends upwards (Thompson & Hunt, 1984).

The positions of the secondary bifurcation points relative to each other is also important. Substitution of (3.25) into (3.35) gives the load at s_a,

$$p^{s_a} = p^a + \frac{b^2}{b^2-2a^2}(p^b - p^a), \tag{3.45}$$

and similarly the load at s_b is

$$p^{s_b} = p^b + \frac{a^2}{a^2-2b^2}(p^a - p^b). \tag{3.46}$$

Rearranging gives,

$$p^{s_a} - p^{s_b} = \frac{3a^2b^2}{\left(b^2 - 2a^2\right)\left(2b^2 - a^2\right)}\left(p^b - p^a\right). \tag{3.47}$$

Take for example the elliptical case of Fig. 3.5(a) where $b > \sqrt{2}a$ and $p^b > p^a$. Substitution into (3.47) shows that the right-hand side is always positive and thus s_a lies above s_b with respect to the load axis. Evolution under parametric increase in load is then as follows. Buckling into a half-waves occurs at the critical load p^a, whereupon the system traces the lower, stable, uncoupled path ($Q_b = 0$). The upper uncoupled path with b half-waves ($Q_a = 0$) intersects the fundamental path at $p^b > p^a$, and is therefore initially unstable with respect to Q_a. An unstable coupled solution path, for which Q_a and Q_b are both non-zero, intersects the lower and upper uncoupled paths at s_a and s_b respectively, projecting onto the base plane as a closed loop as shown. The lower uncoupled path thus loses stability at s_a, where, under dead loading conditions, a dynamic jump takes place to the upper uncoupled path ($Q_a = 0$), which has stabilized at s_b. This is a mode jump from a to b half-waves.

According to this asymptotic description, such jumps are only possible when the coupled path is elliptical, i.e. when $b > \sqrt{2}a$, $p^b > p^a$, and the length is such that the system sits to the left of the relevant intersection point on Fig. 3.3. In addition, mode jumping always involves an increase in wavenumber (and a corresponding decrease in wavelength). The position of s_a is therefore of considerable interest, as it marks the limit of stability of the uncoupled path.

3.4 Numerical solutions

To validate the results given by the two d.o.f. Rayleigh–Ritz approximation above, the nondimensional ODE (3.3) is solved numerically — this effectively includes the full gamut of passive effects and gives "near-exact" solutions. The boundary

value solver AUTO (Doedel *et al.*, 1995) has been used to solve a wide range of problems, one of the more relevant perhaps being the strut on a softening nonlinear foundation (Champneys & Toland, 1993). In addition this package was chosen because, by varying a free parameter (such as load p or length l) for an ODE, it is able to track solution paths and log bifurcation points. This solution technique allows a wide range of results to be generated relatively quickly. Although it is used here as a "black box" solver, a brief description is given below.

The problem is discretized using the method of orthogonal collocation and automatically adapts its mesh to distribute the error from local discretization evenly. The routines for continuation employ predictor–corrector methods which solve the problem in two parts; the corrector iterates from the initial "prediction", using a modified Newton–Raphson method, until a solution within the predefined tolerance is found. However, this technique for parametric continuation fails at limit points, folds and bifurcation points. The alternative methods used, and the numerical detection of bifurcation points, are given in detail elsewhere (Seydel, 1994; Doedel, 1997). Switching between different solution paths which cross at bifurcation points is possible, such that parameter continuation can be performed, for example, along the coupled path of Fig. 3.5(a). In addition to the usual boundary conditions, integral constraints can also be placed on the problem.

3.4.1 Reduction to first-order form

AUTO only solves problems composed from a series of first-order ODEs over the range $0 < \tilde{x} < 1$. Therefore the variables have to be rescaled;

$$\tilde{x} = \frac{x}{l}, \quad \tilde{w} = \frac{w}{l}. \tag{3.48}$$

Using the chain rule, the first derivative of these new variables is

$$\frac{\mathrm{d}\tilde{w}}{\mathrm{d}\tilde{x}} = \frac{\mathrm{d}\tilde{w}}{\mathrm{d}w}\frac{\mathrm{d}w}{\mathrm{d}x}\frac{\mathrm{d}x}{\mathrm{d}\tilde{x}} = \frac{1}{l}\frac{\mathrm{d}w}{\mathrm{d}x}l, = \frac{\mathrm{d}w}{\mathrm{d}x}, \tag{3.49}$$

and using a similar approach,

$$\frac{\mathrm{d}^2\tilde{w}}{\mathrm{d}\tilde{x}^2} = l\frac{\mathrm{d}^2w}{\mathrm{d}x^2}, \quad \frac{\mathrm{d}^3\tilde{w}}{\mathrm{d}\tilde{x}^3} = l^2\frac{\mathrm{d}^3w}{\mathrm{d}x^3}, \quad \frac{\mathrm{d}^4\tilde{w}}{\mathrm{d}\tilde{x}^4} = l^3\frac{\mathrm{d}^4w}{\mathrm{d}x^4}. \tag{3.50}$$

Substituting the above into (3.3) gives

$$\frac{1}{l^3}\frac{\mathrm{d}^4\tilde{w}}{\mathrm{d}\tilde{x}^4} + \frac{p}{l}\frac{\mathrm{d}^2\tilde{w}}{\mathrm{d}\tilde{x}^2} + l\tilde{w} + l^3\tilde{w}^3 = 0, \tag{3.51}$$

which can also be written as four first-order equations,

$$\dot{f}_1 = f_2, \quad \dot{f}_2 = f_3, \quad \dot{f}_3 = f_4, \quad \dot{f}_4 = -\left(pl^2f_3 + l^4f_1 + l^6f_1^3\right), \tag{3.52}$$

where dots denote differentiation with respect to $\tilde{x}$ and,

$$f_1 = \tilde{w} = \frac{w}{l}, \quad f_2 = \frac{\mathrm{d}\tilde{w}}{\mathrm{d}\tilde{x}} = \frac{\mathrm{d}w}{\mathrm{d}x}, \quad f_3 = \frac{\mathrm{d}^2\tilde{w}}{\mathrm{d}\tilde{x}^2} = l\frac{\mathrm{d}^2w}{\mathrm{d}x^2}, \quad f_4 = \frac{\mathrm{d}^3\tilde{w}}{\mathrm{d}\tilde{x}^3} = l^2\frac{\mathrm{d}^3w}{\mathrm{d}x^3}. \tag{3.53}$$

The simply-supported boundary conditions (2.46) become

$$f_1(0) = f_1(1) = f_3(0) = f_3(1) = 0. \tag{3.54}$$

Equations (3.52) with the boundary conditions (3.54) can be solved by AUTO, which gives numerical solutions for f_1, f_2, f_3 and f_4.

3.4.2 Comparison with analytical results

The approximation (3.28) for the uncoupled periodic solutions is found to give good agreement with the numerical results for moderate amplitudes, but as expected the odd-powered harmonics have increasing effect as the amplitude grows.

When $b > \sqrt{2}a$, the coupled results given by AUTO show the same qualitative features as the elliptical asymptotic form of Fig. 3.5. For small and positive $p^b - p^a$, the positions of the secondary bifurcations agree well with predictions (3.45) and (3.46). As expected, there is no coupled path when $p^b < p^a$ (Fig. 3.5(c)).

When $b < \sqrt{2}a$, s_b behaves much as expected, with (3.46) again giving good agreement for moderate amplitudes. Secondary bifurcation s_a is a different matter however. For small and positive $p^a - p^b$ (i.e. just to the right of the relevant compound bifurcation point of Fig. 3.3), p^{s_a} from (3.45) finds reasonable agreement, but the numerics suggest that extra secondary bifurcations also arise at points which are remote from the fundamental path. The coupled behaviour predicted from the numerical results is summarized in Fig. 3.6, which has been produced by separating BVP profiles into the corresponding periodic components. This process highlights the reason for the differing results: the coupled path contains additional contaminating modes. Fig. 3.6(a) shows that the coupled path initially reflects the hyperbolic form shown in Fig. 3.4(a) at $Q_a = 0$, but then bends back to form a loop. When $p^a = p^b$ (Fig. 3.6(b)) a remote bifurcation s_a, not seen in either Fig. 3.4 or Fig. 3.5, exists at a non-zero value p^{s_a}. As the length is increased slightly so that $p^a > p^b$, the remote bifurcation s_a on the upper uncoupled path moves towards a second bifurcation s_a which emerges from the compound point (Fig3.6(c)). The coupled solution thus continues to exist but its scope is limited; as the length is increased further these two points converge and eventually eliminate each other, as seen in Fig. 3.6(d). Thus for moderately large $\left|p^a - p^b\right|$ the response (shown in Figs. 3.6(a) and (d)) is more like the behaviour of Fig. 3.5 — with mode jumping occurring when $p^a < p^b$ and no coupled behaviour for $p^a > p^b$ — than that of Fig. 3.4.

These numerical results clearly show that mode jumping still occurs when $b < \sqrt{2}a$, with the remote bifurcation s_a marking the limit of stability of the uncoupled path. The corresponding amplitude is liable to be much greater than when $b > \sqrt{2}a$, as is the difference between p^{s_a} and p^{s_b}, with presumably a relatively large release in energy associated with the jump. This behaviour is perhaps

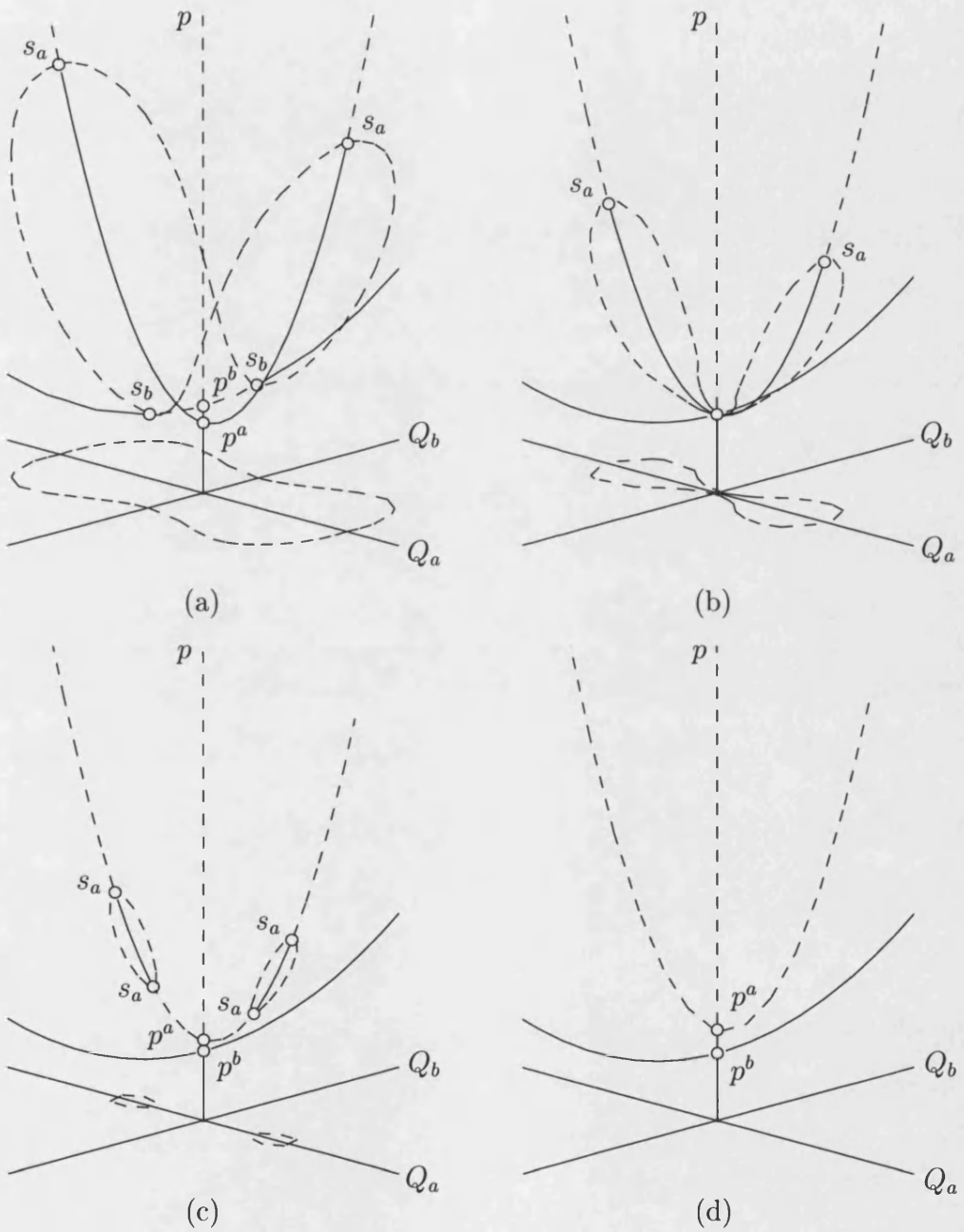

Figure 3.6: Equilibrium paths generated from numerical results when $b < \sqrt{2}a$; (a) $p^a < p^b$, (b) $p^a = p^b$, (c) $p^a > p^b$, (d) $p^a \gg p^b$. Stable paths are shown as solid lines and unstable paths as broken lines.

counter-intuitive: it might be expected that in longer structures, where the interacting modes are closer together, that mode jumping would occur *earlier* in the post-buckling regime. However, later comparisons for a sequence of results shows that this apparent increase in stability is due to the boundary condition effects. Coupled solutions when $p^a > p^b$ are not of interest as these two secondary bifurcations cannot be reached in a normal loading sequence.

3.5 Passive contamination

The comparison of results above shows that the two d.o.f. approximation (3.29) is asymptotic, in the sense that it only holds close to the compound critical state. The agreement at larger amplitudes can be improved by including other modes in the approximation. These are denoted by Greek letters (Thompson & Hunt, 1984) and called "passive" modes because, in contrast to the "active" modes a and b, they have minimal effect close to the primary bifurcation points. Splitting the numerical profiles into separate modes shows that the main interactive contamination comes from a mode of amplitude Q_α, where $\alpha = 2a - b$.

A general scheme for eliminating certain chosen generalized coordinates (Q_α, Q_β etc.) as passive or slave variables is given by Thompson & Hunt (1984). Equivalent to a general Lyapunov–Schmidt reduction (Golubitsky & Schaeffer, 1984), the object is to replace the original potential function with one in a reduced number of degrees of freedom; the coefficients for the new function are obtained in terms of those of the old. If a particular coefficient passes over unaltered from the old to the new function, it is said to be *uncontaminated.* As the original energy function (3.6) is diagonalized and cubic terms are absent, all energy terms up to fourth-order are uncontaminated (Thompson & Hunt, 1984). The list of quartic coefficients (3.25) contains for example terms like $V_{aaa\alpha}$ where $\alpha = 3a$, and $V_{aab\beta}$ where $\beta = 2a \pm b$, which have increasing influence on the solutions as deflections grow in the nonlinear regime. If Q_a and Q_b remain as active coordinates while

Q_α and Q_β are eliminated as passives, sixth and higher-order terms in Q_a and Q_b are all that is produced. A valid asymptotic description is thus obtained simply by ignoring passive effects and truncating the energy expansions after the appropriate quartic terms.

However here interest centres on the location of the secondary bifurcation points which can be found by linear eigenvalue analysis. For the three variable representation of the energy,

$$\begin{aligned} V = {} & \frac{1}{24}V_{aaaa}Q_a^4 + \frac{1}{4}V_{aabb}Q_a^2Q_b^2 + \frac{1}{2}V_{aab\alpha}Q_a^2Q_bQ_\alpha + \frac{1}{4}V_{aa\alpha\alpha}Q_a^2Q_\alpha^2 \\ & + \frac{1}{24}V_{bbbb}Q_b^4 + \frac{1}{4}V_{bb\alpha\alpha}Q_b^2Q_\alpha^2 + \frac{1}{24}V_{\alpha\alpha\alpha\alpha}Q_\alpha^4 \\ & + \frac{1}{2}(p-p^a)V'_{aa}Q_a^2 + \frac{1}{2}(p-p^b)V'_{bb}Q_b^2 + \frac{1}{2}(p-p^\alpha)V'_{\alpha\alpha}Q_\alpha^2, \end{aligned} \tag{3.55}$$

the position of the secondary bifurcation s_a is given by the stability determinant (Thompson & Hunt, 1984)

$$\begin{vmatrix} W_{bb} & W_{b\alpha} \\ W_{b\alpha} & W_{\alpha\alpha} \end{vmatrix} = W_{bb}W_{\alpha\alpha} - W_{b\alpha}W_{b\alpha} = 0, \tag{3.56}$$

where (on the uncoupled path $Q_a \neq Q_b = Q_\alpha = 0$),

$$\begin{aligned} W_{bb} &= \frac{\partial^2 V}{\partial Q_b^2} = \frac{1}{2}V_{aabb}Q_a^2 + V'_{bb}(p-p^b), \\ W_{b\alpha} &= \frac{\partial^2 V}{\partial Q_b \partial Q_\alpha} = \frac{1}{2}V_{aab\alpha}Q_a^2, \\ W_{\alpha\alpha} &= \frac{\partial^2 V}{\partial Q_\alpha^2} = \frac{1}{2}V_{aa\alpha\alpha}Q_a^2 + V'_{\alpha\alpha}(p-p^\alpha). \end{aligned} \tag{3.57}$$

Substituting values for p (3.28) and the coefficients (3.25) gives a complicated quadratic equation in Q_a^2. Using the simplification $b = a+1$ and $\alpha = 2a - b =$

$a-1$ leaves,

$$\frac{9}{64}\frac{l^2}{a^4}\left(6a^2-1\right)Q_a^4 + \frac{3}{16}\frac{\pi^2}{a^2}\left(\left(2a^4+8a^2-2\right)p^a-\left(a-1\right)^2\left(a^2-2a-1\right)\left(p^b+p^\alpha\right)\right)Q_a^2 - \frac{1}{4}\frac{\pi^4}{l^2}\left(\left(a-1\right)^2\left(a+1\right)^2\left(p^a-p^b\right)\left(p^a-p^\alpha\right)\right)=0. \tag{3.58}$$

Solving this equation in MAPLE (Heck, 1996) gives either two or four valid solutions for Q_{s_a} depending on the values of a and l. The load p^{s_a} then follows from (tions for Q_{s_a} depending on the values of a and l. The load p^{s_a} then follows from (3.28).

Fig. 3.6 has been produced from numerical data: however the same diagram constructed using modal solutions of (3.55) is near-identical. To demonstrate this, comparisons between asymptotic results and the full numerical solutions from AUTO are given in Fig. 3.7 for the case where $a = 3$, $b = 4$ and $\alpha = 2a - b = 2$, at a position just to the left of the relevant compound bifurcation point $l = 10.8 < \sqrt{12}\pi$ (3.16). Deflected shapes are plotted for the paths of Fig. 3.6(a) on the left, detailing both uncoupled solutions and the transition from three to four half-waves that takes place in a typical loading sequence. Over the range of deflections shown the two sets of results are barely distinguishable, the differences being shown at an exaggerated scale on the right. The plots show first that the single passive mode Q_α does indeed provide the dominant (passive) effect and secondly that, in this particular regime, the correct form of coupled paths and secondary bifurcations can only be predicted asymptotically with its specific inclusion. Figs. 3.7(b) and (g) clearly show the expected contaminating effects of the first harmonic, $\beta = 3a = 9$ and $\gamma = 3b = 12$ respectively; however, although its exclusion simplifies the energy potential significantly, it does not noticeably effect the accuracy of the solutions. The larger errors in Figs. 3.7(c) and (d) highlight the presence of further passive modes (which again do not affect the position of the secondary bifurcations).

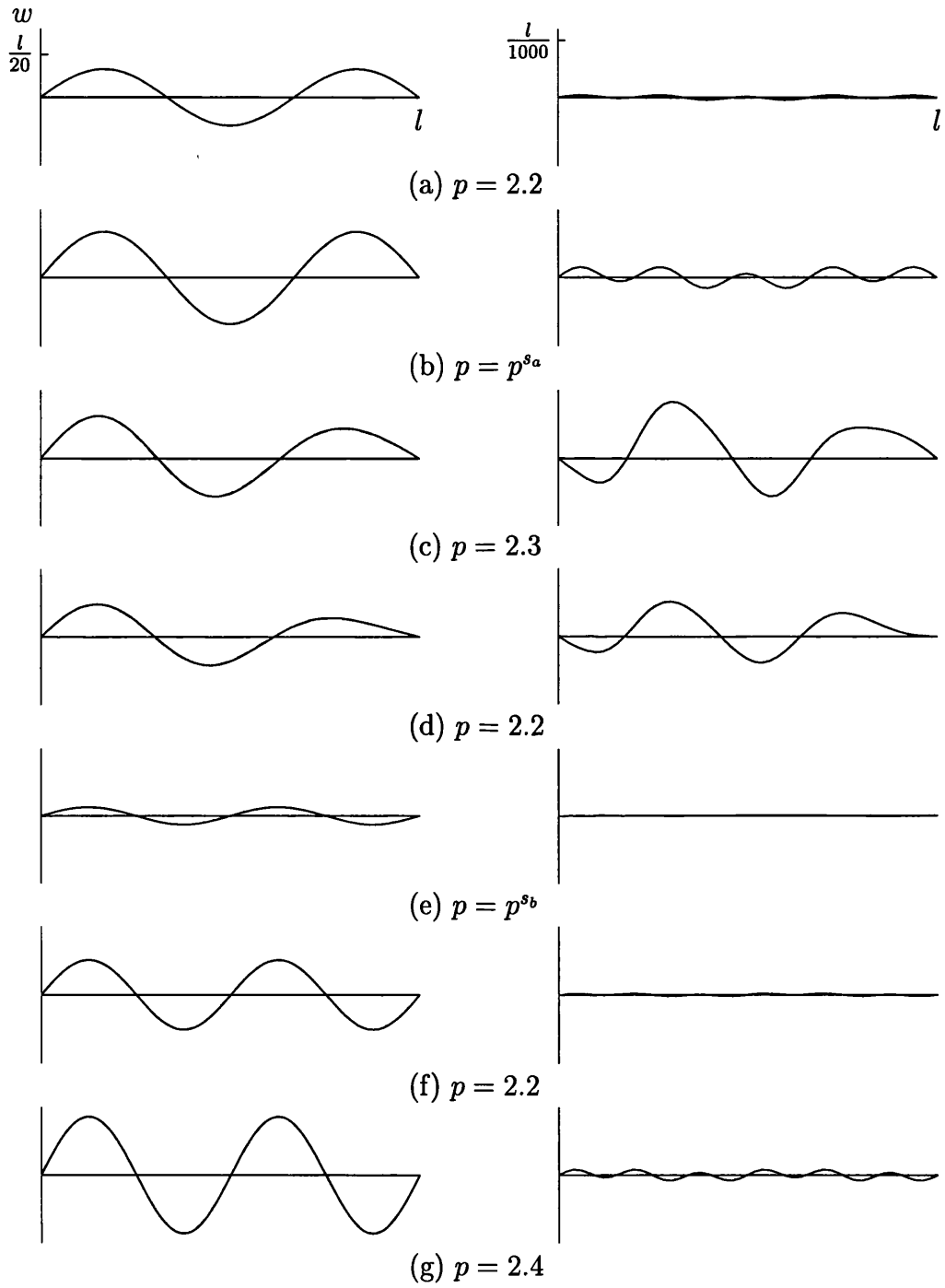

Figure 3.7: Left: solutions at different locations on Fig. 3.6(a); (a) lower uncoupled path, (b) s_a, (c)–(d) unstable coupled path between s_a and s_b, (e) s_b, (f)–(g) upper uncoupled path. Although difficult to distinguish, numerical solutions are shown as solid lines and modal solutions as broken lines. Right: difference between modal and numerical solutions.

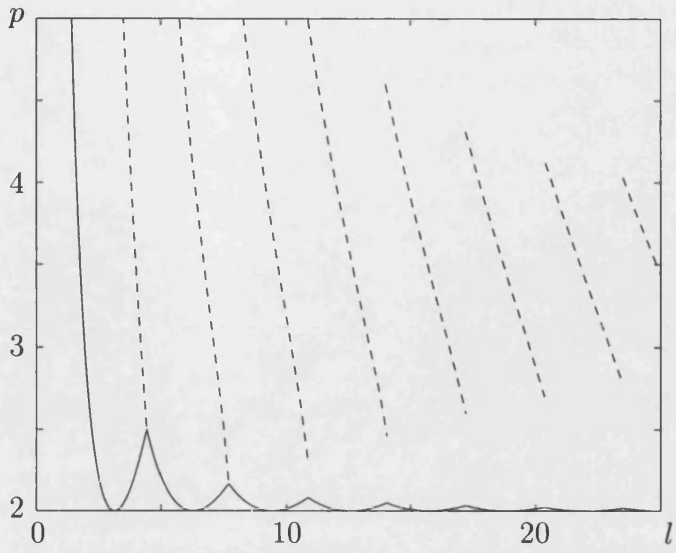

Figure 3.8: Comparison of minimum critical (solid line) and secondary (broken lines) buckling loads.

3.6 Arnol'd tongues

Even for the one set of boundary conditions considered, it is relatively difficult to present results for a wide range of lengths in a concise yet meaningful way. One method is to superimpose the secondary buckling loads for a range of lengths directly onto the critical load plot (Supple, 1970; Nakamura & Uetani, 1979). Fig. 3.8 shows a similar plot for the strut: the left-most two secondary buckling curves (marking the load where jumping from one and two half-waves occurs respectively) intersect the critical load envelope at the corresponding compound bifurcation points; in contrast, but as expected from Fig. 3.6, the other curves start at a load remote from the compound points. Although both critical and secondary buckling loads can be found relatively easily, this plot does not indicate the wavenumber *after* mode jumping or the limit of the coupled behaviour as $l \to \infty$.

Here a new approach is used. Instead of plotting load against length (as in Fig. 3.8), the nondimensional amplitude is plotted against the ratio of the two wavelengths: this can show *all* interactions for *all* strut lengths. It was noted that at compound bifurcation points (Fig. 3.3) the values of λ_1/λ_2 are rational and, in

addition, either two (Fig. 3.6(b)) or four (Fig. 3.6(b)) of the secondary bifurcation points have zero amplitude. This provides a tenuous but not unrealistic link to the portrayal of mode locking in a forced oscillator due to Arnol'd (1965) — described in Section 1.3.2 — where again cusps meet the real line at rational positions. Here there is no forcing frequency, instead there are two natural frequencies of the linearized problem, λ_1 and λ_2, which play the same interactive role. Similarly the nondimensional amplitude of the uncoupled (mode-locked) periodic state, Q_a or Q_b, replaces the amplitude of the nonlinearity as the second parametric dimension. Secondary bifurcation positions are again marked by cusp-shaped tongues; the point where the tongue meets the real line defines the wavenumbers before and after mode jumping. Interestingly however, in this boundary value representation it is points outside, rather than inside, the tongues that define mode-locked states. This is in contrast to the Arnol'd tongues associated with the circle map, but coincides with those relating to the Mathieu equation for example (Jordan & Smith, 1987).

3.6.1 Construction

Take for example the interaction between $a = 2$ and $b = 3$ half-waves, shown schematically in Fig. 3.5, which is summarized for struts of all lengths in Fig. 3.9. The value of λ_1/λ_2 for each of the two modes of interest is fixed by its critical load, p^a or p^b (3.14). While one of these λ values must be linked directly to an integer (a or b), the other in general will not; typically therefore λ_1/λ_2 is irrational. Only when the length is such that two critical loads coincide will both λ values be linked to integers, and λ_1/λ_2 be rational. The compound bifurcation point where $p^a = p^b$ is thus marked by a rational position on the λ_1/λ_2 axis, in this case at $\lambda_1/\lambda_2 = 2/3$. To the left of the relevant compound bifurcation point in Fig. 3.3, p^b increases and the λ_1/λ_2 (3.17) related to it decreases, while at the same time s_b emerges from the compound bifurcation point and moves up the uncoupled path. This is traced by the left-hand arm of the cusp shown in Fig. 3.9.

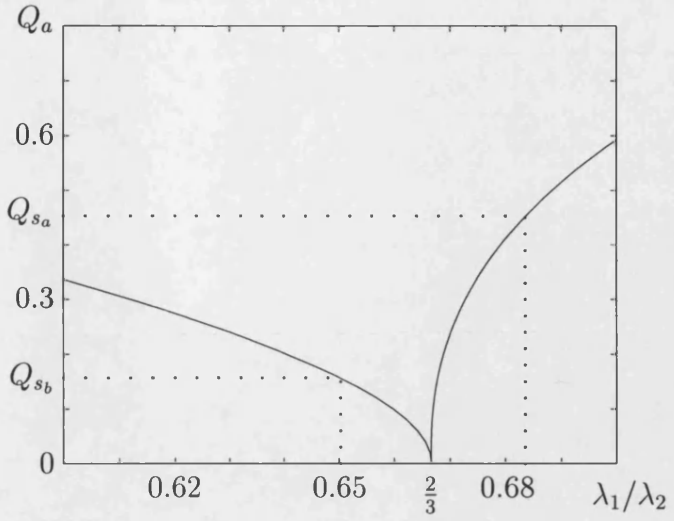

Figure 3.9: Tongue showing interaction between 2 and 3 half-waves.

Of more practical interest is the position of s_a; as p^a reduces, λ_1/λ_2 increases and hence the position of s_a is given by the line to the right of $\lambda_1/\lambda_2 = 2/3$.

When $a = 2$ and $b = 3$, $p^a = p^b$ occurs at $l = \sqrt{6}\pi$ (3.16), so for $l = 7.6 < \sqrt{6}\pi$ say, the coupled behaviour is similar to that shown in Fig. 3.5(a). The values of λ_1/λ_2 at p^a and p^b are 0.684 and 0.650 (given by (3.14)), shown by the vertical dotted lines in Fig. 3.9. The nondimensional amplitudes of the secondary bifurcation points are given by the intersection of these lines with the two arms of the cusp; in this example Q_a and Q_b are approximately 0.45 and 0.16 respectively. The corresponding secondary buckling load can be quickly found by substituting the relevant amplitude into (3.28).

In contrast, when $b < \sqrt{2}a$ — for example $a = 3$ and $b = 4$ — s_a fails to pull in to the compound bifurcation point as p^a and p^b converge. As shown in Fig. 3.6, it remains remote from the fundamental path, and vanishes only when it collides with a further secondary bifurcation on the same uncoupled path, which emerges from the compound bifurcation point in the region to the right of relevant intersection of Fig. 3.3. As $p^a > p^b$ these secondary bifurcations do not affect the global stability, and hence they are represented in Fig. 3.10 by the *broken* line which initially veers to the left. There is thus a certain threshold value of amplitude of s_a below which mode jumping is absent, which is picked

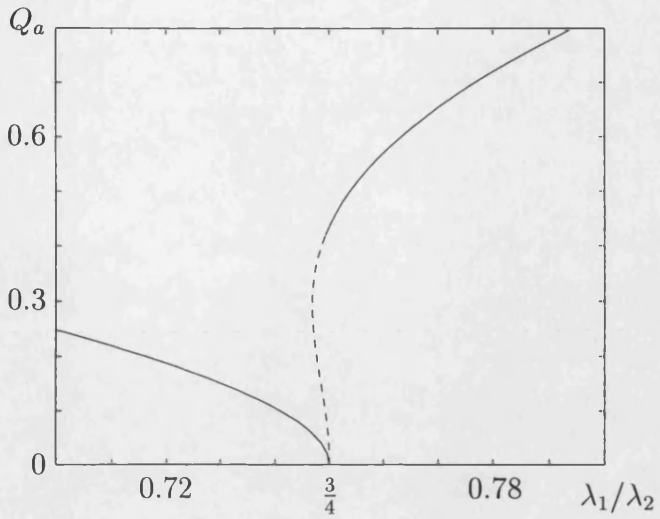

Figure 3.10: Tongue showing interaction between 3 and 4 half-waves.

out at $\lambda_1/\lambda_2 = a/b = 3/4$, where the broken line changes to solid. The secondary bifurcation s_b is again marked by the left-hand arm of the cusp.

3.6.2 Simply-supported strut

An Arnol'd tongues plot summarizes the extent of mode-locking for all possible interactions; however for clarity Fig. 3.11 shows only a handful of tongues and left-hand arms have been truncated. They have been produced by a modal approach which includes the single dominant passive coordinate ($\alpha = 2a - b$); spot checks in AUTO indicate that, as in Fig. 3.7, these curves are barely distinguishable from those that would be produced numerically. Of all the possibilities, only those from positions of stability under increasing load on the lower uncoupled path, depicted by the solid right-hand arms, are practically-relevant. For the simply-supported strut considered here, these cases always involve a jump from mode a to the mode $b = a + 1$. The remainder are from paths that are unstable, either upper uncoupled paths (i.e. p^a is not the minimum critical load) or those lower paths that are already unstable with respect to others waves ($b \neq a + 1$). An example of the latter is the jump from $a = 3$ to $b = 5$ half-waves — a mode jump to $b = 4$ will occur earlier in the post-buckling regime.

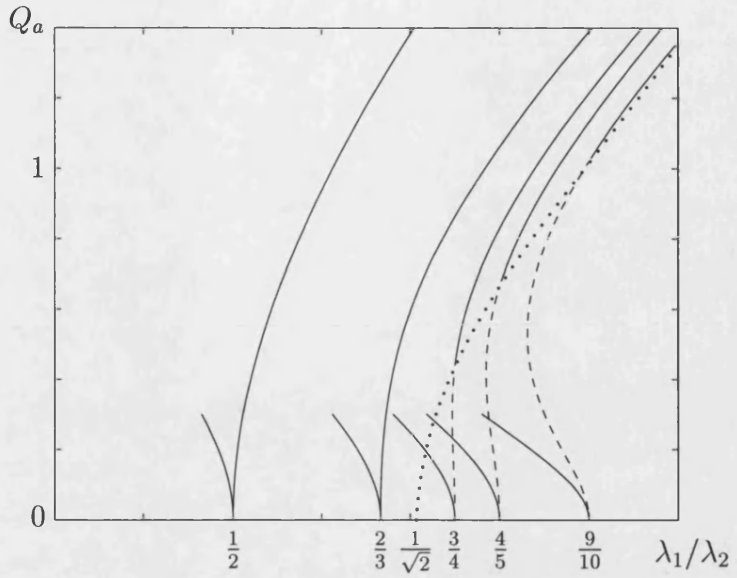

Figure 3.11: Modally produced Arnol'd tongues for (3.58).

With increasing length, more rational positions become available on the real line of λ_1/λ_2, and so more tongues appear. Significantly, although extra tongues appear throughout the space, those describing a loss of initial stability (for which $b = a + 1$) are always born to the right of those that have gone before, with the infinitely-long strut lying at the right-hand edge where $\lambda_1/\lambda_2 = 1$. If a newly established cusp appears to the right of $\lambda_1/\lambda_2 = 1/\sqrt{2}$, Fig. 3.6 shows that the smallest amplitude of secondary buckling is given when $\lambda_1/\lambda_2 = a/b$ for each combination of modes. The locus of these points is shown by the dotted line (again produced using the modal approximation), the region to the right of which can be usefully described as a *safety envelope* inside which no secondary buckling can occur. Tongues with values of $\lambda_1/\lambda_2 < 1/\sqrt{2}$ are outside the safety envelope, with the right hand arm moving initially to the right, and so mode jumping could occur at vanishingly-small amplitudes just above p^a (Fig. 3.5(a)).

What is perhaps more surprising is that the safety envelope increases in the Q_a sense as $\lambda_1/\lambda_2 \to 1$. This implies that, as the strut gets longer and the interacting wavenumbers get relatively closer together, secondary bifurcation is increasingly delayed. This seems counter-intuitive, as it might be thought that the interactions present in shorter systems, where the boundary conditions place

considerable restriction on the choice of wave, would always be available to the less restricted longer strut. This is not the case. Consider for example the interaction between $a = 4$ and $b = 5$, where the worst case scenario takes place when $\lambda_1/\lambda_2 = 4/5$ on the Arnol'd tongue picture of Fig. 3.11. In a system of exactly double the length the critical load plot of Fig. 3.3 reveals that the strut would buckle into $a = 9$ half-waves (rather than $a = 8$), and subsequently jumps to $b = 10$. The worst-case interaction for this latter problem is now at $\lambda_1/\lambda_2 = 9/10$, with the safety envelope showing that secondary bifurcation is inevitably further delayed. However comparing the $\frac{4}{5}$ and $\frac{9}{10}$ tongues for the case where the initial wavelengths are the same, for example $l = 0.95a\pi \Rightarrow \lambda_1/\lambda_2 \approx 0.9$, shows the expected decrease in post-buckling reserve.

3.7 Concluding remarks

This chapter investigates the phenomena of mode locking and mode jumping in the post-buckling of the simply-supported strut on a stiffening elastic foundation, culminating in the summary curves of Fig. 3.11 produced by application of the general theory of elastic stability. Results are checked against numerical runs using the boundary value solver AUTO, with good agreement in the range of interest. This shows that a modal analysis, although asymptotic, can capture the nature of the full behaviour as described by numerical solutions of the differential equation. Initial nonlinear effects, in particular the important secondary bifurcation positions, are seen to be well represented by two modes alone when $|p^a - p^b|$ is small, but less successfully as p^a and p^b separate and push the secondary bifurcations up the uncoupled paths. The complete picture of coupled paths and secondary bifurcations is only successfully portrayed when the dominant passive effect is included.

The mechanism leading to mode jumping has now been described for the relatively simple one-dimensional strut problem. In the next chapter the same

approach is applied to the more difficult plate problem: it will be interesting to see if the qualitative features of the strut behaviour, such as the safety envelope, also appear for the axially-compressed plate.

Chapter 4

Simply-supported plate

For the one-dimensional supercritical strut of the previous chapter only the boundary conditions at each end, which can be varied between the extremes of simply-supported and clamped, have to be specified. In the two-dimensional plate problem these correspond to the boundary conditions on the (short) loaded edges — however those on the long edges and the in-plane constraints also have to be considered. As discussed earlier, many combinations of the numerous possibilities that this introduces have been covered in the literature. Only results for the simplest case — both long and short edges simply-supported — are presented in this chapter, allowing direct comparisons with the strut behaviour and investigation of the effects of the in-plane boundary conditions (shown in Fig. 1.10). Results are again presented in the form of Arnol'd tongues (Arnol'd, 1965), which highlight any changes in stability due the differing in-plane constraints.

The choice of simply-supported edges allows a modal approximation to be used in both the longitudinal and transverse directions (Supple, 1970; Uemura & Byon, 1977). Comparing the results of Nakamura & Uetani (1979) and Maaskant & Roorda (1992) shows that there are numerous passive contaminations in the more difficult plate problem. The previous chapter showed that a *single* dominant passive mode had a significant impact on the coupled behaviour of the supercritical

strut and therefore, if a modal approach is to be successful here, it is important to ensure that all the passive effects are included. Validation with a suitable numerical technique is thus essential, obvious candidates being the numerical partial differential equation (PDE) solvers which can track solution paths and log bifurcation points (Riks *et al.*, 1996; Gervais *et al.*, 1997). However these programs tend to be time consuming and are not suitable for use over a large number of boundary conditions and lengths.

Here a third method is introduced. By noting that the mode interaction causing the loss of stability occurs along the length of the plate, with the transverse profile remaining similar throughout, the coupled PDEs are reduced to a series of ODEs in the longitudinal coordinate x using the Galerkin procedure. These equations can then be solved using AUTO (Doedel *et al.*, 1995). This method has previously been employed with the axially-compressed cylinder (Lord *et al.*, 1997), where again the PDEs were reduced to a series of ODEs solved by AUTO. Limitations of the Rayleigh–Ritz analysis are explored by comparing predictions of the secondary bifurcation points with those given numerically. If the number of contaminating passive modes is large — and this analytical method becomes impractical — the ODE approach may be both more accurate and quicker. The latter will be certainly be faster than full numerical solutions while hopefully retaining its accuracy; to check, results are compared with finite difference solutions.

Finally, the post-buckling behaviour is explored in detail by AUTO, highlighting the increased contaminating effects of the large number of passive modes, especially in the coupled paths.

4.1 Differential equation

The post-buckling of a thin plate is described by the von Kármán large-deflection equations, derived in Chapter 2 (2.49),

$$\begin{aligned} D\nabla^4 w &= \left(Et\ddot{\varphi}'' - P_x\right)\ddot{w} - 2Et\ddot{\varphi}'\ddot{w}' + \left(Et\ddot{\varphi} - P_y\right)\ddot{w}'', \\ \nabla^4\varphi &= \ddot{w}'^2 - \ddot{w}\ddot{w}'', \end{aligned} \tag{4.1}$$

where the first is an equilibrium and the second a compatibility equation. To recap, dots and primes denote partial differentiation with respect to x and y; P_x and P_y are the average applied loads per unit of length in the x and y directions respectively; w is the out-of-plane displacement; and φ is a stress function describing the change from the uniformly compressed state, defined by

$$\sigma_x = E\ddot{\varphi}'' - \frac{P_x}{t}, \quad \tau_{xy} = -E\ddot{\varphi}', \quad \sigma_y = E\ddot{\varphi} - \frac{P_y}{t}. \tag{4.2}$$

4.1.1 Nondimensionalization

As for the strut, the equations are nondimensionalized, giving:

$$\nabla^4\bar{w} = \ddot{\bar{w}}\left(\ddot{\bar{\varphi}}'' - \pi^2 p_x\right) - 2\ddot{\bar{w}}'\ddot{\bar{\varphi}}' + \ddot{\bar{w}}''\left(\ddot{\bar{\varphi}} - \pi^2 p_y\right), \tag{4.3}$$

$$\nabla^4\bar{\varphi} = \ddot{\bar{w}}'^2 - \ddot{\bar{w}}\ddot{\bar{w}}'', \tag{4.4}$$

where

$$\bar{w} = \sqrt{\frac{Et}{D}}w, \quad \bar{\varphi} = \frac{Et}{D}\varphi, \quad p_x = \frac{1}{\pi^2 Et}P_x, \quad p_y = \frac{1}{\pi^2 Et}P_y, \tag{4.5}$$

and dots and primes now denote partial differentiation with respect to $\bar{x}$ and $\bar{y}$, defined by

$$\bar{x} = \sqrt{\frac{Et}{D}}x, \quad \bar{y} = \sqrt{\frac{Et}{D}}y. \tag{4.6}$$

Similarly, the nondimensionalized energy integral (2.38) is,

$$\begin{aligned}\bar{V} = &\frac{1}{2}\int_0^1\int_0^l \left(\ddot{\bar{w}} + \bar{w}''\right)^2 - 2(1-\nu)\left(\ddot{\bar{w}}\bar{w}'' - \dot{\bar{w}}'^2\right) \mathrm{d}\bar{x}\mathrm{d}\bar{y} \\ &+ \frac{1}{2}\int_0^1\int_0^l \left(\ddot{\bar{\varphi}} + \bar{\varphi}''\right)^2 - 2(1+\nu)\left(\ddot{\bar{\varphi}}\bar{\varphi}'' - \dot{\bar{\varphi}}'^2\right) \mathrm{d}\bar{x}\mathrm{d}\bar{y} \\ &- \frac{1}{2}\int_0^1\int_0^l \pi^2 p_x \dot{\bar{w}}^2 \,\mathrm{d}\bar{x}\mathrm{d}\bar{y} \\ &- \frac{1}{2}\int_0^1\int_0^l \pi^2 p_y \bar{w}'^2 \,\mathrm{d}\bar{x}\mathrm{d}\bar{y} \\ &- \int_0^1\int_0^l \bar{\varphi}\left(\nabla^4\bar{\varphi} - \dot{\bar{w}}'^2 + \ddot{\bar{w}}\bar{w}''\right) \mathrm{d}\bar{x}\mathrm{d}\bar{y}. \end{aligned} \tag{4.7}$$

Again the nondimensional values are used and the bar is dropped for the remainder of the chapter.

4.2 Boundary conditions

A simply-supported plate of unit width and length l is considered with the three different sets of in-plane boundary conditions shown in Fig. 1.10. For each case all four edges are simply-supported, i.e. there are no out-of-plane deflections or bending moments at the plate edges;

$$\begin{aligned} &w(0,y) = w(l,y) = w(x,0) = w(x,1) = 0, \\ &\ddot{w}(0,y) = \ddot{w}(l,y) = w''(x,0) = w''(x,1) = 0. \end{aligned} \tag{4.8}$$

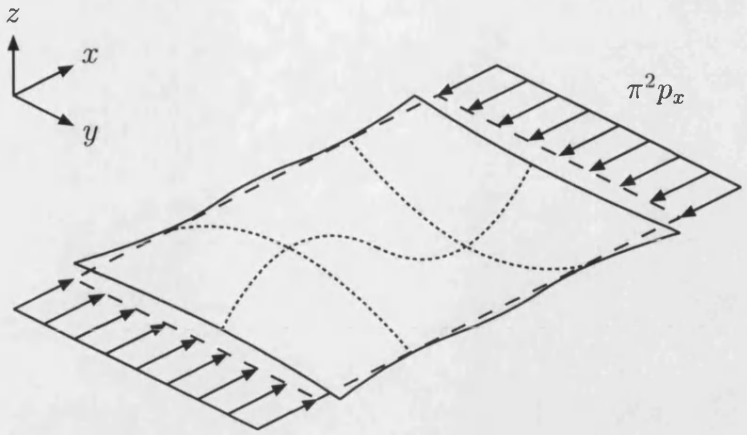

Figure 4.1: Simply-supported plate with free edges. Broken lines show unloaded plate and solid lines the (exaggerated) post-buckling shape.

4.2.1 Free-edged

The simplest loading case occurs when there is a uniform applied load ($\pi^2 p_x$) on the short edges and no applied or reactive stresses on the long edges, as shown in Fig. 4.1. This implies that all edges are free to move in the plane of the plate. However, in this case the coupled behaviour for *all* lengths is described by the general form shown in Fig. 3.4 where no secondary bifurcations occur on the natural loading path (Supple, 1970; Gervais *et al.*, 1997). Therefore mode jumping is absent, and further analysis is not pursued. Unlike the right-hand arms of the Arnol'd tongues shown in Fig. 3.11 which all (eventually) veer to the right, both arms of the cusps relating to this stable behaviour will veer to the left. In addition, this is the least practical of the in-plane boundary conditions considered here: unlike the straight-edged and clamped in-plane cases below (where mode jumping *does* occur), it is not immediately apparent how multiple plates with free-edged boundaries could be used to construct more complex structures.

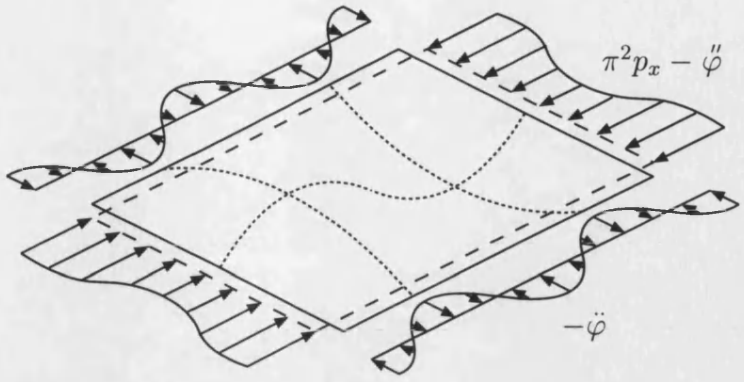

Figure 4.2: Simply-supported plate with straight edges. Broken lines show unloaded plate and solid lines the (exaggerated) post-buckling shape.

4.2.2 Straight-edged

Straight edges implies that the end-shortening Δ, obtained by integration over the length, is constant across the width. Using (2.30), this gives

$$\Delta = \int_0^l \dot{u}\, \mathrm{d}x = \int_0^l \left(\varepsilon_x - \frac{1}{2}\dot{w}^2\right) \mathrm{d}x = \text{constant}. \tag{4.9}$$

A similar equation holds across the width; substituting for ε (2.6) and then σ (2.34) gives (in nondimensional terms),

$$\begin{aligned} \int_0^l \dot{u}\, \mathrm{d}x &= \int_0^l \left(\ddot{\varphi}'' - \pi^2 p_x - \nu(\ddot{\varphi}'' - \pi^2 p_y) - \frac{1}{2}\dot{w}'^2\right) \mathrm{d}x, \\ \int_0^1 \dot{v}'\, \mathrm{d}y &= \int_0^1 \left(\ddot{\varphi}'' - \pi^2 p_y - \nu(\ddot{\varphi}'' - \pi^2 p_x) - \frac{1}{2}\dot{w}'^2\right) \mathrm{d}y. \end{aligned} \tag{4.10}$$

Both should be constant for straight edges. Fig. 4.2 shows that to achieve this, although the total load $p_y = 0$, the stresses at the plate boundaries are no longer uniform, with the variation from the uniformly compressed state being described by φ.

While the boundary conditions on w are relatively simple to define (see equation (4.8)), those on φ are less straightforward. Consider the boundary conditions on the short ($x = 0, l$) edges. As the plate has constant width and zero (w) displacement at each end, symmetry considerations suggest that the values of $\ddot{\varphi}$

will be the same, giving

$$\ddot{\varphi}(l,y) - \ddot{\varphi}(0,y) = 0. \tag{4.11}$$

In the strut problem, positive and negative deflections of equal magnitude give the same foundation energy. The same symmetry applies here, and hence the stress function is independent of the sign of the deflection. The buckle pattern at the intersection of two identically loaded plates, placed end-to-end, will be continuous and antisymmetrical: therefore the corresponding stress distribution must be symmetrical, implying

$$\frac{\partial \sigma_y}{\partial x} = 0 \Rightarrow \frac{\partial \ddot{\varphi}}{\partial x} = \dddot{\varphi} = 0 \text{ at } x = 0, l. \tag{4.12}$$

By definition φ measures the *variation* from the uniformly applied load and hence

$$\int_0^1 \ddot{\varphi} \, \mathrm{d}y = 0 \text{ at } x = 0, l. \tag{4.13}$$

These three constraints — (4.11), (4.12) and (4.13) — combine to satisfy the remaining boundary conditions defined by (2.52); the same arguments can be used on the long edges to satisfy (2.53), giving;

$$\begin{aligned} &\ddot{\varphi}(x,0) - \ddot{\varphi}(x,1) = 0, \\ &\frac{\partial \ddot{\varphi}}{\partial y} = \dddot{\varphi} = 0 \text{ at } y = 0, 1, \\ &\int_0^l \ddot{\varphi} \, \mathrm{d}x = 0 \text{ at } y = 0, 1. \end{aligned} \tag{4.14}$$

4.2.3 Clamped in-plane

For the plate that is clamped in-plane (Fig. 4.3) — such that the long boundaries are restrained from moving in the transverse direction but remain free to move longitudinally — the average transverse applied stress is non-zero. Before buck-

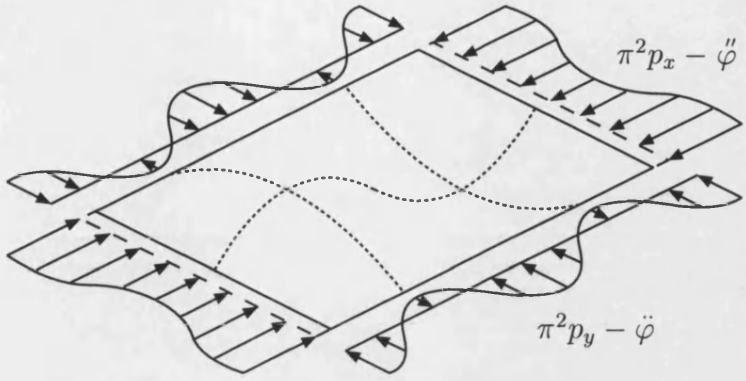

Figure 4.3: Simply-supported plate with long edges clamped in-plane. Broken lines show unloaded plate and solid lines the (exaggerated) post-buckling shape.

ling it is clear that $p_y = \nu p_x$ (where ν is Poisson's ratio); however this no longer holds in the post-buckling regime. Rearranging the second equation of (4.10) and equating to zero gives the following relationship,

$$p_y = \nu p_x + \frac{1}{\pi^2} \int_0^1 \left(\ddot{\varphi} - \nu \varphi'' - \frac{1}{2} \dot{w}^2 \right) \mathrm{d}y. \tag{4.15}$$

The boundary conditions for w and φ are the same as for the straight-edged case.

In the remainder of this chapter the single loading parameter $p \equiv p_x$ will be varied — where necessary p_y is substituted using (4.15).

4.3 Critical loads

The critical loads can be found by linearizing (4.3) and (4.15), to give

$$\nabla^4 w = -\ddot{w} \pi^2 p - w'' \nu \pi^2 p \tag{4.16}$$

for the clamped in-plane boundary conditions of Fig. 4.3. Substituting $w = A \mathrm{e}^{\Lambda \pi x} \sin \pi y$, leads to the characteristic equation,

$$\Lambda^4 + \Lambda^2 (p - 2) + 1 - \nu p = 0. \tag{4.17}$$

When $4 - 4\nu < p < 1/\nu$, Λ^2 is real and negative,

$$\Lambda^2 = -\frac{p-2}{2} \pm \sqrt{\frac{(p-2)^2}{4} + \nu p - 1}, \tag{4.18}$$

leading to four imaginary eigenvalues. As for the strut the two negative eigenvalues can be absorbed by the boundary conditions, leaving

$$\lambda_1 = \sqrt{\frac{p-2}{2} - \sqrt{\frac{(p-2)^2}{4} + \nu p - 1}},$$

$$\lambda_2 = \sqrt{\frac{p-2}{2} + \sqrt{\frac{(p-2)^2}{4} + \nu p - 1}}. \tag{4.19}$$

The deflected shape for a simply-supported plate of length l will typically consist of a single mode of wavenumber a,

$$w = A \sin \lambda \pi x \sin \pi y = Q_a \sin \frac{a \pi x}{l} \sin \pi y, \tag{4.20}$$

and therefore $\lambda = a/l$ (where λ is either λ_1 or λ_2). Substituting this value into (4.17) gives the critical loads for buckling into a half-waves at all plate lengths,

$$p^a = \frac{(a^2 + l^2)^2}{(a^2 + \nu l^2)\, l^2}. \tag{4.21}$$

In dimensional terms the critical loads for a plate of unit width are

$$P^a = \pi^2 D \frac{(a^2 + L^2)^2}{(a^2 + \nu L^2)\, L^2}. \tag{4.22}$$

The values of λ, p^a and P^a for both the free- and straight-edged cases of Figs. 4.1 and 4.2 can be found by substituting $\nu = 0$ into (4.19), (4.21) and (4.22) respectively.

The variations in critical load for the first four mode numbers are shown in Fig. 4.4 over a range of plate lengths. Critical loads for the clamped in-plane plate are lower than those for the straight-edged plate, with their minima occurring

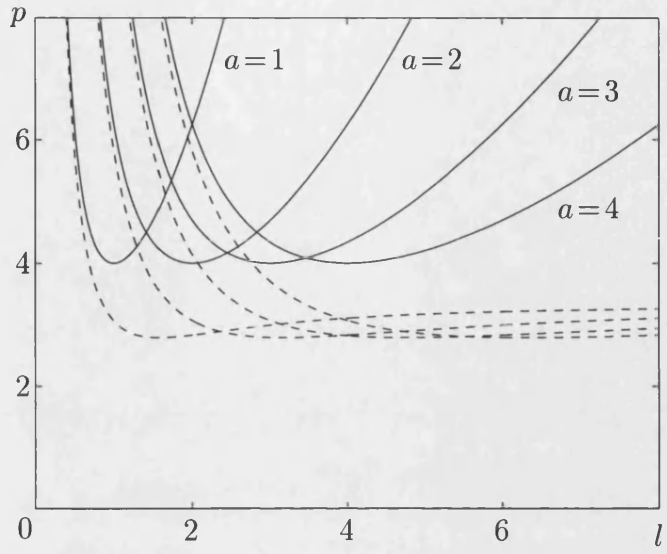

Figure 4.4: Critical load variations with length for (a) straight-edged (solid lines) and (b) clamped in-plane plates with $\nu = 0.3$ (broken lines).

at relatively greater lengths. This is due to pre-buckling compression across the width, causing it to buckle at a load lower than when such compression is absent. At discrete plate lengths, the critical loads for different modes coincide at compound bifurcation points, where the values of λ_1/λ_2 are rational. For the straight-edged plate, $\lambda_1/\lambda_2 \to 0$ as $p \to \infty$ and therefore rational positions (and compound bifurcation points) can occur for all $p > 4$. If the edges are clamped in-plane, λ_2 again tends to infinity as $p \to \infty$, and for short wavelengths the critical loads for the two cases are similar. However, $\lambda_1 = 0$ when $p = 1/\nu$; this corresponds to an infinite wavelength and hence $p^a \to 1/\nu$ as $l \to \infty$ (Fig. 4.4). As a consequence, the compound bifurcation points are restricted to the range $4 - 4\nu < p < 1/\nu$.

4.4 Rayleigh–Ritz formulation

Exact analytical solutions of (4.3) which satisfy simply-supported boundary conditions (4.8) are given by a double-infinite summation (Szilard, 1974),

$$w = \sum_{m=1}^{\infty}\sum_{n=1}^{\infty} Q_{mn} \sin\frac{m\pi x}{l} \sin n\pi y. \tag{4.23}$$

To make the problem practicable a Rayleigh–Ritz approach — with a finite number of modes along the length and width — is used. The stress function φ is found by substituting this function for w into (4.4) and integrating directly. For a two d.o.f. model,

$$w = \left(Q_a \sin\frac{a\pi x}{l} + Q_b \sin\frac{b\pi x}{l}\right) \sin \pi y, \tag{4.24}$$

(where $Q_a \equiv Q_{a1}$ and $Q_b \equiv Q_{b1}$ in (4.23) above) integration of (4.4) gives

$$\begin{aligned}
\varphi = {} & \frac{1}{32}Q_a^2\left(\frac{l^2}{a^2}\cos\frac{2a\pi x}{l} + \frac{a^2}{l^2}\cos 2\pi y\right) \\
& + \frac{1}{4}Q_aQ_b\left(\frac{l^2}{(a+b)^2}\cos\frac{(a+b)\pi x}{l} + \frac{l^2}{(a-b)^2}\cos\frac{(a-b)\pi x}{l}\right. \\
& \qquad - \frac{(a-b)^2l^2}{\left((a+b)^2+4l^2\right)^2}\cos\frac{(a+b)\pi x}{l}\cos 2\pi y \\
& \qquad \left. + \frac{(a+b)^2l^2}{\left((a-b)^2+4l^2\right)^2}\cos\frac{(a-b)\pi x}{l}\cos 2\pi y\right) \\
& + \frac{1}{32}Q_b^2\left(\frac{l^2}{b^2}\cos\frac{2b\pi x}{l} + \frac{b^2}{l^2}\cos 2\pi y\right).
\end{aligned} \tag{4.25}$$

Interestingly, these functions for w and φ satisfy the straight-edged boundary conditions: substituting (4.24) and (4.25) into (4.10), integrating and simplifying,

leaves

$$\int_0^l \dot{u}\,\mathrm{d}x = -\pi^2 p_x l + \nu\pi^2 p_y - \frac{1}{8}\frac{\pi^2}{l}\left(a^2Q_a^2 - b^2Q_b^2\right),$$
$$\int_0^1 \dot{v}\,\mathrm{d}y = -\pi^2 p_y + \nu\pi^2 p_x - \frac{1}{8}\pi^2\left(Q_a^2 + Q_b^2\right), \tag{4.26}$$

which, being independent of x and y, are constant. For the clamped in-plane case p_y (4.15) is defined by

$$p_y = \nu p_x - \frac{1}{8}\left(Q_a^2 + Q_b^2\right). \tag{4.27}$$

4.4.1 Energy integral

Before substituting (4.24) and (4.25) into (4.7) to generate an expression for the total potential energy, some terms can be eliminated. As the expression for φ was derived using the compatibility equation, the last term (which essentially repeats this equation) will be zero. In addition, for the straight-edged case both p_y is zero cancelling the fourth term. Therefore the energy integral reduces to

$$\begin{aligned} V = {} & \frac{1}{2}\int_0^1\int_0^l \left(\ddot{w} + \dot{w}''\right)^2 - 2(1-\nu)\left(\ddot{w}\dot{w}'' - \dot{w}'^2\right)\,\mathrm{d}x\mathrm{d}y \\ & + \frac{1}{2}\int_0^1\int_0^l \left(\ddot{\varphi} + \dot{\varphi}''\right)^2 - 2(1+\nu)\left(\ddot{\varphi}\dot{\varphi}'' - \dot{\varphi}'^2\right)\,\mathrm{d}x\mathrm{d}y \\ & - \frac{1}{2}\int_0^1\int_0^l \pi^2 p\,\dot{w}^2\,\mathrm{d}x\mathrm{d}y. \end{aligned} \tag{4.28}$$

Substituting (4.24) and (4.25) into this equation gives the following energy function;

$$V = \frac{1}{24}\sum_{a=1}^{\infty}\sum_{b=1}^{\infty}\sum_{c=1}^{\infty}\sum_{d=1}^{\infty} V_{abcd}Q_aQ_bQ_cQ_d + \frac{1}{2}\sum_{a=1}^{\infty} V'_{aa}\left(p - p^a\right)Q_a^2, \tag{4.29}$$

which is identical to that of the strut on a stiffening foundation (3.24). As a result, zero and non-zero V_{abcd} terms occur for the same combinations of a, b, c

and d; however the non-zero coefficients (listed in Appendix B) are more complex.

The theory that was used with the simply-supported strut also applies here: equilibrium solutions are given where

$$\frac{\partial V}{\partial Q_a} = \frac{\partial V}{\partial Q_b} = \cdots = 0, \tag{4.30}$$

and a first-order approximation of an uncoupled path by (3.28),

$$p = p^a - \frac{1}{6}\frac{V_{aaaa}}{V'_{aa}}Q_a^2. \tag{4.31}$$

Similarly, the amplitude of the secondary bifurcations s_a using a two mode analysis (4.24) is (Supple, 1967),

$$Q_{s_a} = \frac{6V'_{aa}V'_{bb}}{3V'_{aa}V_{aabb} - V'_{bb}V_{aaaa}}(p^b - p^a). \tag{4.32}$$

4.4.2 Passive contamination

However work on the simply-supported strut in the previous chapter and the simply-supported plate (Nakamura & Uetani, 1979) shows that this two d.o.f. approximation is only accurate for small amplitudes. The approximation for the uncoupled path (i.e. $Q_b = 0$) can be improved by adding either the longitudinal harmonic $\beta = 3a$,

$$w = \left(Q_a \sin\frac{a\pi x}{l} + Q_\beta \sin\frac{\beta\pi x}{l}\right)\sin\pi y, \tag{4.33}$$

or both the longitudinal and transverse harmonics,

$$w = \left(Q_a \sin\frac{a\pi x}{l} + Q_\beta \sin\frac{\beta\pi x}{l}\right)\sin\pi y + \left(Q_{a3} \sin\frac{a\pi x}{l} + Q_{\beta 3} \sin\frac{\beta\pi x}{l}\right)\sin 3\pi y. \tag{4.34}$$

The expression for the coupled path can be improved in a similar manner by including further passive modes, although both (3.55) and (3.56) increase in size and complexity. For example, if the longitudinal harmonic $\beta = 3a$ and three passive modes (α, γ and δ) are used, the positions of the secondary bifurcations s_a are found by solving the stability determinant,

$$\begin{vmatrix} W_{bb} & W_{b\alpha} & W_{b\gamma} & W_{b\delta} \\ W_{b\alpha} & W_{\alpha\alpha} & W_{\alpha\gamma} & W_{\alpha\delta} \\ W_{b\gamma} & W_{\alpha\gamma} & W_{\gamma\gamma} & W_{\gamma\delta} \\ W_{b\delta} & W_{\alpha\delta} & W_{\gamma\delta} & W_{\delta\delta} \end{vmatrix} = 0, \tag{4.35}$$

while inclusion of the transverse harmonics will give an 8×8 matrix and a determinant quadruple the size. Subscripts again denote differentiation with respect to the variable, for example

$$W_{b\alpha} = \frac{\partial^2 V}{\partial Q_b \partial Q_\alpha}. \tag{4.36}$$

Although the coupled solutions will contain numerous passive modes, only those which have interactions with the other passive modes — and therefore have non-zero off-diagonal $W_{b\alpha}$ terms — will affect the position of the secondary bifurcations. In descending order of importance, they are (Nakamura & Uetani, 1979): $\alpha = 2a - b$, $\gamma = 2a + b$, $\delta = 4a - b$, $\epsilon = 4a + b$ etc. (note that β is used for the longitudinal harmonic $3a$).

The secondary bifurcation positions given by this analysis are compared with those from AUTO, and the uncoupled solutions validated with those given by a finite difference approach. (These solution methods are described in the following two sections.) Therefore, unlike other work (Supple, 1970; Uemura & Byon, 1977; Maaskant & Roorda, 1992), the dominant harmonics and passive modes can be identified and the limitations of this approach assessed.

4.5 Reduction to ODEs

The mode interaction which leads to mode jumping occurs along the length of the plate while the profile across the width remains reasonably constant. Therefore, by expressing the transverse deflection as a number of sinusoidal functions, the PDEs can be reduced to a series of ODEs in x using the Galerkin procedure. This effectively includes the full compliment of passive modes along the length, and secondary bifurcation positions can now be found using AUTO (Doedel *et al.*, 1995), with much quicker solution times than for PDE solvers (Riks *et al.*, 1996; Gervais *et al.*, 1997). A similar approach was used when investigating the post-buckling behaviour of axially-compressed cylinders (Lord *et al.*, 1997) where deflection in the circumferential direction was assumed to be periodic.

4.5.1 Galerkin reduction

The Galerkin procedure (see for example Szilard, 1974) defines a series of integrals, each of which is given by one of the assumed functions multiplied by the governing differential equation. These integrals are then evaluated over the range of interest, setting the total residual error associated with each function to zero and, in this application, producing a set of ODEs.

For the plate problem with a single transverse deflection profile (4.24), it can be seen from (4.25) that the expression for stress depends on two transverse functions, and hence w and φ are defined as

$$\begin{aligned} w(x,y) &= w_1(x)\sin\pi y, \\ \varphi(x,y) &= \varphi_1(x) + \varphi_2(x)\cos 2\pi y. \end{aligned} \tag{4.37}$$

Multiplying each of these transverse functions by the relevant von Kármán equa-

tion, (4.3) or (4.4), gives the following three integrals;

$$\begin{aligned}
&\int_0^1 \left(\nabla^4 w - \ddot{w}(\ddot{\varphi} - p_x) + 2\dot{w}\dot{\varphi} - \ddot{w}(\ddot{\varphi} - p_y)\right) \sin \pi y \, \mathrm{d}y = 0, \\
&\int_0^1 \left(\nabla^4 \varphi - \dot{w}^2 + \ddot{w}\ddot{w}\right) \mathrm{d}y = 0, \\
&\int_0^1 \left(\nabla^4 \varphi - \dot{w}^2 + \ddot{w}\ddot{w}\right) \cos 2\pi y \, \mathrm{d}y = 0.
\end{aligned} \tag{4.38}$$

Substitution of (4.37) and evaluation produces three fourth-order ODEs,

$$\begin{aligned}
&\dddot{w}_1 - \pi^2 \ddot{w}_1 (2 - p_x) + \pi^4 w_1 (1 - p_y) \\
&\qquad + \frac{1}{2}\pi^2 \left(2 w_1 \ddot{\varphi}_1 - w_1 \ddot{\varphi}_2 - 4 \dot{w}_1 \dot{\varphi}_2 - 4 \ddot{w}_1 \varphi_2\right) = 0, \\
&\dddot{\varphi}_1 - \frac{1}{2}\pi^2 \left(\dot{w}_1^2 + w_1 \ddot{w}_1\right) = 0, \\
&\dddot{\varphi}_2 - 8\pi^2 \ddot{\varphi}_2 + 16\pi^4 \varphi_2 - \frac{1}{2}\pi^2 \left(\dot{w}_1^2 - w_1 \ddot{w}_1\right) = 0,
\end{aligned} \tag{4.39}$$

where w_1, φ_1 and φ_2 (and their derivatives) will be given by AUTO.

Accuracy can be improved by including the first transverse harmonic, giving two displacement and four stress functions,

$$\begin{aligned}
w(x, y) &= w_1(x) \sin \pi y + w_2(x) \sin 3\pi y, \\
\varphi(x, y) &= \varphi_1(x) + \varphi_2(x) \cos 2\pi y + \varphi_3(x) \cos 4\pi y + \varphi_4(x) \cos 6\pi y.
\end{aligned} \tag{4.40}$$

The Galerkin procedure now produces six fourth-order ODEs.

4.5.2 Boundary conditions

All the boundary conditions on the long ($y = 0, 1$) edges and the integral condition (4.13) are satisfied by the functions defined in (4.37) for both the straight-edged

and clamped in-plane cases. Equation (4.8) implies

$$w_1(0) = w_1(l) = \ddot{w}_1(0) = \ddot{w}_1(l) = 0, \tag{4.41}$$

and the assumption of no applied shear (2.51)

$$\begin{aligned} \ddot{\varphi}(0, y) &= 2\pi\dot{\varphi}_2(0) \sin 2\pi y = 0 \Rightarrow \dot{\varphi}_2(0) = 0, \\ \ddot{\varphi}(l, y) &= 2\pi\dot{\varphi}_2(l) \sin 2\pi y = 0 \Rightarrow \dot{\varphi}_2(l) = 0. \end{aligned} \tag{4.42}$$

Similarly the symmetry condition (4.12) gives,

$$\ddot{\varphi}_1(0) = \ddot{\varphi}_2(0) = \ddot{\varphi}_1(l) = \ddot{\varphi}_2(l) = 0, \tag{4.43}$$

and the integral condition of (4.14)

$$\int_0^l \ddot{\varphi}_1 \, \mathrm{d}x = \int_0^l \ddot{\varphi}_2 \, \mathrm{d}x = 0. \tag{4.44}$$

Note that

$$\int_0^l \ddot{\varphi}_2 \, \mathrm{d}x = 0 \Rightarrow \dot{\varphi}_2(l) - \dot{\varphi}_2(0) = 0, \tag{4.45}$$

and hence if $\dot{\varphi}_2(0) = 0$ then $\dot{\varphi}_2(l) = 0$ is automatically satisfied by (4.44) and can be neglected in (4.42). This leaves a total of eleven boundary conditions: four on w_1, three on φ_1 and four on φ_2. As each equation of (4.39) is fourth order, four boundary conditions are required for w_1, φ_1 and φ_2; therefore another boundary condition is required for φ_1. Equation (4.39) shows that the resulting PDEs are not functions of φ_1 or $\dot{\varphi}_1$, and hence the additional constraint $\dot{\varphi}_1(0) = 0$ can be applied without affecting the results.

Substituting (4.37) into (4.10) gives expressions for the straight-edged constraints,

$$\begin{aligned}\int_0^l \dot{u}\,\mathrm{d}x &= \int_0^l \Big(\nu\pi^2 p_y - \pi^2 p_x - 4\pi^2\varphi_2\cos 2\pi y \\ &\qquad - \nu\big(\ddot{\varphi}_1 + \ddot{\varphi}_2\cos 2\pi y\big) - \frac{1}{2}\dot{w}_1^2\sin^2\pi y\Big)\mathrm{d}x \\ &= \int_0^l \Big(\nu\pi^2 p_y - \pi^2 p_x - \nu\ddot{\varphi}_1 - \frac{1}{4}\dot{w}_1^2 \\ &\qquad - \frac{1}{4}\big(4\nu\ddot{\varphi}_2 + 16\pi^2\varphi_2 - \dot{w}_1^2\big)\cos 2\pi y\Big)\,\mathrm{d}x, \qquad (4.46)\end{aligned}$$

$$\int_0^1 \dot{v}\,\mathrm{d}y = \nu\pi^2 p_x - \pi^2 p_y + \ddot{\varphi}_1 - \frac{1}{4}\pi^2 w_1^2. \qquad (4.47)$$

These constraints are again automatically satisfied. To demonstrate this, the equations for $\dddot{\varphi}_1$ and $\dddot{\varphi}_2$ in (4.39) are summed,

$$\begin{aligned}&\ddddot{\varphi}_1 + \ddddot{\varphi}_2 - 8\pi^2\ddot{\varphi}_2 + 16\pi^4\varphi_2 - \pi^2\dot{w}_1^2 = 0 \\ &\quad\Rightarrow \pi^2\big(16\pi^2\varphi_2 - \dot{w}_1^2\big) = 8\pi^2\ddot{\varphi}_2 - \dddot{\varphi}_1 - \dddot{\varphi}_2, \qquad (4.48)\end{aligned}$$

and substituted into (4.46), giving

$$\int_0^l \nu\pi^2 p_y - \pi^2 p_x - \nu\ddot{\varphi}_1 + \frac{1}{4}\dot{w}_1^2 + \left((2-\nu)\ddot{\varphi}_2 - \frac{1}{4\pi^2}(\dddot{\varphi}_1 + \dddot{\varphi}_2)\right)\cos 2\pi y\,\mathrm{d}x. \qquad (4.49)$$

Any variation in end-shortening across the width can only be due to the final term. Equation (4.44) shows that $\ddot{\varphi}_2$ integrates to zero, leaving

$$\left[-\frac{1}{4\pi^2}(\dddot{\varphi}_1 + \dddot{\varphi}_2)\right]_0^1 \cos 2\pi y, \qquad (4.50)$$

which, using the boundary conditions (4.43), is again zero.

For straight long edges, the first derivative of (4.47),

$$\frac{\partial}{\partial x}\left(\nu\pi^2 p_x - \pi^2 p_y + \ddot{\varphi}_1 - \frac{1}{4}\pi^2 w_1^2\right) = \dddot{\varphi}_1 - \frac{1}{2}\pi^2 w_1\dot{w}_1, \qquad (4.51)$$

must be zero for all x. Using (4.41) and (4.43) shows that this is true at $x = 0$

and differentiating again gives the second equation of (4.39); this implies that (4.51) is zero for all x and hence the long edges remain straight. Equation (4.47) also gives p_y for the clamped in-plane case,

$$p_y = \nu p_x + \frac{\ddot{\varphi}_1}{\pi^2} - \frac{1}{4}w_1^2. \tag{4.52}$$

4.5.3 Reduction to first-order form

Rescaling the variables over a unit length and reducing (4.39) to first-order form allows the equations to be solved by AUTO;

$$\begin{aligned}
&\dot{f}_1 = f_2, \quad \dot{f}_2 = f_3, \quad \dot{f}_3 = f_4,\\
&\dot{f}_4 = 2\pi^2 l^2 f_3(2 - p_x) - \pi^4 l^4 f_1(1 - p_y) - \pi^2 l^3\big(f_1 f_7 - \frac{1}{2}f_1 f_{11} - 2f_2 f_{10} - 2f_3 f_9\big),\\
&\dot{f}_5 = f_6, \quad \dot{f}_6 = f_7, \quad \dot{f}_7 = f_8,\\
&\dot{f}_8 = \frac{1}{2}\pi^2 l^3\big(f_1 f_3 + f_2^2\big),\\
&\dot{f}_9 = f_{10}, \quad \dot{f}_{10} = f_{11}, \quad \dot{f}_{11} = f_{12},\\
&\dot{f}_{12} = 8\pi^2 l^2 f_{11} - 16\pi^4 l^4 f_9 - \frac{1}{2}\pi^2 l^3\big(f_1 f_3 - f_2^2\big),
\end{aligned} \tag{4.53}$$

where,

$$\begin{aligned}
&f_1 = \frac{w_1}{l}, \quad f_2 = \dot{w}_1, \quad f_3 = l\ddot{w}_1, \quad f_4 = l^2\dddot{w}_1,\\
&f_5 = \frac{\varphi_1}{l}, \quad f_6 = \dot{\varphi}_1, \quad f_7 = l\ddot{\varphi}_1, \quad f_8 = l^2\dddot{\varphi}_1,\\
&f_9 = \frac{\varphi_2}{l}, \quad f_{10} = \dot{\varphi}_2, \quad f_{11} = l\ddot{\varphi}_2, \quad f_{12} = l^2\dddot{\varphi}_2.
\end{aligned} \tag{4.54}$$

Rewriting the boundary conditions in this notation gives

$$f_1(0) = f_1(1) = f_3(0) = f_3(1) = 0,$$
$$f_6(0) = \int_0^1 f_7 \, \mathrm{d}\tilde{x} = f_8(0) = f_8(1) = 0,$$
$$f_{10}(0) = \int_0^1 f_{11} \, \mathrm{d}\tilde{x} = f_{12}(0) = f_{12}(1) = 0. \tag{4.55}$$

If the first harmonic is included (4.40) a series of twenty-four first-order ODEs are produced and, although the results will be more accurate, solution times will increase.

4.6 Full numerical solution

Although sophisticated finite element programs which track solution paths and locate secondary bifurcation points have been written (Riks *et al.*, 1996; Gervais *et al.*, 1997), they are not generally available and it is beyond the scope of this work to develop one. Therefore a classical finite difference method is used to validate the uncoupled solutions given by the two methods described above. Using Taylor approximations for the derivatives, this technique generates a series of nonlinear algebraic equations (Szilard, 1974) for (4.3) and (4.4). These are solved using an iterative method, the current solution values being substituted back into the algebraic equations and used to give an improved solution. This procedure is repeated until the change is less than a desired tolerance. Although simple to implement, the general nature of this method leads to long convergence times, especially as this problem has relatively high (fourth-order) derivatives. In addition, many grid points are required to maintain accuracy.

For the clamped in-plane case, (4.15) is used directly to calculate p_y. The other integral conditions cannot be implemented directly — however using the bound-

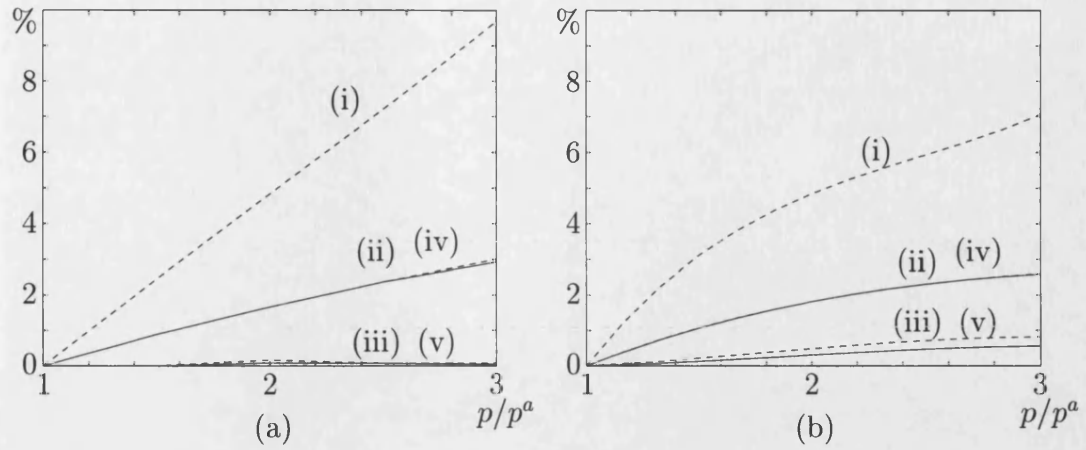

Figure 4.5: Percentage errors in total potential energy (4.28) for (a) straight-edged and (b) clamped in-plane plates. Broken lines compare numerical and Rayleigh–Ritz solutions of (4.29) with (i) one, (ii) two and (iii) four modes. Solid lines compare numerical and AUTO solutions of (iv) (4.37) and (v) (4.40).

ary conditions defined by (4.8) and

$$\dot{\varphi}(0,y) = \dot{\varphi}(l,y) = \acute{\varphi}(x,0) = \acute{\varphi}(x,1) = 0,$$
$$\ddot{\varphi}(0,y) = \ddot{\varphi}(l,y) = \acute{\varphi}(x,0) = \acute{\varphi}(x,1) = 0, \tag{4.56}$$

solutions were found which satisfy both the straight-edged (4.10) and integral (4.13) constraints.

4.7 Validation

4.7.1 Uncoupled paths

Solutions given by the three methods described above are compared by calculating the total potential energy (4.7) of a square plate ($l = 1$) at different loads. The broken lines of Fig. 4.5(a) show percentage differences between the finite difference and Rayleigh–Ritz solutions for the straight-edged plate. Supple (1966) suggests that the deflection with a single mode approximation is reasonably accurate up to $2.5p^a$; however Fig. 4.5 shows that at this load agreement is poor. Addition

of the first harmonic (4.33) gives an error of approximately 3% at $3p^a$, but with inclusion of the transverse harmonics (4.34) this reduces to 0.1%. The solutions of (4.37) and (4.40) by AUTO — shown by the solid lines — are hard to distinguish over the range given from those given by the two- and four-mode Rayleigh–Ritz method; the latter gives excellent agreement with the finite difference solutions. Fig. 4.5(b) shows similar trends for the clamped in-plane case, although with slightly increased errors.

It might be expected that the errors would increase at least linearly with increasing load: that this is not the case in Fig 4.5(b) suggests that the numerical solutions had not fully converged as the solution method used was very slow.

4.7.2 Secondary bifurcations

The maximum amplitude of the secondary bifurcation point which is of interest here occurs at the right-hand edge of Fig. 4.6(a) where $\lambda_1/\lambda_2 = 1$ (implying $p = 4$ and $a = l$ in Fig. 4.4) and $Q_a \approx 8$. Substituting the energy coefficients from Appendix B into (4.31) gives,

$$p = p^a + \frac{1}{16}\left(\frac{a^2}{l^2} + \frac{l^2}{a^2}\right) Q_a^2, \tag{4.57}$$

and hence for $a = l$, $p \approx 12 = 3p^a$. Curve (v) of Fig. 4.5(a) shows that the error for the uncoupled path over this range of loads is negligible and thus the secondary bifurcation positions predicted by AUTO, which includes all the longitudinal passive modes and one transverse mode, should be accurate. In dimensional terms the amplitude is (4.5),

$$\sqrt{\frac{D}{Et}}Q_a = \sqrt{\frac{1}{12(1-\nu^2)}}tQ_a \approx 0.3tQ_a, \tag{4.58}$$

giving a maximum deflection of approximately two-and-a-half times the plate thickness when $Q_a = 8$; for this amplitude the von Kármán equations are still

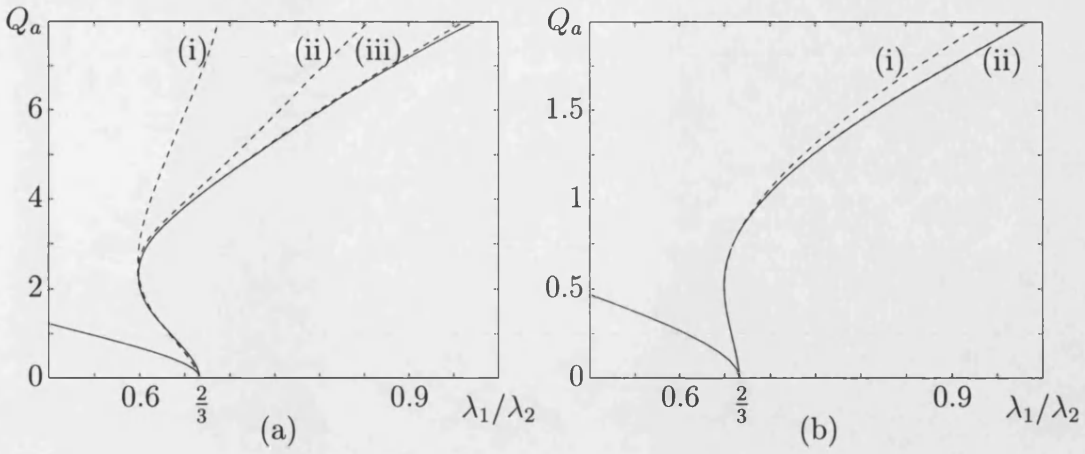

Figure 4.6: Comparison between numerically and modally produced tongues for (a) straight-edged and (b) clamped in-plane plates. Broken lines show modal solutions with (i) 3, (ii) 6 and (iii) 12 modes. Solid lines show AUTO solutions of (4.40).

valid.

The positions of the secondary bifurcation points for the simply-supported strut were found much more quickly using the modal approximation than by using AUTO, especially for large l. If the number of passive modes is small, the same will be true for the plate; the differences between AUTO and three modal approximations are summarized in Figs. 4.6(a) and (b) which show the interaction between two and three half-waves for the two sets of boundary conditions. The simplest modal approximation plotted includes the single passive contamination, $\alpha = 2a - b$; Fig. 4.6(b) shows this only gives good agreement for $Q_a < 1$. This is expected, as agreement between the single mode Rayleigh–Ritz and AUTO solutions for the uncoupled path is poor (curves (i) and (v) of Fig. 4.5(b)). When the effects of the longitudinal harmonic (4.33) and two other passive modes are introduced (giving a, b, $\alpha = 2a - b$, $\beta = 3a$, $\gamma = 2a + b$ and $\delta = 4a - b$), acceptable agreement extends to $Q_a \approx 3$ (curve (ii) of Fig. 4.6(a)). Secondary buckling for the plate with clamped in-plane boundary conditions occurs at relatively low loads, where curve (ii) of Fig. 4.5(b) shows the error using this approximation is less than 1%, and hence the secondary bifurcation positions are indistinguishable from the numerical results (Fig. 4.6(b)). This approximation also gives accurate predictions for s_b as the amplitudes of the secondary bifurcations on the upper

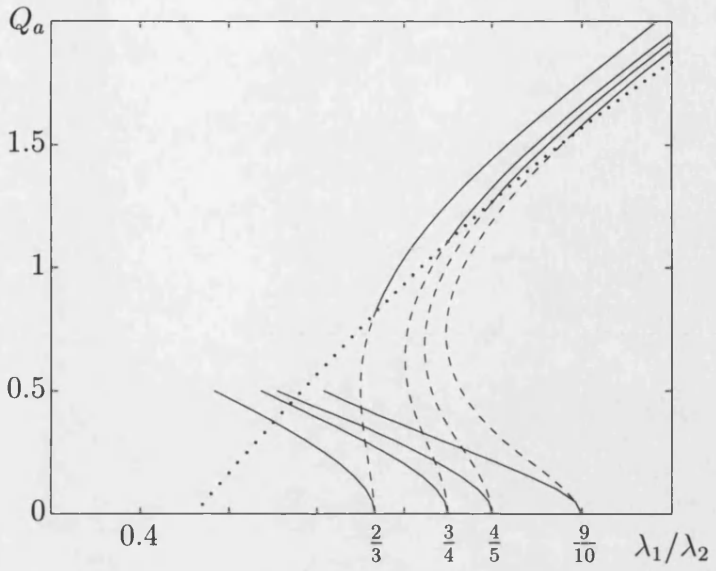

Figure 4.7: Arnol'd tongues produced from AUTO solutions of (4.40) for the clamped in-plane plate.

uncoupled path are also relatively small. Curve (iii) of Fig. 4.6(a) shows that inclusion of the transverse harmonics for each of the six modes listed above gives accurate predictions when $Q_a < 6$. However, this twelve mode approximation gives a very lengthy energy function (4.29) and a 64 element stability matrix (4.35); both are difficult to manipulate and time consuming to solve in MAPLE (Heck, 1996). Therefore, for the straight-edged plate, a modal approximation of sufficient accuracy is not noticeably quicker than AUTO. It also highlights the increase in the number of passive modes as s_a moves away from the primary bifurcation point.

4.8 Arnol'd tongues

The Arnol'd tongues for a plate with clamped in-plane boundary conditions are plotted in Fig. 4.7 using the solutions of (4.40) given by AUTO. Note that λ_1/λ_2 is related to the critical load for each length, and therefore exact values are given by (4.19). As with the strut, most secondary bifurcations occur on uncoupled paths which are already unstable with respect to another mode and therefore have no

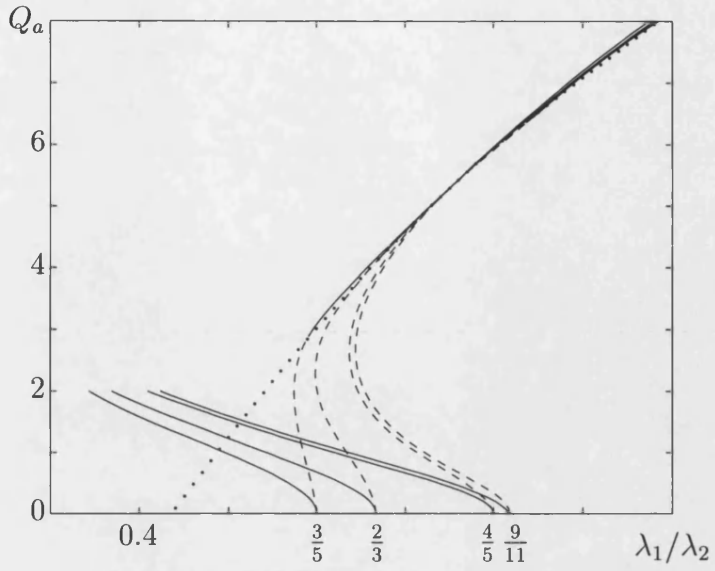

Figure 4.8: Arnol'd tongues produced from AUTO solutions of (4.40) for the straight-edged plate.

practical significance; for clarity, only four tongues which mark secondary bifurcations associated with the initial loss of stability are shown. Two other features are also common to both the strut and the clamped in-plane plate problems: tongues meet the λ_1/λ_2 axis at rational positions (giving the ratio between the number of half-waves before and after mode jumping, a/b) and the case of practical relevance is always $b = a+1$. (The absence of a tongue at $\lambda_1/\lambda_2 = 1/2$ is due to passive contamination and is explored later in Section 4.9.) All the illustrated tongues curve back on themselves and hence there is a *safety envelope* — inside which no secondary buckling can occur — first seen in Fig. 3.11. As the cusps have been constructed from numerical results and not an equation, the safety envelope has been generated by extrapolating from the points on the four curves plotted using a cubic spline in MATLAB (The Math Works, 1993).

The tongues for the straight-edged plate (Fig. 4.8) show the same general behaviour, except that the amplitude of secondary buckling is much greater. Some of the right-hand arms now *cross*, indicating that mode jumping may take place with, say, the mode $b = a + 2$. This is also due to increased contamination from passive modes; the complete picture of the coupled paths is now explored using

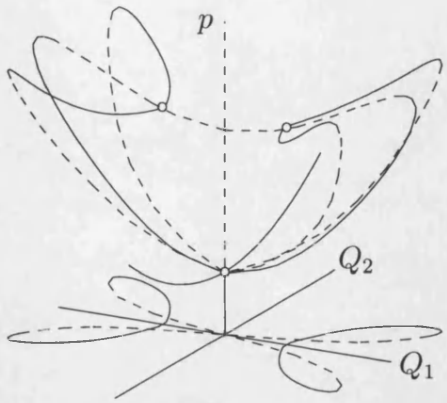

Figure 4.9: Effect of first harmonic at $p^a = p^b$ for the clamped in-plane plate. Stable paths are shown as solid lines and unstable paths as broken lines.

AUTO.

4.9 Passive mode effects

4.9.1 Limit point instability

Even at relatively small amplitudes the effect of the passive modes can be significant; when the primary mode is a single half-wave for example, the amplitude of the first passive harmonic ($\beta = 3a = 3$) also becomes large when Q_a is large. Fig. 4.9 shows the contaminating mechanism by which stability is lost to this harmonic, before the secondary bifurcation marking interaction with a two half-wave solution is encountered. This introduces contamination from $V_{aaa\beta}$, which, being negative (see Appendix B), is destabilizing in nature, whereas V_{aabb} is positive and stabilizing. Thus stability is lost at a limit point which is not picked out by the Arnol'd tongues plot, and accounts for the absence of a tongue at $\lambda_1/\lambda_2 = 1/2$ for both sets of boundary conditions.

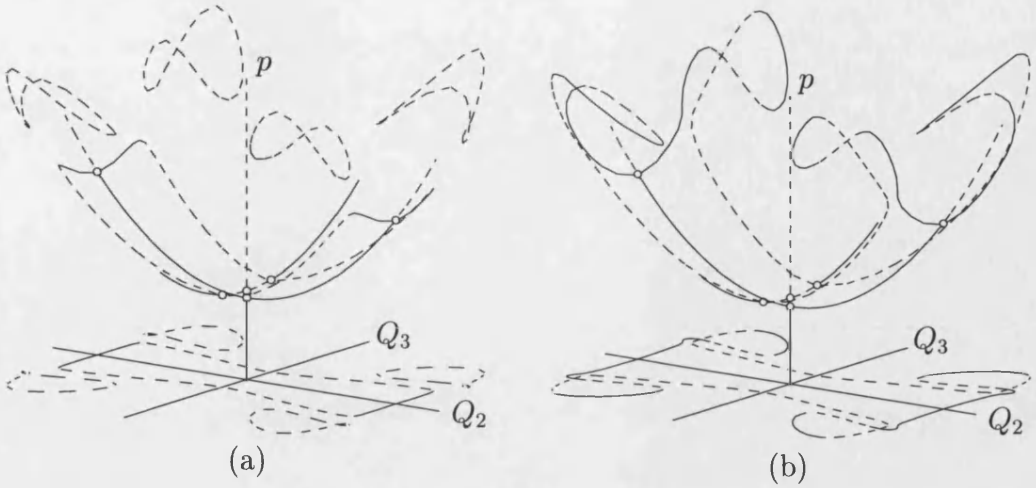

Figure 4.10: Jump from 2 to 3 waves for the clamped in-plane plate, (a) $l = 3.80$, (b) $l = 3.76$. Stable paths are shown as solid lines and unstable paths as broken lines.

4.9.2 Stable secondary bifurcation

For the clamped in-plane plate, secondary buckling from $a = 2$ to $b = 3$ occurs before the uncoupled path is destabilized by the passive harmonic $\beta = 3a = 6$. However, Fig. 4.10(a) shows that at s_a the coupled path is initially stable. Mode jumping is then delayed until a limit point where $p > p^{s_a}$; again, in this instance, the tongue does not show the amplitude where stability is lost. For slightly shorter lengths (Fig. 4.10(b)), the isolated solution path of Fig. 4.10(a) merges with the coupled path. This gives a very complex coupled path, with the amplitudes of some passive modes being greater than Q_a and Q_b, highlighting the increasing effect of passive modes with displacement away from both primary and secondary bifurcation points. Stability is now lost at a higher load than might be expected from Fig. 4.10(a), with the path restabilizing before a jump to the 3 half-wave solution occurs.

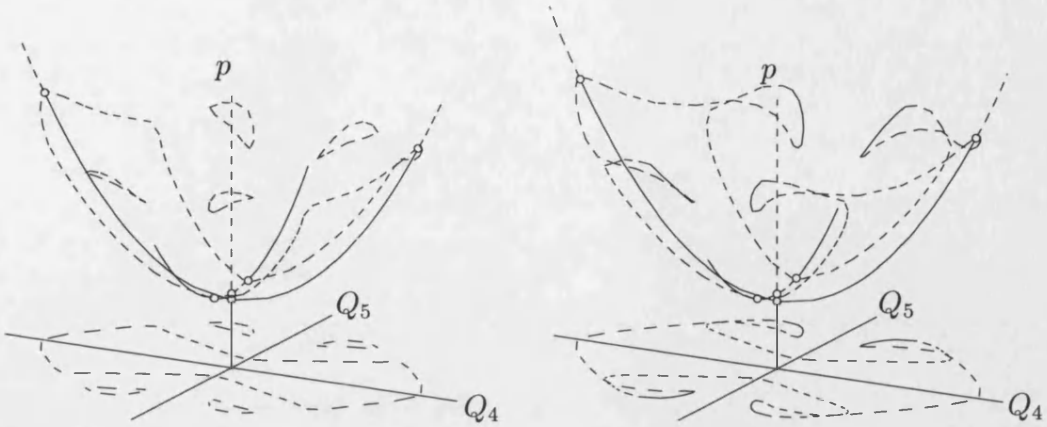

Figure 4.11: Jump from 4 to 5 waves for the clamped in-plane plate, (a) $l = 6.70$, (b) $l = 6.60$. Stable paths are shown as solid lines and unstable paths as broken lines.

4.9.3 Unstable secondary bifurcation

As l increases, the coupled path moves from stable to unstable. Fig. 4.11(a) shows that mode jumping occurs at the secondary bifurcation point when $a = 4$. For slightly shorter lengths (Fig. 4.11(b)) the coupled path again merges with the isolated solution path, and although it restabilizes the load reached is less than p^{s_a}, implying that under dead loading conditions the buckle pattern will change instantaneously.

4.9.4 Crossing of tongues

The amplitudes of s_a for the straight-edged plate are much larger than for clamped in-plane boundary conditions, and hence the effect of the passive modes will be greater and the coupled behaviour more complex. The tongue of $\lambda_1/\lambda_2 = 3/5$ crosses that of $\lambda_1/\lambda_2 = 3/4$, showing that when $a = 3$ interaction can occur with the mode $b = a + 2 = 5$; this coupled path contains only odd modes which have stronger coupling ($V_{3355} > V_{3344}$ for example). When $b = a + 1$, the coupled path is symmetrical with respect to both Q_a and Q_b. However, when a and b are both odd this double-symmetry is broken; flipping one mode through while keeping

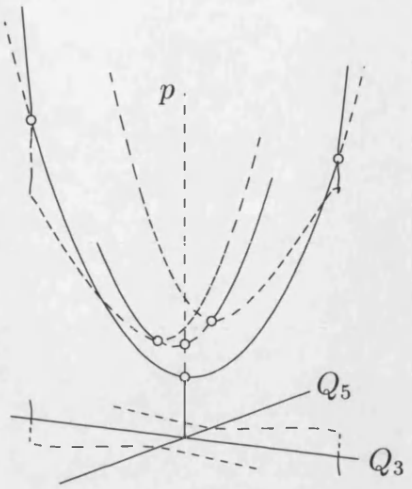

Figure 4.12: Jump from 3 to 5 waves for the straight-edged plate. Stable paths are shown as solid lines and unstable paths as broken lines.

the other unchanged generates a different shape (Hunt, 1986). This is reflected in the plot of Fig. 4.12, in which the coupled path does not project onto the base plane as a closed loop.

4.10 Concluding remarks

The main aims of this chapter were twofold — to extend the investigation and presentation techniques introduced for the simply-supported strut to the more difficult plate problem, and to explore the effect of the in-plane boundary conditions on the post-buckling stability.

The coupled behaviour of the plate is found to be far more complex, with the large number of passive modes meaning that locating secondary bifurcation positions using a Rayleigh–Ritz approach is no longer practical. The most useful results are obtained by reducing the von Kármán equations to a set of ODEs which are solved numerically using AUTO, hence including the destabilizing effects of all longitudinal harmonics and passive modes. Validation with the full numerical solution of the PDEs highlights the effect of transverse harmonics, especially at large amplitudes.

The results, presented using the parameter space of Arnol'd tongues, share a number of features with the strut, the most important being the appearance of a safety envelope. As the boundaries are increasingly constrained against in-plane movement, the amplitude, and hence the load, at which secondary bifurcation occurs reduces: the unrestrained plate of Fig. 4.1 is unconditionally stable; for most lengths the straight-edged plate loses stability at $p > 2p^a$; and the plate with its edges clamped in-plane exhibits little by comparison in the way of post-buckling strength. However it is important to note that this plot shows the amplitude at which secondary buckling occurs and does not indicate the behaviour or stability of the coupled path. In general the coupled path for short plates is stable, with mode jumping only occurring at the secondary bifurcation point for larger aspect ratios.

Chapter 5

Effects of the boundary conditions

The previous two chapters have explored mode jumping for the simply-supported strut, and the simply-supported plate with various in-plane boundary conditions. In addition to introducing the phenomena of mode jumping and the presentation of results in the form of Arnol'd tongues, this work highlights a number of important points, both in the post-buckling stability (with the existence of a safety envelope) and the choice of solution method (due to the effects of passive modes). However these results are perhaps slightly academic, as in most practical applications flat plates are not simply-supported. Therefore this work is now extended to encompass boundary conditions other than simply-supported for both the strut and plate problems.

Simply-supported boundary conditions are special in that the secondary bifurcation points can be found relatively easily using analytical techniques; for other boundary conditions the modulation of the buckle pattern (see Fig. 1.9) means that numerical methods are more suitable. The use of AUTO allows mode jumping to be explored in the full range of boundary conditions — including those lying between the extremes of simply-supported and clamped (Potier-Ferry, 1983) —

which have not been considered in detail for either the strut or plate problems. The entire sequence is described in the space of Arnol'd tongues; by comparing plots for each set of boundary conditions, variations in the post-buckling stability between the different cases can be seen.

Of the two available eigenvalues to express the initial deflected shape, only one is required when the boundaries are simply-supported: now the modulated shape is given (typically) by a quasi-periodic combination of the two. This could have implications for eigenvalue solvers such as VICON (Anderson *et al.*, 1983) and VICONOPT (Williams *et al.*, 1991) which assume eventual repeatability in the buckle pattern, and hence use integer mode numbers when calculating critical loads of prismatic structures (see Fig. 1.4).

The transition between the extremes of simply-supported and clamped is characterized by the behaviour of the strut. Therefore in the plate problem four distinct combinations of simply-supported and clamped boundaries on the long and short edges are investigated, with both straight-edged and clamped in-plane constraints, for the full range of lengths to be considered. Again, comparison of the tongue plots highlights the effects of the boundary conditions.

5.1 Supercritical strut

5.1.1 Energy integral and differential equation

The heuristic strut model shown in Fig. 3.1 is only valid for the extremes of simply-supported and clamped ends. The desire to include intermediate boundary conditions necessitates the inclusion of rotational springs of stiffness $\mathcal{K}$ at either end (Damil & Potier-Ferry, 1986), as shown in Fig. 5.1. These add two terms to the energy function (3.2) which — as they act at discrete points —

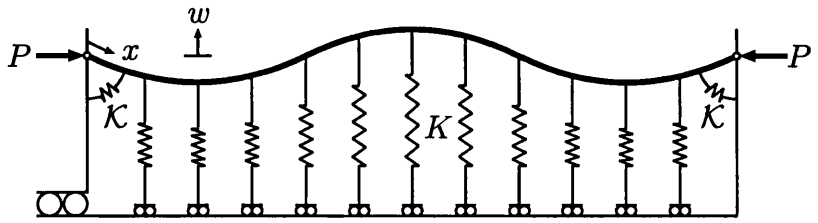

Figure 5.1: Strut on an elastic foundation.

appear outside the integral,

$$V = \int_0^L \left(\frac{1}{2}EI\ddot{w}^2 - \frac{1}{2}P\dot{w}^2 + \frac{1}{2}Kw^2 + \frac{1}{4}Cw^4\right) \mathrm{d}x + \frac{1}{2}\mathcal{K}\left(\dot{w}^2(0) + \dot{w}^2(L)\right). \tag{5.1}$$

At the extremes of simply-supported or clamped ends (where $\mathcal{K} = 0$ and $\mathcal{K} = \infty$ respectively) these additional terms are zero. As before w represents deflection away from the foundation and dots denote differentiation with respect to x.

Again, standard application of the calculus of variations leads to the Euler equation,

$$EI\dddot{w} + P\ddot{w} + Kw + Cw^3 = 0, \tag{5.2}$$

and the following (new) constraints,

$$\left[EI\ddot{w}\delta\dot{w} - EI\dddot{w}\delta w + P\dot{w}\delta w\right]_0^L + \mathcal{K}\dot{w}\delta\dot{w}\big|_0 + \mathcal{K}\dot{w}\delta\dot{w}\big|_L = 0, \tag{5.3}$$

which (as $\delta w = 0$ at each end) leaves,

$$\begin{aligned} w = \mathcal{K}\dot{w} - EI\ddot{w} = 0 \text{ at } x = 0, \\ w = \mathcal{K}\dot{w} + EI\ddot{w} = 0 \text{ at } x = L. \end{aligned} \tag{5.4}$$

Nondimensionalization gives

$$\bar{w}'''' + p\bar{w}'' + \bar{w} + \bar{w}^3 = 0, \tag{5.5}$$

where $\bar{w}$ and p are given by (3.4) and $\bar{x}$ by (3.5). For the boundary conditions (5.4) it is convenient (for the later numerical continuation) to define the nondimensional rotational stiffness as

$$\kappa = \frac{\mathcal{K}}{\mathcal{K} + \sqrt[4]{K(EI)^3}}, \tag{5.6}$$

giving

$$\begin{aligned} \bar{w} &= \kappa\dot{\bar{w}} - (1-\kappa)\ddot{\bar{w}} = 0 \text{ at } \bar{x} = 0, \\ \bar{w} &= \kappa\dot{\bar{w}} + (1-\kappa)\ddot{\bar{w}} = 0 \text{ at } \bar{x} = l, \end{aligned} \tag{5.7}$$

and hence $\kappa = 0$ and $\kappa = 1$ for simply-supported and clamped boundaries respectively.

The nondimensional equation (5.5) is the same as the simply-supported strut (3.3) and hence the characteristic equation (3.8), eigenvalues (3.12) and general solution (3.13) are also the same. In the remainder of this chapter the nondimensional equations are used and the bar dropped.

5.1.2 Critical loads

For the simply-supported case ($\kappa = 0$), the critical loads are given by (3.14) and are shown in Fig. 5.2(a) (repeated from Fig. 3.3). To satisfy the boundary conditions when κ is non-zero, the buckle pattern depends on both values of λ (3.12) and hence is, in general, quasi-periodic; as a result the critical loads cannot be written explicitly. However, solutions are still either symmetric or antisymmetric. Symmetric solutions can be found by considering the general equation

$$w = Q_a \cos\frac{a\pi x}{l} + Q_b \cos\frac{b\pi x}{l} \tag{5.8}$$

— where a and b can now take non-integer values — over the range $-l/2 < x < l/2$. Applying the boundary conditions (5.7) for the clamped case ($\kappa = 1$) gives

$$\begin{aligned} w(l/2) &= Q_a \cos\frac{a\pi}{2} + Q_b \cos\frac{b\pi}{2} = 0, \\ \dot{w}(l/2) &= -\frac{\pi}{l}\left(aQ_a \sin\frac{a\pi}{2} + bQ_b \sin\frac{b\pi}{2}\right) = 0. \end{aligned} \tag{5.9}$$

Combining these two equations to eliminate Q_a leaves

$$lQ_b\left(a \sin\frac{a\pi}{2}\cos\frac{b\pi}{2} - b\cos\frac{a\pi}{2}\sin\frac{b\pi}{2}\right) = 0, \tag{5.10}$$

and using the relationship (3.16)

$$l = \pi\sqrt{ab} \Rightarrow b = \frac{l^2}{a\pi^2} \tag{5.11}$$

effectively leaves the equation in a,

$$a^2\pi^2 \sin\frac{a\pi}{2}\cos\frac{l^2}{2a\pi} - l^2\cos\frac{a\pi}{2}\sin\frac{l^2}{2a\pi} = 0. \tag{5.12}$$

For any given length l, this can be solved numerically for a with the help of an algebraic manipulation package such as MAPLE (Heck, 1996). Substitution of these values into (3.14) gives the critical load. Starting with

$$w = Q_a \sin\frac{a\pi x}{l} + Q_b \sin\frac{b\pi x}{l}, \tag{5.13}$$

will give antisymmetric solutions and those for $0 < \kappa < 1$ can also be found by using a similar approach.

The lowest two critical loads for three different non-zero values of κ are shown in Figs. 5.2(b)–(d). One curve marks symmetric solutions and the other antisymmetric solutions, with the number of maxima and minima increasing with length such that the symmetry or antisymmetry of the solution is preserved. Fig. 5.2(d) is also familiar from the buckling of plates with clamped short edges (Wittrick, 1952; Bulson, 1970). Fig. 5.3 shows that as the rotational stiffness κ increases

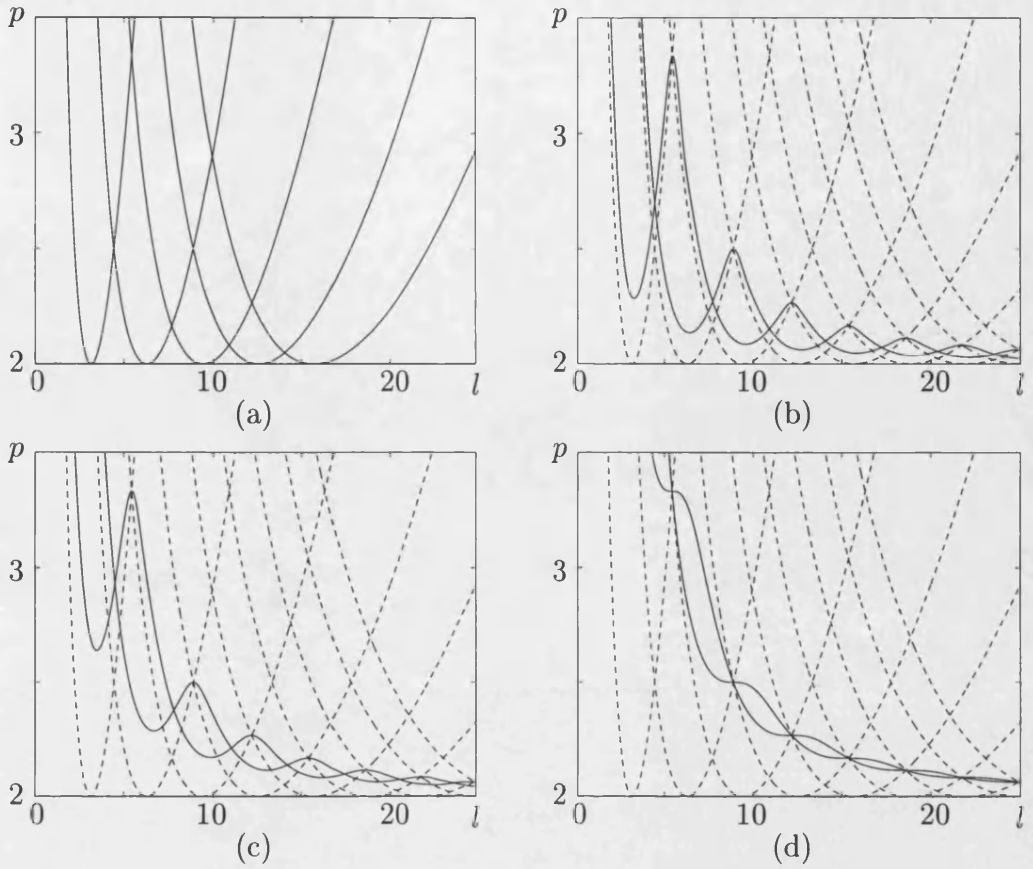

Figure 5.2: Lowest two critical loads for (a) $\kappa = 0$, (b) $\kappa = 0.2$, (c) $\kappa = 0.4$ and (d) $\kappa = 1$. Broken lines show critical loads for the simply-supported strut ($\kappa = 0$).

there is increased modulation of the buckle pattern (Damil & Potier-Ferry, 1986). The corresponding critical loads also increase, and $p = 2$ is only approached as $l \to \infty$ — where the effect of the boundary conditions reduces — rather than at the discrete lengths ($l = a\pi$) of the simply-supported case.

The curves all pass through the rational positions $\lambda_1/\lambda_2 = a/a + 2$, where a is odd for the symmetric case and even for the antisymmetric case, and modulated periodicity replaces the quasi-periodic response. At these positions, $w = \dot{w} = \ddot{w} = 0$ at both ends of the strut, and thus the critical loads are independent of the value of κ. Interestingly, the compound bifurcation points for the clamped case also occur at $\lambda_1/\lambda_2 = a/a + 2$: for example, interaction between buckle patterns with 4 and 5 maxima and minima is now marked by $\lambda_1/\lambda_2 = 4/6$. For other non-zero values of κ the compound bifurcation points occur at irrational

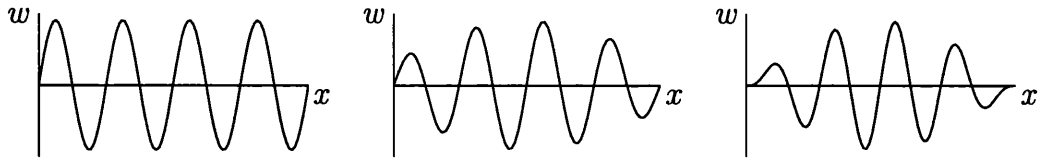

(a) (b) (c)

Figure 5.3: Linear buckle patterns for $l = 25$ and (a) $\kappa = 0$, (b) $\kappa = 0.5$ and (c) $\kappa = 1$.

positions between $a/a+1$ and $a/a+2$, corresponding to the quasi-periodic nature of the response.

5.1.3 Solution method

The nonlinear behaviour of the simply-supported strut is periodic (Fig. 5.4(a)) and hence a Galerkin or Rayleigh–Ritz technique is often used (Supple, 1970; Nakamura & Uetani, 1979). When κ is non-zero the post-buckling behaviour is more complex; although unclear from Fig. 5.4, the wavelengths decrease as the amplitude increases and modulation is concentrated at each end, creating a boundary layer effect (Damil & Potier-Ferry, 1986). Therefore a modal approach is not practical because, unlike the simply-supported case, the buckle pattern cannot be approximated with sufficient accuracy by a small number of modes.

The ODE (5.5) is thus solved numerically using the boundary value solver AUTO (Doedel *et al.*, 1995). The rescaled first-order equations are given by (3.52) and the boundary conditions (5.7) by

$$\begin{aligned} f_1(0) &= 0, \quad l\kappa f_2(0) - (1-\kappa) f_3(0) = 0, \\ f_1(1) &= 0, \quad l\kappa f_2(1) + (1-\kappa) f_3(1) = 0. \end{aligned} \tag{5.14}$$

In addition to varying the load or length as before, the rotational stiffness κ can also be altered, thereby allowing the full range of post-buckling behaviours to be investigated relatively easily.

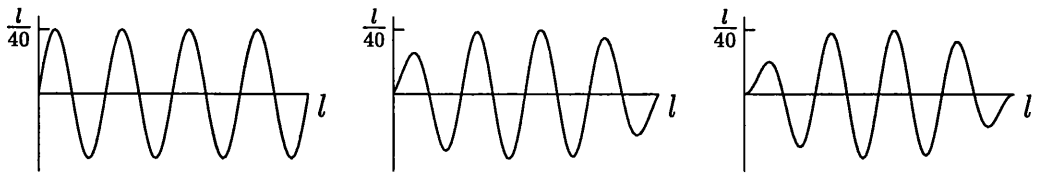

Figure 5.4: Nonlinear buckle patterns for $p = 2.3$, $l = 25$ and (a) $\kappa = 0$, (b) $\kappa = 0.5$, (c) $\kappa = 1$.

5.1.4 Arnol'd tongues

Tongues for the simply-supported case, repeated from Fig. 3.11, are shown in Fig. 5.5(a). The area to the top right of Fig. 5.5(a), where the curves are seen to bounce off the line $\lambda_1/\lambda_2 = 1$ (representing the minima of Fig. 5.2(a) where $p = 2$), is an artifact of the plot; switching λ_1 and λ_2 would allow them to carry through without discontinuity. The curves are presented this form to demonstrate the evolution as κ increases from zero.

When κ is non-zero the combination of the boundary layer and quasi-periodic behaviour means that in the nonlinear regime the response cannot be broken into distinct "integer" modes. As a result the maximum amplitude of the deflection is plotted and the vertical axis has been relabeled $w_{\max}$. However, mode jumping still occurs from symmetric to antisymmetric solutions, or vice versa, such that the number of maxima or minima increases by one. Figs. 5.5(b)–(d) show that the tongues of Fig. 5.5(a) move to the left and change shape as the rotational stiffness κ is increased. A typical cusp point moves from rational position $a/a+1$ at $\kappa = 0$, through intermediate irrational positions, to rational position $a/a+2$ at $\kappa = 1$, reflecting the movement of the compound bifurcation points of Fig. 5.2. For $0 < \kappa \leq 1$, all curves miss the $\lambda_1/\lambda_2 = 1$ line; this reflects the fact that, only as $l \to \infty$, do the critical loads approach $p = 2$. As κ increases, the safety envelope both decreases in size and moves to the right; thus stiffening the boundaries reduces the post-buckling reserve against mode jumping and limits it to progressively longer systems. For the fully clamped conditions of Fig. 5.5(d), both arms of the tongues are again seen to veer to the left; in the absence of the

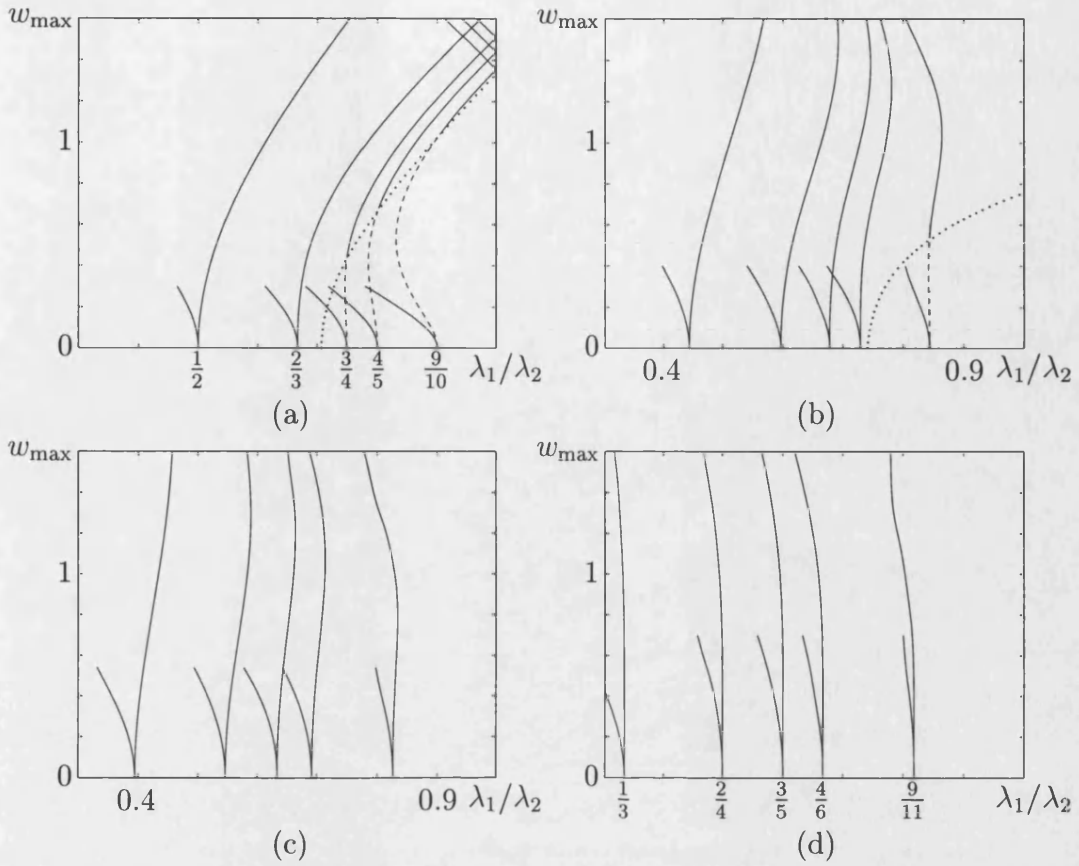

Figure 5.5: A selection of Arnol'd tongues for (a) $\kappa = 0$, (b) $\kappa = 0.2$, (c) $\kappa = 0.4$ and (d) $\kappa = 1$. Left-hand arms have been truncated for clarity.

safety envelope this is simply due to the fact that, to the left of the compound bifurcation points of Fig. 5.2(d), both critical loads increase.

For simply-supported boundary conditions, a jump from a periodic mode of wavenumber a to one of $a + 1$ necessarily involves a sudden reversal of the first derivative $\dot{w}$ at one of the boundaries. It was noted earlier that w, $\dot{w}$ and $\ddot{w}$ all vanish at the $(a,\ a + 2)$ compound bifurcations of Fig. 5.2(d), and this gives a clue to the mechanism for collapse of the safety envelope. A new half-wave can evolve smoothly at a clamped end, without the sudden switch in $\dot{w}$ required with simple supports. These special conditions restrict the ability of the system to lock into a specific mode, with the effect that, as the two critical points converge on the fundamental path, all secondary bifurcation points draw into the compound bifurcation point and the safely envelope is eliminated.

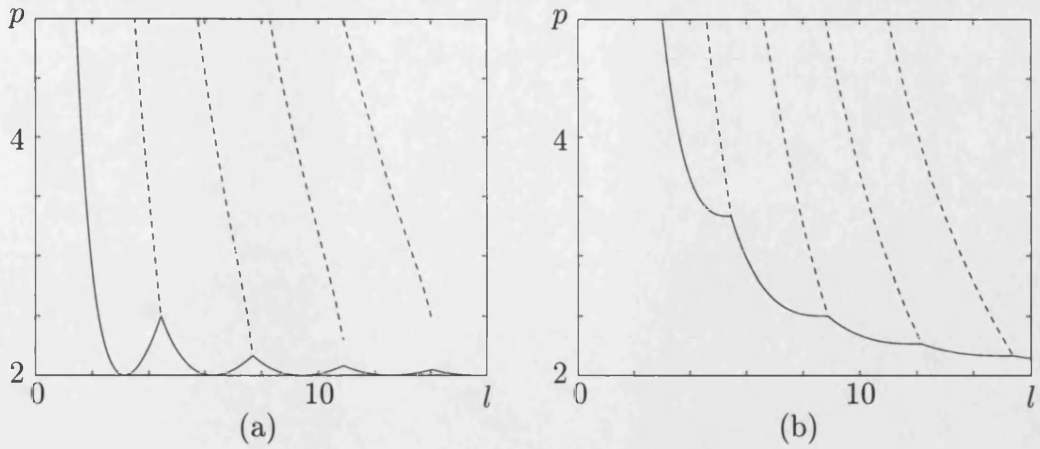

Figure 5.6: Comparison of minimum critical (solid lines) and secondary buckling loads for a strut with (a) simply-supported and (b) clamped ends.

It is intriguing that in all cases the jump is from symmetric mode to antisymmetric or vice versa. For simply-supported boundaries the position of the cusp on the real line at $a/a+1$ clearly identifies the periodic modes involved, but for the other boundary conditions it is more difficult to interpret how such a transfer is linked to either the irrational positions or $a/a+2$.

Fig. 5.2 shows that the critical loads vary considerably with κ and, although they determine the relevant values of λ_1/λ_2, it is important to note that Arnol'd tongue plots only represent the post-buckling behaviour and do not account for differences in critical loads. When $l < 5$, for example, the critical loads for the clamped case are significantly greater than those for simple supports, and thus mode jumping occurs at a higher load, as shown in Fig. 5.6. In contrast, when l is large the critical loads are similar and hence the simply-supported strut, with the greater reserve of post-buckling stability, has the higher secondary buckling load.

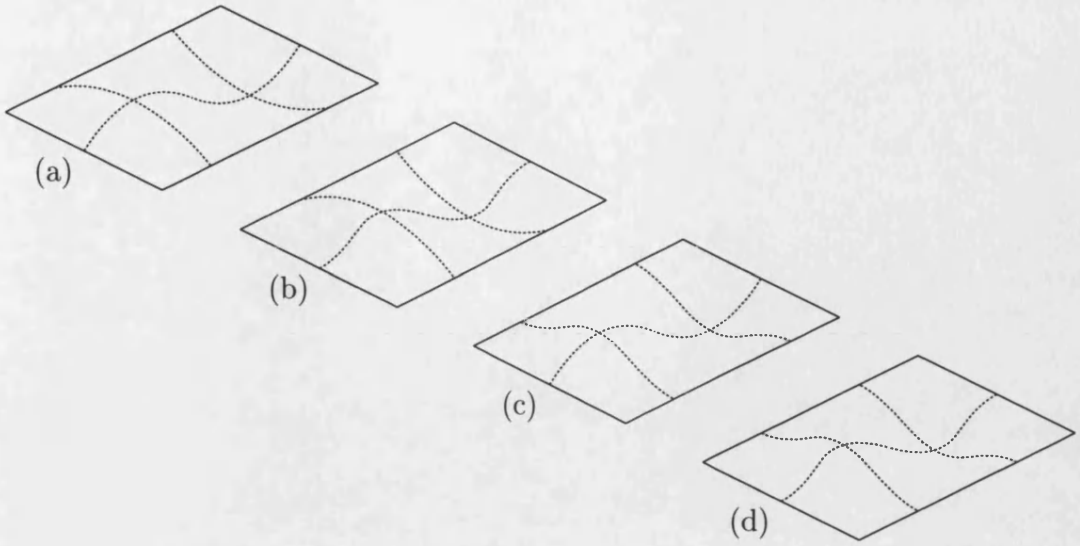

Figure 5.7: Plate buckle patterns for different flexural boundary conditions; (a) all edges simply-supported (A), (b) short edges clamped (B), (c) long edges clamped (C), (d) all edges clamped (D). Applied loads have been omitted for clarity.

5.2 Axially-compressed plate

5.2.1 Boundary conditions

From the similarities between the simply-supported strut and plate, it is reasonably safe to assume that the safety envelope for the plate will also disappear as the short edges are increasingly clamped. Therefore only four combinations of simply-supported and clamped boundary conditions (shown in Fig. 5.7),

A. all edges simply-supported,

B. long edges simply-supported and short edges clamped,

C. long edges clamped and short edges simply-supported,

D. all edges clamped,

in conjunction with two different in-plane constraints,

I. straight-edged,

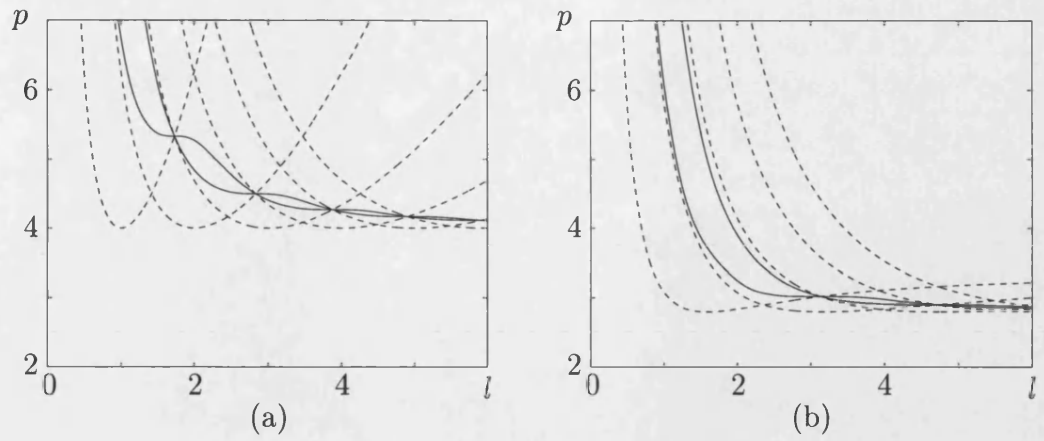

Figure 5.8: Critical loads for the (a) straight-edged (I) and (b) clamped in-plane (II) plates with simply-supported long edges. Broken and solid lines indicate simply-supported (A) and clamped (B) short edges respectively.

II. clamped in-plane,

are considered. This allows the von Kármán equations (2.49) and the constraints on w and φ to be used unaltered.

Unlike the free-edged plate with simply-supported boundaries (case A, Fig. 4.1) which has no instabilities on the natural loading path, mode jumping has been predicted for the free-edged plate with boundary conditions B and D by Gervais *et al.* (1997). However most practical applications will either be straight-edged or clamped in-plane, and so mode jumping in the free-edged plate is not pursued here.

5.2.2 Critical loads

The critical loads for cases AI and AII are given by (4.21) and are shown by the broken lines in Figs. 5.8(a) and (b) respectively. With clamped short edges (B), the solution now necessarily involves both wavelengths and the critical loads cannot be written explicitly. Using the same method as for the strut, outlined above, the critical loads are found numerically by MAPLE. The lowest two critical loads are shown by the solid lines in Fig. 5.8 (Wittrick, 1952; Bulson, 1970). Again

one curve marks symmetric solutions and the other antisymmetric solutions, with the compound bifurcation points for case B occurring at $a/a + 2$.

With clamped long edges the exact deflection is given by a combination of trigonometric and hyperbolic functions (Allen & Bulson, 1980). Unfortunately this solution changes slightly with different interacting modes and the plate lengths. However a good approximation for this transverse profile, suggested by Koiter & Pignataro (1976), is

$$w(y) = y^2(1-y)^2. \tag{5.15}$$

Substituting $w = Ae^{\Lambda\pi x}y^2(1-y)^2$ into (4.16) leads to the characteristic equation,

$$\Lambda^4\pi^4 + \Lambda^2\pi^2(\pi^2 p - 24) - 12\nu\pi^2 p + 504, \tag{5.16}$$

and two imaginary eigenvalues:

$$\begin{aligned}
\lambda_1 &= \frac{1}{\pi}\sqrt{\frac{\pi^2 p - 24}{2} - \sqrt{\frac{(\pi^2 p - 24)^2}{4} + 12\nu\pi^2 p - 504}}, \\
\lambda_2 &= \frac{1}{\pi}\sqrt{\frac{\pi^2 p - 24}{2} + \sqrt{\frac{(\pi^2 p - 24)^2}{4} + 12\nu\pi^2 p - 504}}.
\end{aligned} \tag{5.17}$$

Again assuming an integer number of half-waves ($\lambda = a/l$) gives the critical load for the simply-supported case,

$$p^a = \frac{\left(\pi^2 a^2 + 12l^2\right)^2 + 360l^4}{\left(a^2\pi^2 + 12\nu l^2\right)\pi^2 l^2}. \tag{5.18}$$

with the values of λ and p^a for the straight-edged boundary conditions found by substituting $\nu = 0$. The variations in the critical loads for cases C and D are shown in Fig. 5.9 for a range of plate lengths (Wittrick, 1952; Bulson, 1970). Critical loads are significantly greater than those shown in Fig. 5.8, although those for the clamped in-plane plate are again lower than those for the straight-edged plate.

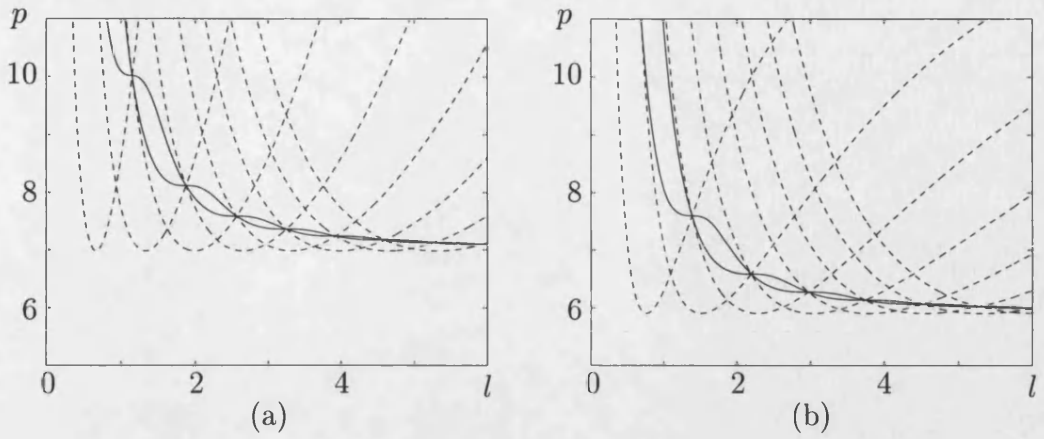

Figure 5.9: Critical loads for the (a) straight-edged (I) and (b) clamped in-plane (II) plates with clamped long edges. Broken and solid lines indicate simply-supported (C) and clamped (D) short edges respectively.

5.2.3 Reduction to ODEs

The PDEs are again reduced to a series of ODEs in x using the Galerkin procedure. The transverse functions and boundary conditions for cases AI and AII are given in Chapter 4. With clamped short edges (B) the same functions (4.40) are used with the following boundary conditions on w,

$$\begin{aligned} w_1(0) = w_1(l) = w_2(0) = w_2(l) = 0, \\ \dot{w}_1(0) = \dot{w}_1(l) = \dot{w}_2(0) = \dot{w}_2(l) = 0, \end{aligned} \tag{5.19}$$

and the same constraints on φ, satisfying the straight-edged conditions.

For clamped long edges the transverse profile (5.15) is used with the first harmonic,

$$w_2(y) = 1296y^4(1-y)^4 - 104y^3(1-y)^3 - 91y^2(1-y)^2, \tag{5.20}$$

(chosen by trial-and-error) which gives good agreement with the (slightly varying) exact solution. The boundary conditions on w for cases C and D are given by (4.41) and (5.19) respectively. The same functions and constraints are used for φ.

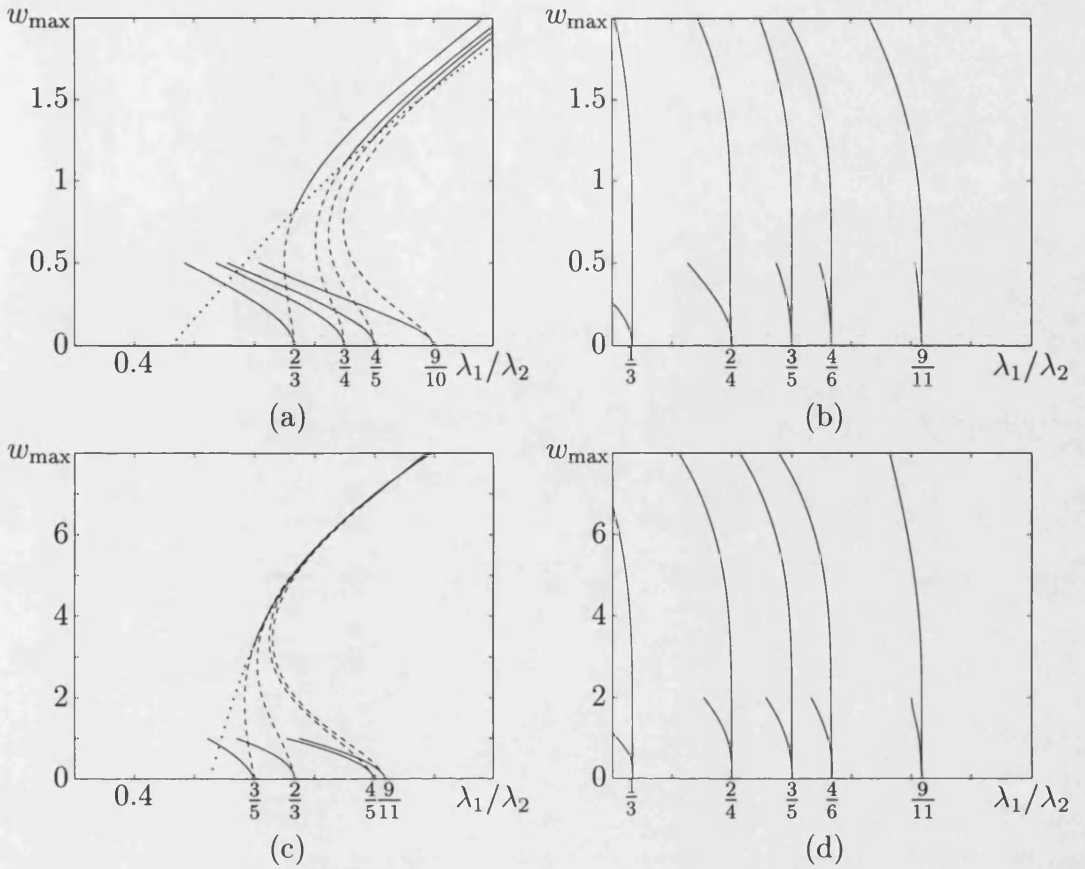

Figure 5.10: Arnol'd tongues produced from AUTO results for the clamped in-plane plate; (a) A, (b) B, (c) C, (d) D. For clarity, left-hand arms are truncated and some tongues are omitted.

5.2.4 Arnol'd tongues

Arnol'd tongues for the clamped in-plane plate (II) are plotted in Fig. 5.10, with the cusps for case A being repeated from Fig. 4.7. For the strut system, increases in flexural stiffness of the boundaries led to changes in the size and position of the safety envelope. The same changes are seen in the plate system. With clamped short edges (case B, Fig. 5.10(b)) the cusp points occur at the rational positions $a/a+2$ and both secondary bifurcation points draw into the compound bifurcation point eliminating the safely envelope. This has considerable practical implications: mode jumping can now occur at loads fractionally above the critical load.

For plates with clamped long edges (C and D), shown in Figs. 5.10(c) and (d), the

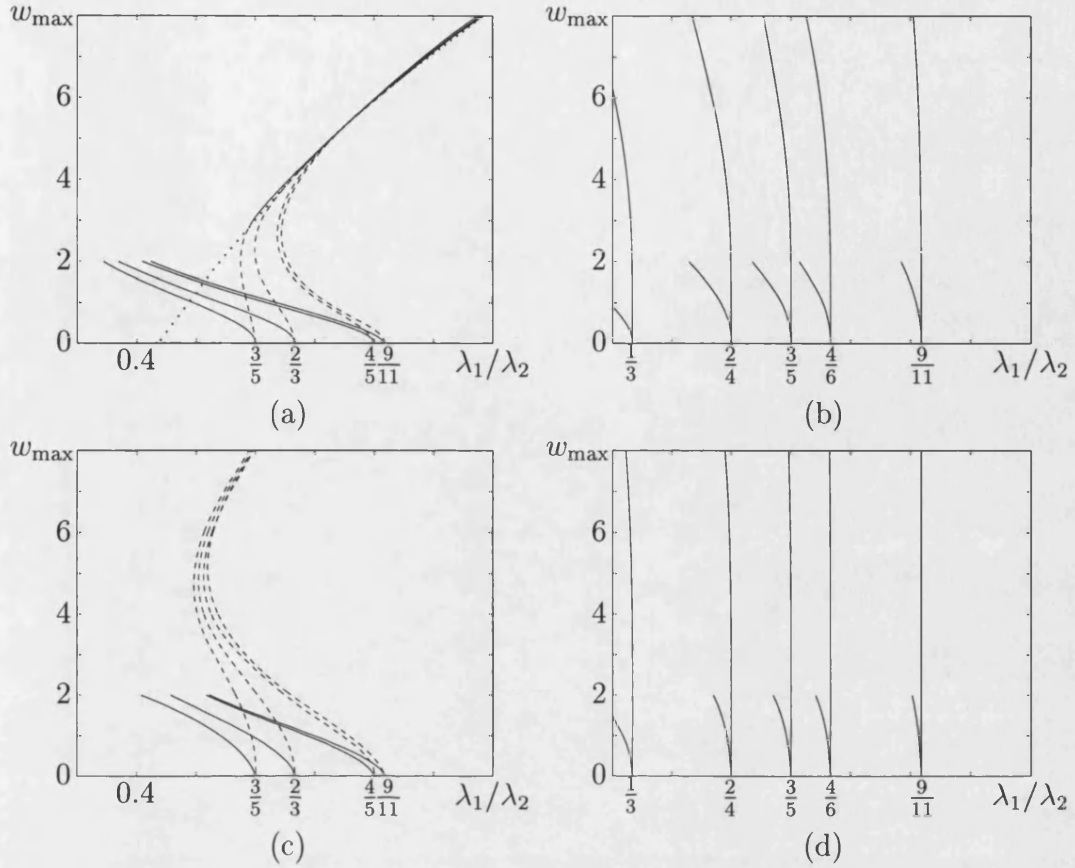

Figure 5.11: Arnol'd tongues produced from AUTO results for the straight-edged plate; (a) A, (b) B, (c) C, (d) D. For clarity, left-hand arms are truncated and some tongues are omitted.

same behaviour is seen except that the amplitude of the secondary bifurcations is much greater than for the corresponding simply-supported cases. A possible explanation is that the clamped edges reduces the wavelength across the width, making it much more difficult to move from positive to negative deflections. The increased amplitudes also means that there is more contamination from passive modes and hence some of the right-hand arms cross, indicating that for case C mode jumping can take place with the mode $b = a + 2$.

The Arnol'd tongues for the straight-edged plate (I) are plotted in Fig. 5.11. Apart from the notable increase in secondary buckling amplitudes (and loads) the pattern repeats that of the clamped in-plane case shown in Fig. 5.11: some tongues for cases A and C cross; the safety envelope disappears when the short edges are clamped; and the plates with clamped long edges have more post-

buckling reserve than those with simply-supported long edges.

Again the minimum critical loads vary considerably with the boundary conditions (Figs. 5.8 and 5.9) and hence when l is small mode jumping for cases C and D will occur at a higher load than for A and B. In contrast, when l is large the plates with simply-supported short edges (A and C) will have the higher secondary buckling loads.

5.3 Concluding remarks

Boundary conditions are shown to have considerable influence on the critical loads and post-buckling stability of the supercritical elastic struts. Several important features emerge, which pass over directly to the more difficult problem of elastic plates under compression and take on considerable practical importance. As the rotational stiffness is increased, the corresponding Arnol'd tongue plots show a significant drop in post-buckling stability and the elimination of the safety envelope, implying that mode jumping can occur at vanishingly small amplitudes just above the critical load. Short structures compensate for this with an increase in critical load, but as l is increased the difference in critical loads for different boundary conditions diminishes, and the clamped case has the lowest secondary buckling load.

The influence of the in-plane boundary conditions on the critical loads and post-buckling stability of compressed thin elastic plates is also found to be significant. Restricting the in-plane movement, from straight-edged to clamped in-plane, leads to a decrease in post-buckling stability. In contrast, and perhaps most importantly from a practical point of view, clamping up the long edges gives an considerable increase in critical loads for both the straight-edged and clamped in-plane cases.

Chapter 6

Conclusions and further work

This thesis gives a systematic appraisal of the phenomenon of mode jumping in the supercritical post-buckling of axially-compressed struts and plates. The problem is treated from two perspectives, the general theory of elastic stability as described nearly three decades ago (Thompson & Hunt, 1973), and with the modern numerical continuation code AUTO (Doedel *et al.*, 1995); analysis is combined with numerical experimentation in a search for the underlying destabilizations. Results are presented in a form reminiscent of Arnol'd tongues (Arnol'd, 1965) which shows the limit of mode locking, or instigation of mode jumping, for any length of system in a succinct manner. The appearance of Arnol'd tongues — or at least an Arnol'd tongue-like plot — which are usually associated with nonlinear mappings or dynamical systems running in time, is perhaps unexpected in a boundary value problem. However, as with subcritical behaviour, it is again abundantly clear that the dynamical systems analogy has much to offer nonlinear statics.

It is well known that the subcritical strut has led to a greater understanding of more complex problems which exhibit localized behaviour. Here the supercritical response of the strut on a stiffening foundation is usefully allied to axially-compressed flat plates; in both strut and plate problems an initially stable peri-

odic response is found to lose stability at a secondary bifurcation point, followed by a "mode jump" to a different solution with a shorter wavelength. These modes will sometimes have the same critical load, and the *compound bifurcation point* thus produced might thus seem a possible source of small amplitude jumps early in the post-buckling regime. However the tongue plots clearly show that with simply-supported boundary conditions protection against this effect is provided within a so-called "safety envelope". Surprisingly perhaps, the threshold value of amplitude (and load) marking the limit of this unconditional stability increases with increasing length.

The culmination of this work is a sequence of Arnol'd tongue plots which allow results from different boundary conditions to be compared in a consistent manner. Most plate applications are not truly simply-supported and hence, from a practical point of view, it is essential to be aware that restraint against rotational movement at the short edges leads to a reduction in post-buckling reserve. This is highlighted by the collapse of the safety envelope implying that, for a wide range of boundary conditions, mode jumping can occur early in the post-buckling regime. However some comfort can be gained by restricting flexural movement of the long edges which is known to give an considerable increase in the critical load.

Comparisons of analytical and numerical results show that the post-buckling behaviour is only successfully portrayed analytically with the inclusion of contaminating passive modes. Therefore, in the majority of cases, accurate post-buckling solutions are only given by numerical methods which effectively include the full gamut of passive effects. The increased complexity of the plate behaviour also highlights a limitation of the Arnol'd tongue plots: they do not indicate the stability of the coupled paths. In the strut problem all the coupled paths are unstable and so the tongues also mark the point where mode jumping occurs. For the simply-supported plate this is not the case; in general the coupled paths for short plates are stable and those at large aspect ratios unstable.

Finally, it is important to note that although the response for the case with simple supports is periodic, for other boundary conditions it is typically quasi-periodic — this could affect the calculation of critical loads by methods which assume repeatability and thus rely on integer mode numbers.

6.1 Further work

The recent developments in numerical methods — in particular the algorithms used by AUTO — and increases in computing power have enabled this extensive investigation into the effects of boundary conditions on the post-buckling response. Small increases in flexural stiffness are found to give a significant decrease in stability and therefore, rather than imperfections due to an initial out-of-flatness, differences between previous experimental and theoretical results may be caused by imperfect boundary conditions. This theoretical study would be complimented by a new series of experiments: if deviations from the desired simple or clamped supports were measured, these results could then be compared with predictions for the corresponding model generated by AUTO.

Other logical extensions of this work include the modelling of imperfections due to out-of-flatness, the use of orthotropic material properties (Brunelle & Oyibo, 1983) and different loading conditions (Fig. 1.3), all of which are relatively simple additions to the existing von Kármán equations. (In contrast, the modelling of anisotropic, layered or thick plates would require more complex three-dimensional models.)

The post-buckling of axially-compressed cylinders (Fig. 1.6) is governed by the von Kármán–Donnell equations, which are similar to those describing plate behaviour. As with the plate the initial post-buckling response is periodic (although in this case it is unstable); however for "long" cylinders *localized* solutions emerge from secondary bifurcation points close to the flat state (Hunt *et al.*, 1999). Pe-

riodicity and localization are thus inherently interlinked and therefore it may be interesting to investigate — by searching for homoclinic solutions via the eigenvalues of the periodic state (see for example Providência e Costa, 1994) — whether mode jumping in thin plates is also accompanied by some form of localization phenomenon.

Appendix A

Calculus of variations

For the plate the energy integral (2.37) is of the form

$$V = \int_0^1 \int_0^L \mathcal{L}(\dot{w}, \acute{w}, \ddot{w}, \grave{w}, \acute{\acute{w}}, \ddot{\varphi}, \grave{\varphi}, \acute{\varphi}) \, \mathrm{d}x\mathrm{d}y, \tag{A.1}$$

where dots and primes above the variables denote partial differentiation with respect to x and y respectively. The first variation δV of the Lagrangian $\mathcal{L}$ is given by

$$\delta V = \int_0^1 \int_0^L \left\{ \frac{\partial \mathcal{L}}{\partial \dot{w}} \delta \dot{w} + \frac{\partial \mathcal{L}}{\partial \acute{w}} \delta \acute{w} + \frac{\partial \mathcal{L}}{\partial \ddot{w}} \delta \ddot{w} + \frac{\partial \mathcal{L}}{\partial \grave{w}} \delta \grave{w} + \frac{\partial \mathcal{L}}{\partial \acute{\acute{w}}} \delta \acute{\acute{w}} \right.$$
$$\left. + \frac{\partial \mathcal{L}}{\partial \ddot{\varphi}} \delta \ddot{\varphi} + \frac{\partial \mathcal{L}}{\partial \grave{\varphi}} \delta \grave{\varphi} + \frac{\partial \mathcal{L}}{\partial \acute{\varphi}} \delta \acute{\varphi} \right\} \mathrm{d}x\mathrm{d}y. \tag{A.2}$$

Integrating by parts gives

$$\int_0^1 \int_0^L \frac{\partial \mathcal{L}}{\partial \dot{w}} \delta \dot{w} \, \mathrm{d}x\mathrm{d}y = \int_0^1 \left\{ \left[\frac{\partial \mathcal{L}}{\partial \dot{w}} \delta w \right]_0^L - \int_0^L \frac{\partial}{\partial x} \left(\frac{\partial \mathcal{L}}{\partial \dot{w}} \right) \delta w \, \mathrm{d}x \right\} \mathrm{d}y$$
$$= \int_0^1 \left[\frac{\partial \mathcal{L}}{\partial \dot{w}} \delta w \right]_0^L \mathrm{d}y - \int_0^1 \int_0^L \frac{\partial}{\partial x} \left(\frac{\partial \mathcal{L}}{\partial \dot{w}} \right) \delta w \, \mathrm{d}x\mathrm{d}y,$$

$$\int_0^1\int_0^L \frac{\partial\mathcal{L}}{\partial\ddot{w}}\delta\ddot{w}\,\mathrm{d}x\mathrm{d}y = \int_0^1\left[\frac{\partial\mathcal{L}}{\partial\ddot{w}}\delta\dot{w}\right]_0^L\mathrm{d}y - \int_0^1\int_0^L \frac{\partial}{\partial x}\left(\frac{\partial\mathcal{L}}{\partial\ddot{w}}\right)\delta\dot{w}\,\mathrm{d}x\mathrm{d}y$$

$$= \int_0^1\left[\frac{\partial\mathcal{L}}{\partial\ddot{w}}\delta\dot{w} - \frac{\partial}{\partial x}\left(\frac{\partial\mathcal{L}}{\partial\ddot{w}}\right)\delta w\right]_0^L\mathrm{d}y$$

$$+ \int_0^1\int_0^L \frac{\partial^2}{\partial x^2}\left(\frac{\partial\mathcal{L}}{\partial\ddot{w}}\right)\delta w\,\mathrm{d}x\mathrm{d}y,$$

$$\int_0^1\int_0^L \frac{\partial\mathcal{L}}{\partial\ddot{w}'}\delta\ddot{w}'\,\mathrm{d}x\mathrm{d}y = \int_0^1\left[\frac{\partial\mathcal{L}}{\partial\ddot{w}'}\delta\dot{w}'\right]_0^L\mathrm{d}y - \int_0^1\int_0^L \frac{\partial}{\partial x}\left(\frac{\partial\mathcal{L}}{\partial\ddot{w}'}\right)\delta\dot{w}'\,\mathrm{d}x\mathrm{d}y$$

$$= \int_0^1\left[\frac{\partial\mathcal{L}}{\partial\ddot{w}'}\delta\dot{w}'\right]_0^L\mathrm{d}y - \int_0^L\left[\frac{\partial}{\partial x}\left(\frac{\partial\mathcal{L}}{\partial\ddot{w}'}\right)\delta w\right]_0^1\mathrm{d}x$$

$$+ \int_0^1\int_0^L \frac{\partial^2}{\partial x\partial y}\left(\frac{\partial\mathcal{L}}{\partial\ddot{w}}\right)\delta w\,\mathrm{d}x\mathrm{d}y. \tag{A.3}$$

Expressions for the other components can be derived in a similar manner; adding them together leads to the first variation,

$$\delta V = \int_0^1\left[\frac{\partial\mathcal{L}}{\partial\dot{w}}\delta w + \frac{\partial\mathcal{L}}{\partial\ddot{w}}\delta\dot{w} - \frac{\partial}{\partial x}\left(\frac{\partial\mathcal{L}}{\partial\ddot{w}}\right)\delta w + \frac{\partial\mathcal{L}}{\partial\ddot{w}'}\delta\dot{w}'\right]_0^L\mathrm{d}y$$

$$+ \int_0^L\left[\frac{\partial\mathcal{L}}{\partial\dot{w}'}\delta w + \frac{\partial\mathcal{L}}{\partial\ddot{w}'}\delta\dot{w}' - \frac{\partial}{\partial y}\left(\frac{\partial\mathcal{L}}{\partial\ddot{w}'}\right)\delta w + \frac{\partial}{\partial y}\left(\frac{\partial\mathcal{L}}{\partial\ddot{w}}\right)\delta w\right]_0^1\mathrm{d}x$$

$$+ \int_0^1\int_0^L\left\{-\frac{\partial}{\partial x}\left(\frac{\partial\mathcal{L}}{\partial\dot{w}}\right) - \frac{\partial}{\partial y}\left(\frac{\partial\mathcal{L}}{\partial\dot{w}'}\right)\right.$$

$$\left. + \frac{\partial^2}{\partial x^2}\left(\frac{\partial\mathcal{L}}{\partial\ddot{w}}\right) + \frac{\partial^2}{\partial x\partial y}\left(\frac{\partial\mathcal{L}}{\partial\ddot{w}'}\right) + \frac{\partial^2}{\partial y^2}\left(\frac{\partial\mathcal{L}}{\partial\ddot{w}'}\right)\right\}\delta w\,\mathrm{d}x\mathrm{d}y$$

$$+ \int_0^1\left[\frac{\partial\mathcal{L}}{\partial\ddot{\varphi}}\delta\dot{\varphi} - \frac{\partial}{\partial x}\left(\frac{\partial\mathcal{L}}{\partial\ddot{\varphi}}\right)\delta\varphi + \frac{\partial\mathcal{L}}{\partial\ddot{\varphi}'}\delta\dot{\varphi}'\right]_0^L\mathrm{d}y$$

$$+ \int_0^L\left[\frac{\partial\mathcal{L}}{\partial\ddot{\varphi}'}\delta\dot{\varphi}' - \frac{\partial}{\partial y}\left(\frac{\partial\mathcal{L}}{\partial\ddot{\varphi}'}\right)\delta\varphi + \frac{\partial}{\partial x}\left(\frac{\partial\mathcal{L}}{\partial\ddot{\varphi}'}\right)\delta\varphi\right]_0^1\mathrm{d}x$$

$$+ \int_0^1\int_0^L\left\{\frac{\partial^2}{\partial x^2}\left(\frac{\partial\mathcal{L}}{\partial\ddot{\varphi}}\right) + \frac{\partial^2}{\partial x\partial y}\left(\frac{\partial\mathcal{L}}{\partial\ddot{\varphi}'}\right) + \frac{\partial^2}{\partial y^2}\left(\frac{\partial\mathcal{L}}{\partial\ddot{\varphi}'}\right)\right\}\delta\varphi\,\mathrm{d}x\mathrm{d}y. \tag{A.4}$$

Substituting (2.37), noting that all edges are supported (i.e. $\delta w = 0$ on the boundaries) and simplifying leaves

$$\begin{aligned}
\delta V = &\int_0^1 \Big[\big(D(\ddot{w} + \nu w'') - Et\varphi w''\big)\delta\dot{w} + 2\big(D(1-\nu) + Et\varphi\big)\dot{w}'\delta\dot{w}'\Big]_0^L \mathrm{d}y \\
&+ \int_0^L \Big[\big(D(w'' - \nu\ddot{w}) - Et\varphi\ddot{w}\big)\delta w'\Big]_0^1 \mathrm{d}x \\
&+ \int_0^1 \int_0^L \Big(D\nabla^4 w - \big(Et\varphi'' - P_x\big)\ddot{w} + 2Et\dot{\varphi}'\dot{w}' - \big(Et\ddot{\varphi} - P_y\big)w''\Big)\delta w \,\mathrm{d}x\mathrm{d}y \\
&- \int_0^1 Et\Big[\big(\ddot{\varphi} - \nu\varphi''\big)\delta\dot{\varphi} - \big(\ddot{\varphi} - \nu\varphi''\big)\delta\varphi + 2(1+\nu)\dot{\varphi}'\delta\dot{\varphi}\Big]_0^L \mathrm{d}y \\
&- \int_0^L Et\Big[\big(\varphi'' - \nu\ddot{\varphi}\big)\delta\varphi' - \big(\varphi''' - \nu\ddot{\varphi}'\big)\delta\varphi + 2(1+\nu)\ddot{\varphi}'\delta\varphi\Big]_0^1 \mathrm{d}x \\
&+ \int_0^1 \int_0^L \Big(\nabla^4\varphi - \dot{w}^2 + \ddot{w}w''\Big)\delta\varphi \,\mathrm{d}x\mathrm{d}y, \qquad \text{(A.5)}
\end{aligned}$$

where $\nabla^4 w = \ddot{w}'' + 2\,\ddot{w}'' + w''''$ and $\nabla^4\varphi = \ddot{\varphi}'' + 2\,\ddot{\varphi}'' + \varphi''''$.

Appendix B

Energy coefficients

The algebraic manipulation package MAPLE (Heck, 1996) was used to calculate the non-zero energy coefficients of (4.29). For the straight-edged plate these are;

$$V_{aaaa} = \frac{3}{32}\pi^4 l\left[1+\frac{a^4}{l^4}\right],$$

$$V_{aabb} = \frac{1}{32}\pi^4 l\left[4+\frac{a^2b^2}{l^4}+\frac{(a-b)^4}{\left((a+b)^2+4l^2\right)^2}+\frac{(a+b)^4}{\left((a-b)^2+4l^2\right)^2}\right],$$

$$V_{aaab} = -\frac{3}{32}\pi^4 l \quad \text{for } b=3a,$$

$$V_{aabc} = \frac{1}{32}\pi^4 l\left[3+\frac{(a+b)^2(3a-b)^2}{\left((a-b)^2+4l^2\right)^2}\right] \quad \text{for } c=2a-b,$$

$$= -\frac{1}{32}\pi^4 l\left[3+\frac{(a-b)^2(3a+b)^2}{\left((a+b)^2+4l^2\right)^2}\right] \quad \text{for } c=2a+b,$$

$$V_{abcd} = \pm\frac{1}{64}\pi^4 l\left[6+\frac{(a-b)^2(a+b+2c)^2}{\left((a+b)^2+4l^2\right)^2}+\frac{(a-c)^2(a+2b+c)^2}{\left((a+c)^2+4l^2\right)^2}+\frac{(b-c)^2(2a+b+c)^2}{\left((b+c)^2+4l^2\right)^2}\right] \quad \text{for } d=\pm(-a-b-c),$$

$$= \pm\frac{1}{64}\pi^4 l\left[6+\frac{(a+b)^2(a-b-2c)^2}{\left((a-b)^2+4l^2\right)^2}+\frac{(a+c)^2(a-2b-c)^2}{\left((a-c)^2+4l^2\right)^2}\right.$$
$$\left.+\frac{(b-c)^2(2a-b-c)^2}{\left((b+c)^2+4l^2\right)^2}\right] \quad \text{for } d=\pm(-a+b+c),$$

$$= \pm\frac{1}{64}\pi^4 l\left[6+\frac{(a+b)^2(a-b+2c)^2}{\left((a-b)^2+4l^2\right)^2}+\frac{(a-c)^2(a-2b+c)^2}{\left((a+c)^2+4l^2\right)^2}\right.$$
$$\left.+\frac{(b+c)^2(2a-b+c)^2}{\left((b-c)^2+4l^2\right)^2}\right] \quad \text{for } d=\pm(a-b+c),$$

$$= \pm\frac{1}{64}\pi^4 l\left[6+\frac{(a-b)^2(a+b-2c)^2}{\left((a+b)^2+4l^2\right)^2}+\frac{(a+c)^2(a+2b-c)^2}{\left((a-c)^2+4l^2\right)^2}\right.$$
$$\left.+\frac{(b+c)^2(2a+b-c)^2}{\left((b-c)^2+4l^2\right)^2}\right] \quad \text{for } d=\pm(a+b-c),$$

$$V'_{aa} = -\frac{1}{4}\pi^4\frac{a^2}{l}, \tag{B.1}$$

where a, b, c and d are all different. With clamped in-plane boundary conditions the following coefficients change;

$$V_{aaaa} = \frac{3}{32}\pi^4 l\left[3+\frac{a^4}{l^4}\right],$$

$$V_{aabb} = \frac{1}{32}\pi^4 l\left[6+\frac{a^2b^2}{l^4}+\frac{(a-b)^4}{\left((a+b)^2+4l^2\right)^2}+\frac{(a+b)^4}{\left((a-b)^2+4l^2\right)^2}\right],$$

$$V'_{aa} = -\frac{1}{4}\pi^4\left[\frac{a^2}{l}+\nu l\right]. \tag{B.2}$$

References

Aalami, B., & Williams, D. G. 1975. *Thin plate design for transverse loading.* London: Crosby Lockwood Staples.

Acheson, D. J. 1993. A pendulum theorem. *Proc. R. Soc. Lond.*, A **443**(1917), 239–245.

Allen, H. G., & Bulson, P. S. 1980. *Background to buckling.* London: McGraw-Hill.

Anderson, M. S., Williams, F. W., & Wright, C. J. 1983. Buckling and vibration of any prismatic assembly of shear and compression loaded anisotropic plates with an arbitrary supporting structure. *Int. J. Mech. Sci.*, **25**, 585–596.

Arnol'd, V. I. 1965. Small denominators I: Mappings of the circumference onto itself. *Am. Math. Soc. Transl. Series 2*, **46**, 213–284.

Bauer, L., & Reiss, E. L. 1965. Nonlinear buckling of rectangular plates. *SIAM J. Appl. Math.*, **13**(3), 603–626.

Bazant, Z. P., & Cedolin, L. 1991. *Stability of structures.* Oxford: Oxford University Press.

Brunelle, E. J., & Oyibo, G. A. 1983. Generic buckling curves for specially orthotropic rectangular plates. *AIAA Journal*, **21**(8), 1150–1156.

Bulson, P. S. 1970. *The stability of flat plates.* London: Chatto & Windus.

Carnoy, E. G., & Hughes, T. J. R. 1983. Finite element analysis of a flat plate under uniaxial compression. *Int. J. Nonlin. Mech.*, **18**(2), 167–175.

Champneys, A. R., & Thompson, J. M. T. 1996. A multiplicity of localized buckling modes for twisted rod equations. *Proc. R. Soc. Lond.*, A **452**, 2467–2491.

Champneys, A. R., & Toland, J. F. 1993. Bifurcation of a plethora of large amplitude homoclinic orbits for Hamiltonian systems. *Nonlinearity*, **6**(5), 665–721.

Champneys, A. R., Hunt, G. W., & Thompson, J. M. T. 1997. *Localization and solitary waves in solid mechanics.* Vol. 355. Special Issue of *Phil. Trans. R. Soc. Lond.*

Cheng, C., & Shang, X. 1997. Mode jumping of simply-supported rectangular plates on a nonlinear elastic foundation. *Int. J. Nonlin. Mech.*, **32**(1), 161–172.

Chia, C-Y. 1980. *Nonlinear analysis of plates.* London: McGraw-Hill.

Chien, C.-S. 1989. Secondary bifurcations in the buckling problem. *J. Comp. and App. Math.*, **25**, 277–287.

Chien, C.-S., & Chen, M.-S. 1997. Multiple bifurcation in the von Kármán equations. *SIAM J. Sci. Comp.*, **18**(6), 1737–1766.

Chilver, A. H. 1967. Coupled modes of elastic buckling. *J. Mech. Phys. Solids*, **15**, 15–28.

Chou, S. M., & Rhodes, J. 1997. Review and compilation of experimental results on thin-walled structures. *Comput. Struct.*, **65**(1), 47–67.

Cox, H. L. 1963. *The buckling of plates and shells.* Oxford: Pergamon.

Craggs, J. W. 1973. *Calculus of variations.* George Allen & Unwin.

Croll, J. G. A., & Walker, A. C. 1972. *Elements of structural stability.* London: Macmillan.

Damil, N., & Potier-Ferry, M. 1986. Wavelength selection in the post-buckling of a long rectangular plate. *Int. J. Solids Structures*, **22**(5), 511–526.

Das, S., Datta, S., Shadev, D., Verma, M. K., & Mehrotra, R. 1996. The dynamical response of a three-junction network. *Phys. D*, **91**(3), 292–300.

Doedel, E. J. 1997. Nonlinear numerics. *J. Franklin Inst.*, **334B**(5–6), 1049–1073.

Doedel, E. J., Wang, X. J., & Fairgrieve, T. F. 1995. *AUTO94: Software for continuation and bifurcation problems in ordinary differential equations.* Tech. rept. CRPC-95-2. California Institute of Technology.

Dowling, P. J., Knowles, P. R., & Owens, G. W. 1988. *Structural steel design.* London: Butterworths.

Dwight, J. B., & Ratcliffe, A. T. 1969. The strength of thin plates in compression. *Pages 3–34 of:* Rockey, C. K., & Hill, H. V. (eds), *Thin-walled steel structures.* London: Crosby Lockwood.

Ellinas, C. P., Supple, W. J., & Walker, A. C. 1984. *Buckling of offshore structures.* London: Granada.

Euler, L. 1744. *Methodus inveniendi lineas curvas maximi minimive proprietate gaudentes.* Appendix: De curvis elasticis. Lausanne and Geneva.

Everall, P. R. 1999. Arnol'd tongues and quasi-periodicity in the post-buckling of stable elastic structures. *Pages 165–168 of:* Bettess, P. (ed), *ACME'99: The seventh annual conference of the Association for Computational Mechanics in Engineering, Durham.*

Everall, P. R., & Hunt, G. W. 1999a. Arnol'd tongue predictions of secondary buckling in thin elastic plates. *J. Mech. Phys. Solids*, **47**(10), 2187–2206.

Everall, P. R., & Hunt, G. W. 1999b. Quasi-periodic buckling of an elastic structure under the influence of changing boundary conditions. *Proc. R. Soc. Lond.*, A **455**(1988), 3041–3051.

Everall, P. R., & Hunt, G. W. 1999c. Mode jumping in the buckling of struts and plates: a comparative study. *Int. J. Nonlin. Mech.* To appear.

Everall, P. R., & Hunt, G. W. 1999d. A numerical investigation of the stability of supercritical elastic buckling. *In: Proceedings of the European Conference on Computational Mechanics, Munich.*

Falconer, B. H., & Chapman, J. C. 1953. Compressive buckling of stiffened plates. *The Engineer*, **195**, 789.

Foppl, A. 1907. *Vorlesungen über technische Mechanik.* Leipzig: Teubner.

Galias, J. 1995. On a discrete-time nonlinear system associated with the second-order digital filter. *SIAM J. Appl. Math.*, **55**(6), 1782–1799.

Gervais, J. J., Abderrahmann, O., & Pierre, R. 1997. Finite element analysis of the buckling and mode jumping of a rectangular plate. *Dynamics and stability of systems*, **12**, 161–185.

Golubitsky, M., & Schaeffer, D. G. 1984. *Singularities and groups in bifurcation theory.* Applied mathematical sciences; 51. New York: Springer-Verlag.

Harding, J. E., & Hobbs, R. E. 1979. The ultimate load behaviour of box girder web panels. *The Structural Engineer*, **57B**(3), 49–54.

Hardy, G. H. 1940. *A mathematicians apology.* Cambridge: Cambridge University Press.

Heck, A. 1996. *Introduction to Maple.* New York: Springer-Verlag.

Hibbitt, Karlsson & Sorensen, Inc. 1997. *ABAQUS/Standard: User's manual.* Michigan, USA: Hibbitt, Karlsson & Sorensen, Inc.

Hilborn, R. C. 1994. *Chaos and nonlinear dynamics.* Oxford: Oxford University Press.

Holder, E. J., & Schaeffer, D. G. 1984. Boundary conditions and mode jumping in the von Kármán equations. *SIAM J. Math. Anal.*, **15**(3), 446–458.

Hui, D., & Hansen, J. S. 1980. The swallowtail and butterfly cuspoids and their application in the initial post-buckling of single-mode structural systems. *Q. Appl. Math.*, **38**(1), 17–36.

Hunt, G. W. 1986. Hidden (a)symmetries of elastic and plastic bifurcation. *Appl. Mech. Rev.*, **39**(8), 1165–1186.

Hunt, G. W., & Everall, P. R. 1999. Arnol'd tongues and mode jumping in the supercritical post-buckling of an archetypal elastic structure. *Proc. R. Soc. Lond.*, A **455**(1981), 125–140.

Hunt, G. W., & Wadee, M. K. 1991. Comparative lagrangian formulations for localized buckling. *Proc. R. Soc. Lond.*, A **434**, 485–502.

Hunt, G. W., Bolt, H. M., & Thompson, J. M. T. 1989. Structural localization phenomena and the dynamical phase-space analogy. *Proc. R. Soc. Lond.*, A **425**, 245–267.

Hunt, G. W., Lord, G. J., & Champneys, A. R. 1999. Homoclinic and heteroclinic orbits underlying the post-buckling of axially-compressed cylindrical shells. *Comput. Meth. Appl. Mech. Engng.*, **170**, 239–251.

Ikeda, K., & Nakazawa, M. 1998. Bifurcation hierarchy of a rectangular plate. *Int. J. Solids Structures*, **35**(7–8), 593–617.

Jensen, D. W., & Lagrac, P. A. 1988. Influence of mechanical couplings on the buckling and post-buckling of anisotropic plates. *AIAA Journal*, **26**(10), 1269–1277.

Johnson, B. H. 1990. *Near-coincident doubly-symmetric branching systems: elastic post-buckling behaviour and imperfection sensitivity.* Ph.D. thesis, University of Surrey.

Jordan, D. W., & Smith, P. 1987. *Nonlinear ordinary differential equations.* Oxford applied mathematics and computing science series. Oxford: Clarendon Press.

Kirchhoff, G. R. 1877. Vorlesungen über Mathematische Physik. *Mechanik*, 450.

Koiter, W. T. 1945. *On the stability of elastic equilibrium.* Ph.D. thesis, Delft, Amsterdam. English translation: NASA TT-F10-833 (1967).

Koiter, W. T., & Pignataro, M. 1976. *A general theory for the interaction between local and overall buckling of stiffened panels.* Tech. rept. WTHD 83. Delft University of Technology, Delft, The Netherlands.

Kot, M., Sayler, G. S., & Schultz, T. W. 1992. Complex dynamics in a model microbial system. *Bulletin Math. Biology*, **54**(4), 619–648.

Levy, S. 1942. *Bending of rectangular plates with large deflections.* Tech. rept. TR 737. NACA.

Levy, S., Goldenberg, D., & Zibritosky, G. 1944. *Simply-supported long rectangular plates under combined axial load and normal pressure.* Tech. rept. TN 949. NACA.

Lord, G. J., Champneys, A. R., & Hunt, G. W. 1997. Computation of localized post-buckling in long axially-compressed cylindrical shells. *Phil. Trans. R. Soc. Lond.*, **355**(1732), 2137–2150.

Lord, G. J., Champneys, A. R., & Hunt, G. W. 1998. Computation of homoclinic orbits in partial differential equations: an application to cylindrical shell buckling. *SIAM J. Sci. Comp.* To appear.

Love, A. E. H. 1892. *A treatise on the mathematical theory of elasticity.* New York: Dover.

Maaskant, R., & Roorda, J. 1992. Mode jumping in biaxially-compressed plates. *Int. J. Solids Structures*, **29**(10), 1209–1219.

Magnus, R., & Poston, T. 1977. *On the full unfolding of the von Kármán equations at a double eigenvalue.* Tech. rept. Battelle Advanced Studies Centre.

Matkowsky, B. J., & Putnick, L. J. 1974. Multiple buckled states of rectangular plates. *Int. J. Nonlin. Mech.*, **9**, 89–103.

Matkowsky, B. J., Putnick, L. J., & Reiss, E. L. 1980. Secondary states of rectangular plates. *SIAM J. Appl. Math.*, **38**(1), 38–51.

Mindlin, R. D. 1951. Influence of rotary inertia and shear on flexural motions of isotropic elastic plates. *ASME J. Appl. Mech.*, **18**, 31.

Murray, N. W. 1973. Buckling of stiffened panels loaded axially and in bending. *The Structural Engineer*, **51**(8), 285–301.

Nakamura, T., & Uetani, K. 1979. The secondary buckling and post-secondary buckling behaviours of rectangular plates. *Int. J. Mech. Sci.*, **21**, 265–286.

Nakazawa, M., Iwakuma, T., Kuranishi, S, & Hidaka, M. 1993. Instability phenomena of a rectangular elastic plate under bending and shear. *Int. J. Solids Structures*, **30**(20), 2729–2741.

Poston, T., & Stewart, I. 1978. *Catastrophe theory and its applications.* London: Pitman.

Potier-Ferry, M. 1983. Amplitude modulation, phase modulation and localization of buckling patterns. *Pages 149–159 of:* Thompson, J. M. T., & Hunt, G. W. (eds), *Collapse: the buckling of structures in theory and practice.* Cambridge: Cambridge University Press.

Powell, S. M., Williams, F. W., Asker, A. S., & Kennedy, D. 1998. Local post-buckling analysis for perfect and imperfect longitudinally-compressed plates and panels. *Pages 595–603 of: Proceedings of 39th AIAA/ASME/ASCE/*

AHS/ASC Structures, Structural Dynamics, and Materials Conference, Long Beach, CA.

Providência e Costa, P. M. M. P. 1994. *Post-buckling behaviour of uniform cellular structures.* Ph.D. thesis, Imperial College of Science, Technology and Medicine, London.

Pugh, S. A., Schell, M., & Ross, J. 1986. Effects of periodic perturbations on the oscillatory combustion of acetaldehyde. *J. Chem. Phys.*, **85**(2), 868–878.

Reissner, E. 1947. On bending of elastic plates. *Q. Appl. Math.*, **5**, 55–68.

Rhodes, J., & Harvey, J. M. 1971. The post-buckling behaviour of thin flat plates in compression with unloaded edges elastically restrained against rotation. *ASCE J. Eng. Mech.*, **13**(2), 82–91.

Riks, E., Rankin, C. C., & Brogan, F. A. 1996. On the solution of mode jumping phenomena in thin-walled shell structures. *Comput. Meth. Appl. Mech. Engng.*, **136**, 59–92.

Romeo, R., & Frulla, G. 1994. Nonlinear analysis of anisotropic plates with initial imperfections and various boundary conditions subjected to combined biaxial compression and shear loads. *Int. J. Solids Structures*, **31**(6), 763–783.

Sandefur, J. T. 1990. *Discrete dynamical systems.* Oxford: Clarendon.

Schaeffer, D. G., & Golubitsky, M. 1979. Boundary conditions and mode jumping in the buckling of rectangular plates. *Commum. Math. Phys.*, **69**, 209–236.

Sewell, M. J. 1965. The static perturbation technique in buckling problems. *J. Mech. Phys. Solids*, **13**, 247–265.

Sewell, M. J. 1970. On the branching of equilibrium paths. *Proc. R. Soc. Lond.*, A **315**, 490–518.

Seydel, R. 1994. *Practical bifurcation and stability analysis: from equilibrium to chaos.* Interdisciplinary Applied Mathematics, vol. 5. New York: Springer-Verlag.

Sharman, P. W., & Humpherson, J. G. 1968. An experimental and theoretical investigation of simply-supported thin plates subjected to lateral load and uniaxial compression. *Aero. J. Roy. Aero. Soc.*, **72**, 431–436.

Sridharan, S. 1983. Doubly symmetric interactive buckling of plate structures. *Int. J. Solids Structures*, **19**(7), 625–641.

Stein, M. 1959a. *The phenomenon of change in buckle pattern in elastic structures.* Tech. rept. R39. NASA.

Stein, M. 1959b. *Loads and deformation of buckling in rectangular structures.* Tech. rept. R40. NASA.

Stoll, F. 1994. Analysis of the snap phenomenon in buckled plates. *Int. J. Nonlin. Mech.*, **29**(2), 123–138.

Stroebel, G. J., & Warner, W. H. 1973. Stability and secondary bifurcation for von Kármán plates. *J. Elasticity*, **3**(3), 185–202.

Suchy, H., Troger, H., & Weiss, R. 1985. A numerical study of mode jumping of rectangular plates. *Z. angew. Math. Mech.*, **65**(2), 71–78.

Supple, W. J. 1966. *Coupled buckling modes of structures.* Ph.D. thesis, University of London.

Supple, W. J. 1967. Coupled branching configurations in the elastic buckling of symmetric structural systems. *Int. J. Mech. Sci.*, **9**, 97–112.

Supple, W. J. 1968. On the change in buckle pattern in elastic structures. *Int. J. Mech. Sci.*, **10**, 737–745.

Supple, W. J. 1970. Changes of waveform of plates in the post-buckling range. *Int. J. Solids Structures*, **6**, 1243–1258.

Supple, W. J. (ed). 1973. *Structural instability.* Guildford: IPC Science and Technology Press.

Swanson Analysis Systems, Inc. 1992. *ANSYS: User's manual.* Houston, USA: Swanson Analysis Systems Inc. Revision 5.0.

Szilard, R. 1974. *Theory and analysis of plates — classical and numerical methods.* New Jersey: Prentice-Hall.

The Math Works, Inc. 1993. *MATLAB: High-performance numeric computation and visualization software.* Natick, Massachussets, USA: The Math Works Inc. Version 4.2.

Thompson, J. M. T., & Hunt, G. W. 1973. *A general theory of elastic stability.* London: Wiley.

Thompson, J. M. T., & Hunt, G. W. 1984. *Elastic instability phenomena.* Chichester: Wiley.

Thompson, J. M. T., & Stewart, H. B. 1986. *Nonlinear dynamics and chaos: geometrical methods for engineers and scientists.* Chichester: Wiley.

Thompson, J. M. T., & Supple, W. J. 1973. Erosion of optimum designs by compound brancing phenomena. *J. Mech. Phys. Solids*, **21**, 135–144.

Timoshenko, S. P., & Gere, J. M. 1961. *Theory of elastic stability.* New York: McGraw-Hill (Engineering Societies monograph).

Timoshenko, S. P., & Goodier, J. N. 1970. *Theory of elasticity.* New York: McGraw-Hill.

Timoshenko, S. P., & Woinowsky-Krieger, S. 1959. *Theory of plates and shells.* New York: McGraw-Hill (Engineering Societies monograph).

Uemura, M., & Byon, O. 1977. Secondary buckling of a flat plate under uniaxial compression. Part 1: Theoretical analysis of simply supported flat plate. *Int. J. Nonlin. Mech.*, **12**(6), 355–370.

Uemura, M., & Byon, O. 1978. Secondary buckling of a flat plate under uniaxial compression. Part 2: Analysis of clamped plate by FEM and comparison with experiments. *Int. J. Nonlin. Mech.*, **13**(1), 1–12.

Uetani, K. 1974. *Secondary buckling of an axially-compressed elastic bar supported by a nonlinear hardening foundation.* Orally presented at IUTAM Symp. Buckling of Structures, Harvard University.

von Kármán, T. 1910. Festigkeitsprobleme im maschinenbau. *Enzyklopädie der mathematischen Wissenschaften*, **4**, 348–351.

von Kármán, T., Sechler, E. E., & Donnell, L. H. 1932. The strength of thin plates in compression. *Trans. ASME, J. Appl. Mech.*, **54**, 53–57.

Wadee, M. A. 1999. Experimental evaluation of interactive buckle localization in compression sandwich panels. *J. Sand. Struct. Mat.*, **1**(3), 230–250.

Wadee, M. K., & Bassom, A. P. 1999. Effects of exponentially small terms in the perturbation approach to localized buckling. *Proc. R. Soc. Lond.*, **455**(1986), 2351–2370.

Wadee, M. K., Hunt, G. W., & Whiting, A. I. M. 1997. Asymptotic and Rayleigh–Ritz routes to localized buckling solutions in an elastic instability problem. *Proc. R. Soc. Lond.*, A **453**(1965), 2085–2107.

Walker, A. C. 1984. A brief review of plate buckling research. *Pages 375–398 of:* Rhodes, J., & Spence, J. (eds), *Behaviour of thin-walled structures.* London: Elsevier.

Watson, A. 1998. *Stability analysis and design of prismatic thin-walled structures.* Ph.D. thesis, University of Wales.

Wicks, P. J. 1988. A classification of behaviour in doubly-symmetric compound branching. *Int. J. Mech. Sci.*, **30**, 821–833.

Williams, D. G., & Aalami, B. 1979. *Thin plate design for in-plane loading.* London: Granada.

Williams, D. G., & Walker, A. C. 1975. Explicit solutions for the design of initially deformed plates subject to compression. *Proc. Instn. Civ. Engrs*, **59**, 763–787.

Williams, F. W., Kennedy, D., & Butler, R. 1991. VICONOPT: Program for exact vibration and buckling analysis or design of prismatic plate assemblies. *AIAA Journal*, **11**, 1927–1928.

Winful, H. G., Chen, Y. C., & Liu, J. M. 1986. Frequency locking, quasi-periodicity and chaos in modulated self-pulsing semiconductor lasers. *Appl. Phys. Lett.*, **48**(10), 616–618.

Winter, G. 1947. Strength of thin structures with flanges. *Trans. ASCE*, **112**, 527–554.

Wittrick, W. H. 1952. Correlatoin between some stability problems for orthotropic and isotropic plates under biaxial and uniaxial direct stress. *Aero. Quarterly*, **4**, 83–92.

Wu, B. 1993. Secondary buckling of a strut on an elastic foundation under axial compression. *Acta Mechanica Sinica*, **25**, 443–451.

Yamaki, N. 1959. Post-buckling behaviour of rectangular plates with small initial curvature loaded in edge compression. *ASME J. Appl. Mech.*, **26**, 407–414.

Yamaki, N. 1960. Post-buckling behaviour of rectangular plates with small initial curvature loaded in edge compression (continued). *ASME J. Appl. Mech.*, **27**, 335–342.

Yamaki, N. 1984. *Elastic stability of circular cylindrical shells.* Applied Mathematics and Mechanics Series, vol. 27. New York: Elsevier.

Zienkiewicz, O. C. 1977. *The finite element method.* London: McGraw-Hill.